First Order Assessment of Heat Transfer due to the Loss of Inventory in a Spent Fuel Pool

By:

Vernon W Fillis

Mini-dissertation presented in partial fulfilment of the requirements for the degree of Masters of Engineering specializing in Nuclear Power in the Faculty of Engineering and the Built Environment at the University of Cape Town

Supervisor:

Prof: A.G. Malan

Industrial Co-supervisor: Dr I. Malgas

August 2017

Abstract

The Fukushima Daiichi Nuclear Power Plant accident created renewed international interest in the behaviour of spent fuel subsequent to a complete loss of water inventory in a spent fuel pool (SFP). The study conducted in this dissertation serves as a starting point in gaining an understanding of the thermal hydraulics and associated heat transfer processes involved when spent fuel assemblies (SFAs) become uncovered in air. The complete loss of cooling in a SFP is a complex 3-D problem, hence several simplifications were necessary in this research to narrow the scope. Further, due to the complexity of this topic, the results obtained serves purely as a first order approximation. Accordingly, the Flownex systems CFD code (version 8.6.1.2630) was used to simulate the thermal response of the uncovered SFAs in the SFP of a typical Pressurised Water Reactor (PWR) during a severe accident scenario. Two network models were developed. The first was to identify the dominant heat transfer mechanisms with-in the spent fuel pool and it therefore accounted for a range of physics. This included convective heat transfer through the composite SFA channel walls, conduction along the vertical axial direction of the SFAs and through the inner and outer rack wall as well as through the fuel building (FB) roof and side walls. The model also took into account the radiative heat transfer from the cladding surface of the composite SFAs to the FB roof and side walls. This network model informed that the heat transfer with-in the SFA during the considered extreme accident scenario is dominated by radiative heat transfer. This informed the development of an improved 2-D network model using conduction elements which were specially calibrated in this work to account for radiative heat loss. An effective conduction for the fuel volume which is dependent on temperature was determined and was used to assess the severe accident. Transient results showed that the spent fuel may reach cladding oxidation temperature within circa 10.5 hrs after a complete loss of inventory.

Declaration

I, Vernon William Fillis, know the meaning of plagiarism and declare that all the work in the document, save for that which is properly acknowledged, is my own. This dissertation has been submitted to the Turnitin module and I confirm that my supervisor has seen my report and any concerns revealed by such have been resolved with my supervisor. I have not previously in its entirety or in part submitted it for obtaining any qualification.

Signed by candidate

Vernon W Fillis

Acknowledgements

First and foremost, the author expresses his gratitude to God, for His divine guidance without which the completion of this task would not have been possible.

I would like to acknowledge the following people:

- To my wife, Alicia, thank you for your endless support, encouragement and understanding, and to my children (Athayla and Jaron), thank you guys for allowing me the space to complete this research.

- I would like to express great gratitude to my supervisor, Professor Arnaud Malan for his expert technical guidance and supervision throughout the development of this research and to my industrial co-supervisor, Dr Isaac Malgas, for his input and support.

- I would like to express great appreciation to Mr William Theron (ESTEQ) for the training on the software package Flownex and the Flownex support team [M-Tech Industrial (PTY) LTD] for their technical support in using the Flownex code.

- Lastly, I would like to thank my sponsor, Eskom and the Operations Readiness Management team for providing me the opportunity and time to execute this research and for their support throughout the programme.

Table of Contents

List of Figures

List of Tables

Nomenclature

Symbols	Description	Unit
A	Cross sectional area	m^2
A_s	Surface area	m^2
c_p	Specific heat capacity	kJ/kg.K
D_H	Hydraulic diameter	m
$F_i(t_\propto, T_\propto)$	Sum of decay heat	MeV/fission
$G(t)$	Correction factor which account for neutron capture in fission products	-
h_c	Convective heat transfer coefficient	$W/m^2.K$
k	Thermal conductivity	W/m.K
L	Pipe length	m
$\dot{m}_e$	Exit mass flow from control volume	kg/s
$\dot{m}_i$	Inlet mass flow from control volume	kg/s
$P_d(t,T)$	Total fission product decay heat power at t seconds after shutdown	kW
$\acute{P}_d(t,T)$	Decay heat power	kW
$\acute{P}_{di}(t,T)$	Uncorrected decay heat power	kW
$P_{i\propto}$	Average power of reactor at specific operating period	kW
P_{oi}	Total inlet pressure	Pa
P_{oe}	Total outlet pressure	Pa
$\Delta P_{0,losses}$	Total pressure losses through control volume	Pa

Q_i	Total energy per fission	MeV/fission
Q	Total heat input	kW
q'''	Heat rate per unit volume	W/m^3
R	Outer radius	m
r	Radial location	m
ΔT	Total temperature difference	K
T_∞	Ambient temperature	K
T_0	Mean total temperature in element	K
T	Total operating period of reactor	s
T_s	Surface temperature	K
t	Time after shutdown	s
V	Fluid velocity	m/s
3-D	Three Dimensional	-

Greek Symbols	**Description**	
ψ	Fissions per initial fissile atom	-
ρ	density	[kg/m^3]
$\propto$	Index specifying an operating period at constant power	-
∞	Infinite time $T \equiv 10^{13}$	s
ε	Emissivity	-
$\forall$	Control volume	m^3

List of Abbreviations

BWR	Boiling Water Reactor
CFD	Computational Fluid Dynamics
CHTE	Composite Heat Transfer Element
FA	Fuel Assembly
FB	Fuel Building
FR	Fuel Rod
F12	View Factor
GWd/MTU	Gigawatt-days per Metric Ton of Uranium
HTE	Heat Transfer Element
IRW	Inner Stainless Steel Rack Wall
ORW	Outer Stainless Steel Rack Wall
NPP	Nuclear Power Plant
Pu-239	Plutonium-239
Pu-241	Plutonium-241
PWR	Pressurised Water Reactor
SFA	Spent Fuel Assembly
SFP	Spent Fuel Pool
SFR	Spent Fuel Rod
SRGM	Simplified Representative Geometric Model
Sr-92	Strontium-94

U-235	Uranium-235
U-238	Uranium-238
US NRC	United States Nuclear Regulatory Commission
Xe-140	Xenon-140
Zr	Zirconium

1. Introduction

1.1 Purpose

The purpose of this research is to provide a first order estimate of the time that it will take for spent fuel cladding to reach the cladding oxidation temperature during a complete loss of inventory in the spent fuel pool (SFP) under a beyond design basis loss of coolant accident. The estimation will serve as input in establishing timelines as to when an Emergency Plan (EP) needs to be implemented. This time period estimation may also assist in developing appropriate coping strategies for preventing the onset of oxidation and/or mitigating the consequences thereof. The results obtained in this mini-dissertation are approximations and detailed analyses needs to be executed with sophisticated 3-D modelling software in the interest of increased certainty and accuracy.

1.2 Background

Nuclear energy is used in various forms of commercial electricity generation. Nuclear power for electricity generation is harnessed in the reactor vessel of various types of Pressurised Water Reactors (PWRs) through the energy released from fission of uranium-235. Uranium -235 is enriched from 0.7% and is converted to uranium oxide powder and pressed into fuel pellets. The pellets are placed in tubes known as fuel rods [1]. The fuel rods (FRs) are bundled together into larger fuel assemblies (FAs) and placed vertically in the core of the reactor vessel as illustrated in Figure 1 below.

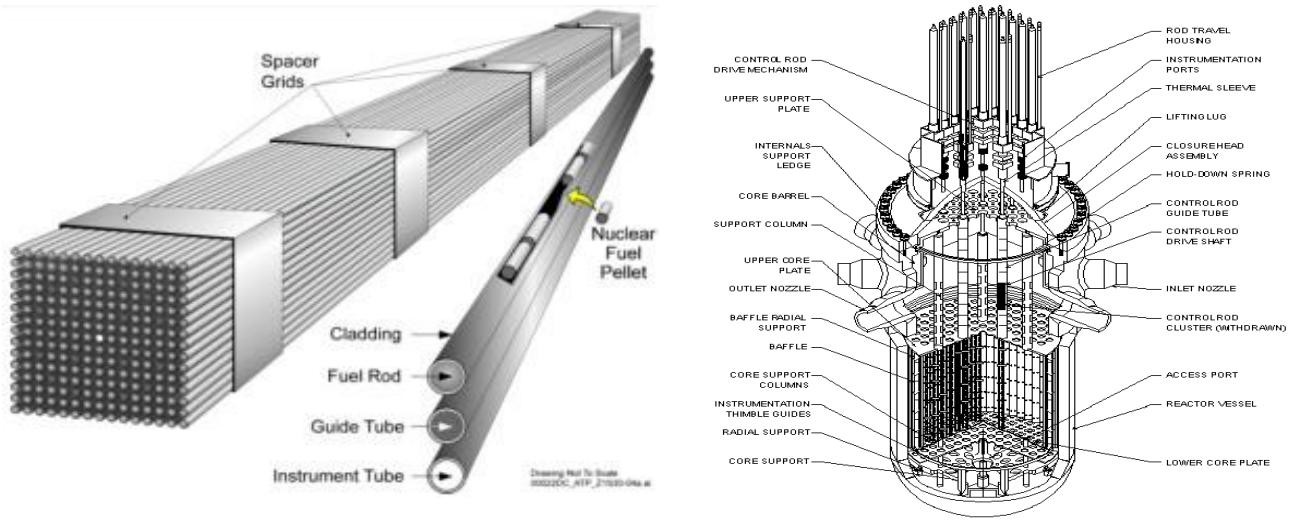

Figure 1: Nuclear Fuel Assembly-DOE Hanson [2], and a typical cut away view of PWR Vessel [3]

From the fission reaction in a PWR, many different fission fragments are formed which are contained within the fuel rods. A typical fission reaction is represented by the following equation [4]:

$$n + {}^{235}_{92}U \longrightarrow {}^{140}_{54}Xe + {}^{94}_{38}Sr + 2n + 200 \text{ MeV}$$

where n denotes a neutron and ${}^{235}_{92}U$ refers to the uranium-235 atom with which the neutron reacts. Further, ${}^{140}_{54}Xe$ and ${}^{94}_{38}Sr$ refers to the daughter elements xenon-140 and strontium-94 respectively.

From the fission reaction above, daughter elements such as xenon-140 and strontium-94 are produced and approximately 200 MeV is released per fission reaction, making nuclear energy potentially dangerous if the chain reaction in a typical PWR is not controlled. When operating Nuclear Power Plants (NPPs), safety is one of the most important considerations and there are many safety requirements that must be adhered to in the design of the PWR to secure safe operation [5]. Keeping the reactor core and SFP cool remains an important activity.

Fukushima Daiichi NPP Accident

On March 11, 2011, the Tohoku earthquake followed by a tsunami resulted in unprecedented damage to the Fukushima Daiichi Nuclear Power Plant (NPP) [6]. The damage caused to the facility by the earthquake was not the direct cause of the eventual accident. It was the effect of a large tsunami that followed which resulted in the loss of all safety functions to protect the fuel that led to the severe accident. Reactor units 1 to 3 were at power, and reactor units 4 to 6 in refuelling outage (unit 4 was completely unloaded) at the time. When the earthquake occurred, all the operating units were automatically shut down as per design requirement. When the Tsunami wave reached the plant, it flooded the emergency back-up diesel generators and the loss of all AC electrical power resulted in a station blackout.

It was the failure of the emergency diesel generators that resulted in the failure of the reactor Core Isolation pumps for units 1 to 3 to remove steam from the reactor core. The decay heat from the reactor cores in conjunction with the reactor coolant ensured the units` continued production of steam. In turn, this resulted in increased pressure in the Boiling Water Reactor (BWR) pressure vessel and reduced liquid levels in the reactor core. As a result, approximately 75% of the core was uncovered and cladding temperatures increased to above 1200 °C [7]. Zirconium (Zr) oxidation, which is a chemical reaction between the Zirconium fuel cladding and the cooling water, commenced. Note that Zirconium oxidation in steam can start at cladding temperatures as low as 650°C [8]. However the United States Nuclear Regulatory Commission (US NRC) regulatory guide 1.224 indicates that Zirconium-steam oxidation at cladding temperatures less or equal to 650°C is insignificant with regards to breakaway oxidation and hydrogen accumulation due the low

oxidation rate. Katliatka, *et al.*, 2013 [9] also indicated that intensive cladding oxidation starts above 1200°C which is the threshold for fast oxidation. The US NRC limit for licensing applications is 1204°C and it includes significant safety margins for Zr [10]. Sailor (1987) reported that Zirconium alloy has a melting point of 1900 °C [11]. The metallic Zirconium is oxidized by the protons of water to form hydrogen gas [12] as:

$$Zr + 2\,H_2O \longrightarrow ZrO_2 + 2\,H_2$$

where Zr denotes the Zirconium element and H_2O the water molecule with which it reacts. Further, ZrO_2 refers to the Zirconium oxide formed and H_2 denotes the hydrogen gas produced from the reaction.

Spent Fuel Pools

The lack of cooling capability of the spent fuel pools as a result of the failure of the Fuel Pool Cooling pumps (as depicted in Figure 2) was of further concern to the operators. Due to maintenance in Unit 4 at the time of the accident, the entire core was stored in the SFP. Based on the relatively higher decay heat in comparison with the other fuel pools, it was estimated that the SFP in Unit 4 would dry out in 10 days and for the other units, it would take a few weeks. On 15 March, 2011, an explosion and fire occurred in the SFP of unit 4 which led to hydrogen generation and fuel rod damage.

Figure 2 below, shows a schematic of the design and layout of the reactor and spent fuel buildings.

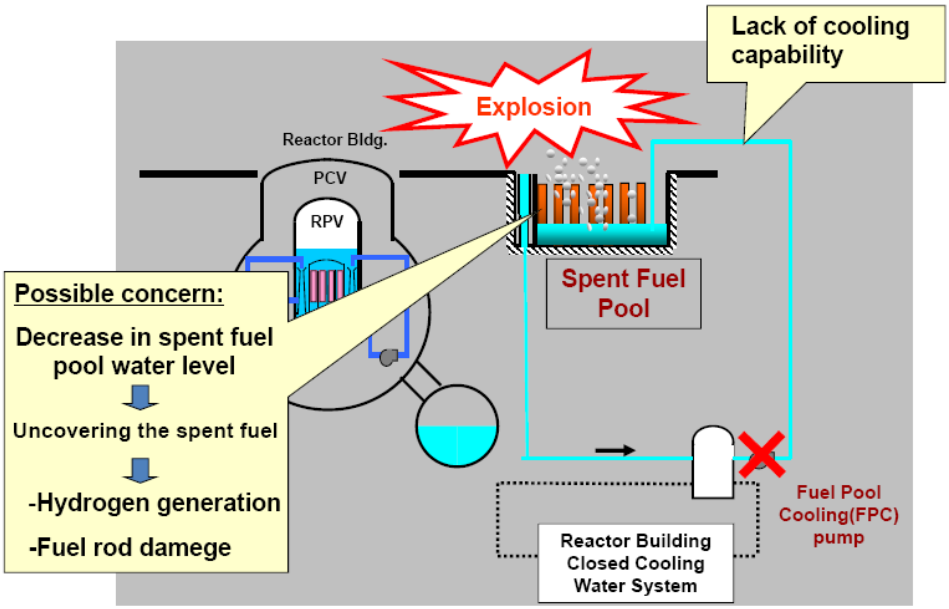

Figure 2: Schematic of the Spent Fuel Pool Cooling circuit of the Fukushima Daiichi BWR plant [13]

Based on the design of the power plant (as depicted in Figure 2) there was minimal retention of fission products. This led to a large release of fission products to the environment [7]. Although

the operators eventually restored active cooling to the SFPs, it was an important activity to keep the spent fuel pool filled with water at all times in order to reduce the scale of the disaster [14]. This accident reinforced that even additional sources of power such as Diesel generators cannot always adequately mitigate the loss of power in a generic spent fuel pool cooling system [15]. More so, loss of cooling capability to the reactor core or SFP can rapidly escalate into a disaster.

Above 900°C, air oxidation is more efficient than that of steam oxidation [16] which occurs as follows:

$$Zr + O_2 \longrightarrow \mathrm{Zr}O_2$$

where O_2 denotes an oxygen molecule with which Zirconium cladding reacts to form Zirconium oxide.

The consequences of overheating and melting of the fuel in these assemblies during the loss of cooling can be severe and is to be avoided [17].

Figure 3 below, shows a design and layout of a typical spent fuel pool (SFP).

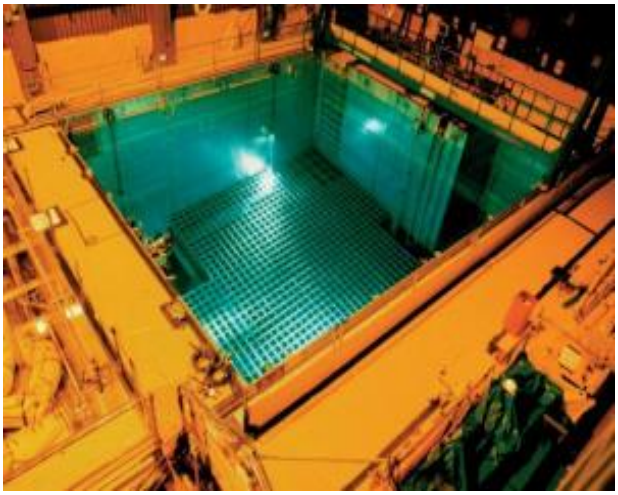

Figure 3: Typical Spent Fuel Pool -NRC Photo [2]

Spent Fuel and Decay Heat

The most common light water reactors today use natural or enriched uranium as nuclear fuel. The fuel is biologically safe before it has been irradiated in the reactor core [18]. Spent nuclear fuel, also called used nuclear fuel, is fuel that has been irradiated in a nuclear power reactor. It is no longer efficient in sustaining a nuclear reaction due to its relatively high level of fuel burnup [19]. Periodically, one-third of the nuclear fuel in an operating reactor is replaced with fresh fuel [20]. Typically these periods ranges from 12 to 24 months [21].

Fuel burnup (also known as fuel utilization) refers to the amount of energy extracted from the nuclear fuel source and it provides a measure of the uranium burned in the reactor. It is commonly

expressed in gigawatt-days per metric ton of uranium (GWd/MTU) and it depends on how long the fuel remains in the core and the power level reached. Burnup values have increased significantly over time, which results in effectively extracting more energy from fuel rods.

Spent fuel decay heat results in the fuel due to the beta decay of fission products into more stable elements. It is produced after a nuclear power reactor has been shut down and the fission chain reaction stopped. At the moment of a shutdown, about 7% of the core power remains due to decay heat, which continues to decrease over time.

Total fission product decay heat power at t seconds after shutdown can be calculated using the following equation [22]:

$$P_d(t,T) = \acute{P}_d(t,T) \text{ x } G(t) \tag{1.1.1}$$

where $\acute{P}_d(t,T)$ denotes the total fission product decay heat power (uncorrected for neutron capture in fission products). Further, $G(t)$ accounts for the captured neutrons by fission products, and is calculated as:

$$G\ (t) = 1.0 + (3.24 \text{ x } 10^{-6} + 5.23 \text{ x } 10^{-10} t) T^{0.4} \psi \tag{1.1.2}$$

where T denotes the total operating period and ψ refers to fissions per initial fissile atom.

The sum of the uncorrected decay heat power for the different fission products can be calculated from:

$$\acute{P}_d(t,T) = \sum_{i=1}^{4} \acute{P}_{di}\ (t,T) \tag{1.1.3}$$

where $\acute{P}_{di}(t,T)$ denotes the fission product decay heat power contribution to $\acute{P}_d(t,T)$ by ith fissionable nuclide (uncorrected for neutron capture in fission products) and t refers to the time after shutdown.

Fission products typically used are U-235, U-238, Pu-239 and Pu-241. The uncorrected decay heat power $\acute{P}_{di}(t,T)$ can be calculated from:

$$\acute{P}_{di}(t,T) = \sum_{\propto=1}^{N} \frac{P_{i\propto} F_i(t_\propto, T_\propto)}{Q_i} \tag{1.1.4}$$

where $P_{i\propto}$ denotes the total power of the reactor and $F_i(t_\propto, T_\propto)$ refers to the decay heat power at t seconds after shutdown while the reactor was operating for T seconds. Further, Q_i refers to the energy released per fission reaction (approximately 200MeV/fission).

$F_i(t_\propto, T_\propto)$ can be calculated by using the decay heat values given in tables of the American Nuclear Society Report [23] as:

$$F_i(t_\propto, T_\propto) = F_i(t_\propto, \infty) - F_i(t_\propto + T_\propto, \infty) \quad (1.1.5)$$

where $F(t, \infty) = F(t, 10^{13})$

Typically the entire core is discharged to the SFP during a re-fuelling outage subsequent to the core having been subcritical for more than 10 days (refer to Appendix A, for a typical core discharge decay heat load distribution after 10 days as well as average uranium mass per SFA). At this time the decay heat has sufficiently decreased to below 1% of the initial core power. Consequently, the longer the spent fuel has been subcritical, the lower the decay heat load from the fuel [24]. To maintain cooling of the spent fuel assemblies (SFAs) in water filled SFPs, heat exchangers are used to remove the decay heat [19]. As discussed in earlier sections (with reference to the SFPs of the Fukushima Daiichi NPS accident), failure of SFP cooling can lead to fuel assembly (FA) cladding reaching excessive temperatures over a very short period of time due to the spent fuel decay heat.

Spent Fuel Pool and Criticality Prevention

SFPs are typically made of reinforced concrete several centimetres thick, with steel inside liners providing a watertight environment. The water medium serves both as biological shielding for personnel and to cool the assemblies [20]. SFPs are typically rectangular in cross-section and approximately 12 m deep (Figure 3).

About 6.1 m of water is needed to provide sufficient radiation shielding and the additional depth provides sufficient safety margin for re-arrangement of SFAs in the SFP without the need for additional shielding to protect workers (Figure 4).

Figure 4 below, shows a SFA transferred into a SFP at a nuclear power plant.

Figure 4: Spent Fuel Assembly Transferred into a Spent Fuel Pool at a Nuclear Power Plant [25]

As pointed out above, decay heat is continuously removed from the SFA by circulating the water through heat exchangers and back to the SFP. The SFP water temperature is normally maintained below 60°C under normal operating conditions. The water quality is also strictly controlled to prevent the fuel or its cladding from degrading [21]. The spent fuel cooling system is typically designed to remove residual heat loads ranging between 1 to 11 MW to cater for normal operation as well as refuelling outages.

SFPs were originally designed to serve as a short-term fuel storage arrangement prior to SFAs being shipped away for intermediate storage or reprocessing. In some countries, no plans exist for the shipping of spent fuel and hence it has been accumulated in the SFPs for many years [18]. SFPs house storage racks, also referred to as storage cells, in which the SFAs are vertically placed. These racks were designed to provide adequate spacing to prevent criticality and to promote natural convection in the water medium [16]. The rack walls also incorporate boron-10 or other neutron-absorbing material to ensure the spent fuel remains sub-critical [21]. The development of high-density spent fuel storage racks to expand the SFP inventory capacity has also occurred. This has allowed SFAs to be stored closer to each other without violating the criticality or temperature limits for the system [26].

Except for the differences in the detailed designs of spent fuel racks and capacity, the configuration of most SFPs is similar for most NPPs [8]. Maintaining structural integrity of the assemblies after a seismic event is a standard design requirement [20]. The SFP and its supporting systems are located within structures that also protect it against natural phenomena (seismic events and tsunamis) and flying debris. For many of the operating NPPs around the world, SFPs are near full capacity. Hence, these utilities have moved some of the older spent fuel into dry storage casks. The spent fuel is typically cooled for at least 5 years in the pool before being transferred to a “dry cask” [20]. The storage of spent fuel in “dry casks” will not be dealt with in this dissertation.

Spent Fuel Cooling via Air

Although there is a very low likelihood of a complete loss of SFP water under normal design basis accident frequencies (about 10^{-6} per pool per year [17]), the consequences of such a severe accident are unacceptable [27]. The study of the heat transfer of SFAs as conducted in this dissertation is therefore important for the development of strategies to mitigate the consequences of this severe accident.

Figure 5 below, shows a simplified cross section of the front view of a typical SFP and Fuel Building (FB) during the loss of inventory.

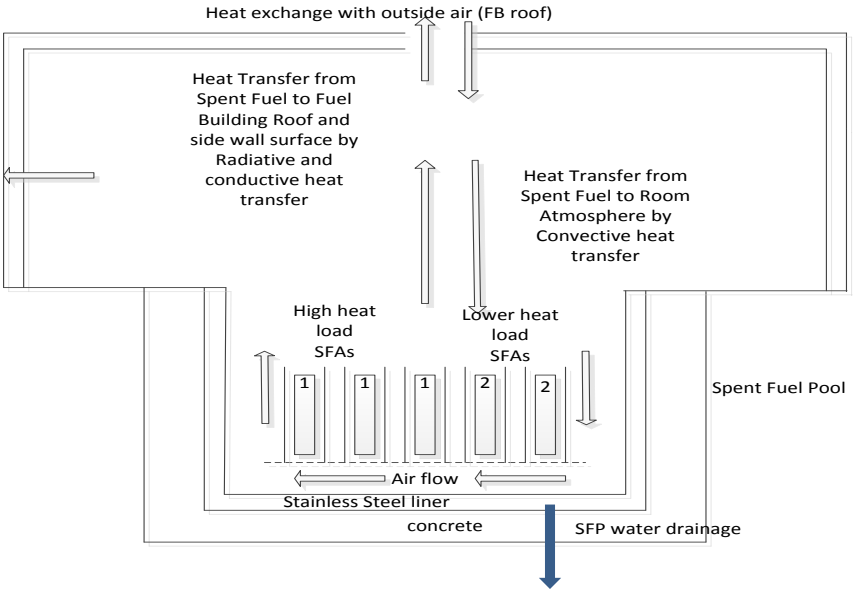

Figure 5: Heat flow path during loss of inventory in a spent fuel pool

Depending on the decay heat of the SFAs at the time of complete loss of inventory, initial cooling will be through steam production from the wetted surfaces of the SFAs as well as the SFP inner wall. Natural convection will be established due to temperature differences between the FB structure and the high and low decay heat SFAs. Air will enter the SFA racks at the bottom, moving upwards through the fuel rod channel walls. As the air travels upwards through the fuel rod channel wall, it increases in temperature. It is further postulated [16] that during a complete loss of SFP inventory, the temperature of the fuel elements will increase. The increase in temperature is of considerable concern as the Zirconium-air oxidation reaction becomes self-sustaining between 700°C - 1200°C [17]. Note that the potential of reaching elevated temperatures depends largely on the decay heat load of the SFAs in the pool [16]. Therefore, the higher the decay heat load (typically during a core discharge to the SFP after a refuelling outage) the higher the likelihood of reaching these elevated temperatures.

The focus of this research is to assess the cladding temperatures of uncovered SFAs in a typical PWR spent fuel pool (with varying heat loads, including the worst case accident scenario). This will be done for loss-of-inventory conditions wherein the SFAs are cooled solely via natural air convection. An outcome of this research includes the determination of the time period at which severe cladding oxidation will commence for an unloaded core. Predicted cladding temperatures will also assist future research into investigating optimum cooling solutions under such conditions. The specific loss of inventory scenario that will be considered in this work is outlined next.

Severe Accident Scenario Description

Under normal operation, the spent fuel heat load in the SFPs of typical PWRs is under 1 MW. This heat load is however much increased during a refuelling outage where the entire reactor core is discharged to a SFP. For this scenario, the complete core has been discharged to the SFP with each assembly having an average heat load of 34 kW (refer to Appendix A for a typical core discharge decay heat load distribution and average uranium mass per SFA). For the accident scenario, all assemblies were considered to have the same average mass. As a result, a total heat load of 5.44MW (160 fuel assemblies) to be cooled by the spent fuel cooling system. This translates into 75 kW/TU in Zone 1 (the zone containing the unloaded core as per Figure 5 and described next).

To depict a possible "worst case scenario", SFAs are loaded into zones in the SFP as per Figure 6, below. The figure depicts a simplified front view cross section indicating the zone arrangement in the SFP.

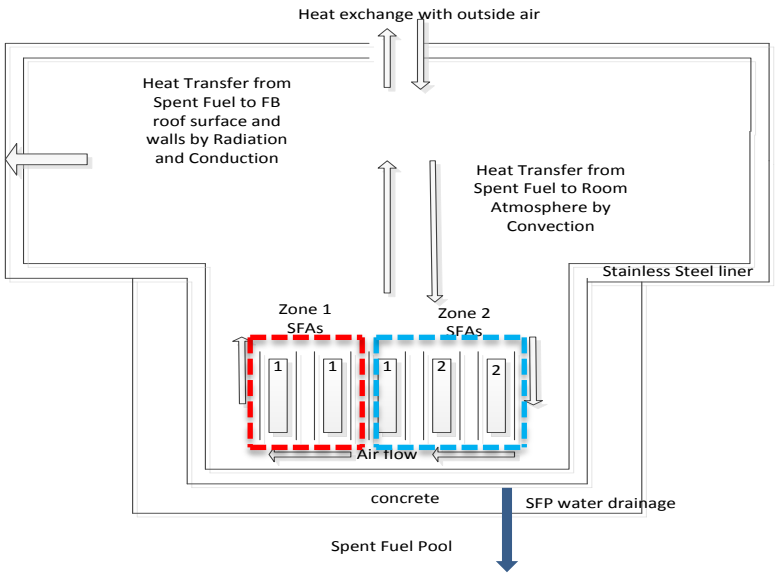

Figure 6: Front view cross section indicating the zone arrangement in the SFP

The fully unloaded core is in Zone 1 while the older SFAs are located in Zone 2. With the unloaded core in the SFP, a severe accident (e.g. earthquake) results in a large break in the SFP floor. The pool inventory drains instantaneously. Unable to maintain SFP inventory level, the result is an instant uncover of the SFAs. For this scenario, Zone 2 will consist of 710 assemblies (the fuel already stored in the SFP with a constant residual heat of 1.5 kW per SFA). The total heat load in Zone 2 is therefore 1.065 MW. This translates into 3.25 kW/MTU in Zone 2, assuming an average uranium mass of 0.462 tons per fuel assembly (Appendix A).

Table 1; below indicate the parameters of the SFAs in the SFP.

Zones of SFAs	**Amount of SFAs in zone**	**Assumed storage time in SFP**	**SFAs decay heat, kW**	**Zone power, MW**	**Zone power density, kW/TU**
Zone 1	160	10 days	34	5.44	75
Zone 2	710	>1 year	1.5	1.065	3.25

Table 1: Parameters of SFA in SFP

Due to the impracticality of conducting an in-situ experiment as depicted in Figure 6, mathematical modelling is required.

A literature review into the thermal hydraulics and associated heat transfer processes of various thermal hydraulic computer-based modelling codes used in similar applications have been conducted. Following is a brief summary of the work done to date in this regard.

1.3 Literature Review (Modelling Codes)

For the purpose of the discussion below, only literature that was directly applicable to the focus of the mini-dissertation was considered. Various computational fluid dynamics (CFD) codes (from one to three dimensional) have been developed to thermodynamically assess the SFP thermal response to a loss of inventory. This has allowed quantifying the heat transfer processes involved and predicting the cladding temperatures resulting from SFAs uncovered in air and is discussed next. Note that one-dimensional (1-D) refers to pipe-network or systems CFD codes.

SFUEL Code

Benjamin *et al.*, 1979 [16] used the SFUEL code which is a systems CFD code to investigate the effect of spent fuel assembly rack configuration on heat transfer in a drained pool and the effect of ventilation rate and base plate hole size on peak cladding temperatures. A limitation of the code was the source of uncertainty in the heat-up predictions due to the natural circulation flows. Sailor *et al.* [11] also suggested uncertainties in the SFUEL calculations due to uncertainties in the zirconium oxidation rates. The research by Benjamin et al., 1979 does not address the question of Zircaloy oxidation propagation after clad melting and relocation.

Conclusions from the results of the code indicated that decay heat of fuel significantly affects the heat-up calculations. Base plate hole size significantly affects heat-up calculations, the bigger the hole size, the lower the peak cladding temperature. Although the code focussed on modelling the effect on building ventilation rates and base plate hole sizes on spent fuel heat-up, the code indicated that decay heat of fuel significantly affect the heat-up calculations. The latter effect will be taken into account when the accident scenario is developed using a thermal hydraulic code.

SFUEL1W Code

Sailor *et al.*, 1987 [11] produced a modified version of the SFUEL code. Their key investigation areas were to determine the conditions which could lead to Zirconium cladding failure as a result of cladding rupture, propagation of a cladding fire to older stored fuel assemblies and releases and consequences for various cladding failure scenarios. A limitation of the code was that it did not explicitly analyse the melting of the zirconium cladding and that the largest source of uncertainty was the natural convective flowrate. Note that accounting for cladding melting also does not form part of this work.

Conclusions from the results of the code indicated that spent fuel heat-up also depends largely on the decay heat. If the decay heat level is sufficient to heat the rods to 900°C, zirconium oxidation becomes self-sustaining. This result will be taken into account in this dissertation. Calculations also indicated that, for plants using a high-density storage rack configuration, a factor of five reduction

in zirconium fire probability (given loss of pool inventory) can be achieved by improved air forced circulation capability. The likelihood of a zirconium clad fire initiation depends largely on the decay heat level and the storage rack configuration. High-density storage racks restrict natural convective flows hence the potential for self-sustaining oxidation still exists even after a year of spent fuel cooling. The temperature to achieve self-sustaining cladding oxidation was found to be greater than 850°C for heat load and storage configuration.

FLUENT version 5 Code

Boyd C.F, 2000 [24]] used the FLUENT (version 5) 3-D CFD code to predict fuel heat up and natural circulation flow paths throughout the SFP and the upper containment building during a complete loss of inventory. The predictions were on 3-D natural circulation flow fields in and around the pool, the racks, and the containment building. Limitations of the code were that physical models for radiation and clad chemistry were not incorporated. The CFD predictions were, therefore, more applicable at low temperatures (below 600°C).

Conclusions from the results indicated that the computed CFD predictions gave valuable insights into the three-dimensional natural circulation air flows. Peak cladding temperatures were significantly affected by the ventilation rate. Although the results indicated that physical models for clad chemistry and radiative heat transfer were not found to be applicable at low cladding temperatures, these are important to take into account when an accident scenario is modelled. These were as a result given due consideration in this dissertation.

SHARP Code

Nourbakhsh *et al.*, 2002 [8] used the SHARP code (Spent-Fuel Heat up: Analytical Response Program) to investigate the heat-up of the spent fuel elements by using the transient conduction equation in the axial direction. SHARP is essentially a pipe-network CFD code. Two cases were considered for heat removal from the building. In the 1st case, ventilation was provided to keep the room air at ambient conditions and in the 2nd case, no chimney effect or forced ventilation existed. Similar to the FLUENT CFD code used by Boyed C.F, 2000 [24], the SHARP code also considered radiation heat transfer of low importance due to the relatively low fuel rod temperatures (<650°C).

Conclusions from the results of the study indicated that spent fuel heat up is strongly affected by total decay heat production in the pool, availability of open spaces for forced convection air flows, and the building ventilation rate. Results from the code indicated that the extent of heat removal from the spent fuel building atmosphere significantly affects the spent fuel heat-up characteristics. Base plate hole sizes were also found to have a significant effect on the heat up of spent fuel. The zirconium cladding failure could occur at temperatures as low as 650°C if thermal loading is

sustained for extended hours. This will be taken into account when the accident scenario is developed using a thermal hydraulic code.

MELCOR Code

J. Cardoni, 2010 [28] used the MELCOR (version 1. 8.6) code to investigate the behaviour of pressurized water reactor (PWR) fuel assemblies under loss of inventory conditions. This model, which is a 2-D CDF code, was developed to accurately represent an experimental assembly, material and masses. Uranium oxide fuel was simulated by Magnesium oxide. The decay power was simulated using a uniform fission product decay power distribution. Limitations of the model were that the SFP fuel assembly and the rack have unique features not found in an actual spent fuel and that MELCOR had no input options for nichrome or steel mass in the fuel or cladding regions of the fuel rod model. Another limitation of the model was that MgO filler was packed into the Zircaloy cladding; therefore, no fuel-cladding gap was modelled in the experiment.

Conclusions from the results of the code indicated that based on a 5W heater adding heat over an 8hr period, 2.2 W was transferred by convective heat vs 0.2 W from oxidation heat vs 0.75W heat transferred to walls. Although the simulation focussed on an experiment with low heat input, the results indicated that convective heat transfer is dominant at low heat input and that heat transfer to the walls plays also a significant role during a loss of inventory conditions at low decay heat input.

ATHLET-CD Code

Katliatka, *et al.*, 2013 [9] used the ATHLET-CD code which is a 2-D CFD code to execute an analysis of the possible consequences of fuel overheating as a result of pool drainage as well as the evaluation of accident mitigation measures the late injection of water.

Conclusions from the results of the code indicated that the developed models allowed the modelling of various phenomena: uncovering and heat up of fuel rods; steam-zirconium reaction; and quenching of hot fuel rods by water. While benchmarking of the ATHLET-CD calculation results with calculations performed by RELAP/SCDAPSIM (3-D CFD) and ASTEC (2-D CFD) showed good agreement of the calculated fuel temperatures, some disagreement of hydrogen mass generation existed. Although the code focussed on the effect of steam-zirconium oxidation reaction and accident mitigation measures it indicated that this effect should not be ignored at elevated cladding temperatures. In this dissertation, the effect of cladding oxidation chemistry will not be taken into account but will be appropriately referenced during the discussion of the results.

A summary of the predicted peak cladding temperatures for various heat loads, days after reactor shutdown and ventilation modes for the respectively discussed modelling codes are presented in Table 2. Also listed is the spatial dimension used to describe the SFP where 1-D refers to a systems or pipe network type of approach.

Author, Code (1-D,2-D/3-D)	**Natural / Forced Convection**	**Fuel Load/Fuel Assembly**	**Days after Reactor Shutdown**	**Peak Cladding Temperatures**	**Self-Sustaining Clad Oxidation**
SFUEL (1-D) [Benjamin *et al.*, 1979 [16]]	Forced convection	86.56 kW/MTU	10	700°C (Ventilation rate of 72.6 cm/s)	850 - 950°C
SFUEL1W (1-D) Modified version of SFUEL [Sailor *et al.*, 1987 [11]	Forced convection	90kW/MTU	10	Natural convection flowrates were a large source of uncertainty	>850°C.
FLUENT (version 5)(3-D) [Boyd C.F, 2000 [24]]	Forced convection	0.92kW/MTU	720	540 °C	
SHARP (1-D) [Nourbakhsh *et al.*, 2002 [8]]	Forced convection	9kW/MTU	420 420	446°C (High ventilation rate of 18.87 m^3/s) 583°C (with low ventilation rates 5.66 m^3/s)	650°C if thermal loading is sustained for extended hours.
MELCOR (2-D) [C. Cardoni 2010] [28]	Natural convection	5kW (experiment)	0.3	527°C	
ATHLET-CD (2-D)	Natural convection	55kW/MTU 1.6kW/MTU	8 1344	Maximal 1900°C, 100000 s after fuel uncover, before water injection 540 °C	Slow oxidation started at 700°C Intensive cladding oxidation starts above 1200°C (fast oxidation threshold)
ASTEC (2-D)		55kW/MTU	8	Maximal 2100°C, 100000 s after fuel uncover, before water injection	
RELAP/SCDAPSIM –(3-D) Katliatka, *et al.*, 2013 [9]		55kW/MTU	8	Maximal 2200°C, 100000 s after fuel uncover, before water injection	

Table 2: Summary of Peak Cladding and Clad Oxidation Temperatures from Various Modelling Codes in Literature

The listed variation in predicted peak cladding temperatures from the literature is attributed to various factors. As would be expected, forced convection has a significant effect during a loss of inventory. In addition, factors that have shown to have a significant effect on peak cladding temperatures are the storage rack configuration and decay heat of the SFAs. The cited literature also indicated that for natural convection conditions, the peak cladding temperatures from 1-D modelling is comparable and similar to 2 and 3-D modelling codes. This included similar predicted peak cladding temperatures under accident scenario conditions. This is important for this work, as the 1-D codes are considerably less costly to develop and use as compared to 2-D and 3-D versions. Therefore, in order to develop a first order assessment of the heat transfer of the

uncovered SFAs under varying heat load scenarios and natural convection conditions in a typical SFP, a 1-D network modelling approach, will be used in this work. The Flownex software was used for this purpose.

1.4 Project Objectives

The project objectives were the following:

- To construct a Flownex network model of two composite Spent Fuel Assemblies (SFAs) representing the SFAs' high and low heat load in a typical SFP.
- To compare the model via application to geometries and heat loads of Boyd C.F, 2000 [24] who employed 3-D model (FLUENT version 5 code). The models will be compared in terms of predicted cladding temperatures.
- To describe quantitatively the overall thermal response under steady state and transient conditions when these composite SFAs becomes uncovered in air.
- To assess the thermal response of the model under severe accident scenario conditions.
- To determine the time period at which severe cladding oxidation will start under the severe accident transient simulation.

1.5 Limitations of the Research

The governing equations used to derive the heat transfer model are only one dimensional. The derived model is not applicable beyond zirconium cladding oxidation temperatures and does not take into account the energy effect of zirconium cladding oxidation chemistry.

1.6 Outline of Dissertation

Chapter 1: Background to the Problem

This chapter provided background to the problem and important issues associated when spent fuel becomes uncovered by reviewing the most important aspects of the Fukushima Daiichi Nuclear Power Plant accident. It provides a short literature review on nuclear fuel and spent nuclear fuel and past models that were used to assess the cladding temperatures of spent fuel during a complete loss of inventory. The main project objectives and research limitations are also discussed.

Chapter 2: Spent Fuel Model Geometry and Heat Modes

In this chapter, the Simplified Representative Geometric Model (SRGM) of the Fuel Building (FB) and Spent Fuel Pool (SFP) is described. The FB, SFP, storage rack, fuel assembly and fuel rod characteristics and dimensions are listed and the main assumptions in the model are discussed. All the heat transfer modes accounted for in the Flownex network model are described.

Chapter 3: Thermal Hydraulic Theory

The governing equations and the thermal hydraulic theory applied in the Flownex network model are presented and described. The methodology of scaling up the SFAs to represent composite SFAs of Zones 1 and 2 respectively are discussed. The governing equations of heat transfer in the SFP and heat removal to the FB are detailed.

Chapter 4: The Flownex Network Model

The constructed Flownex network model is discussed in detail in this chapter. The Flownex network model is also compared by applying the geometries and heat loads from the Fluent (version 5) code used by Boyd C.F, 2000 [24]. An assessment of the Flownex network model was done using the accident scenario conditions. Reasons for the inability of solving the Flownex network model using the severe accident scenario conditions are discussed.

Chapter 5: The Modified 2-D Flownex Network Model of the SFP

In this chapter, the development of an improved 2-D network model uses conduction elements to simulate higher heat load and temperature scenarios by accounting for radiative heat transfer within the SFAs. An effective conduction for the fuel volume which is dependent on temperature was determined and used to assess the severe accident scenario (beyond design basis) in the SFP therefore discretizing the entire SFP into smaller fuel zones.

Chapter 6: Assessment of the Modified 2-D Flownex Network Model of the SFP

The accident scenario condition was applied to the modified 2-D Flownex network model to obtain average cladding/Fuel zone temperatures at the all the discretized Fuel zones and to assess the network model under transient conditions. The transient analyses for the severe accident scenario and results are discussed.

Chapter 7: Overall Conclusions and Recommendations

This chapter concludes the study and final results including recommendations for future research are presented.

In the next chapter, detailed dimensional characteristics of the Fuel Building (FB), Spent Fuel Pool (SFP), Spent Fuel Assemblies (SFAs) and the spent fuel storage racks will be discussed . This information will be used to construct the Flownex network model. The heat modes that will be taken into account in the Flownex network model will also be discussed in more detail.

2. Spent Fuel Model Geometry and Heat Modes

In order to facilitate an understanding of the construction of the Flownex network model for heat transfer assessment, the geometrical detail of the FB, the SFP and the SFAs are provided in this section. The heat modes considered in the network model during a loss of inventory will be discussed in later sections of this chapter.

2.1 Simplified Representative Geometric Model description (SRGM)

Figure 7, below shows the dimensions of the FB and SFP that are used in the SFP network model.

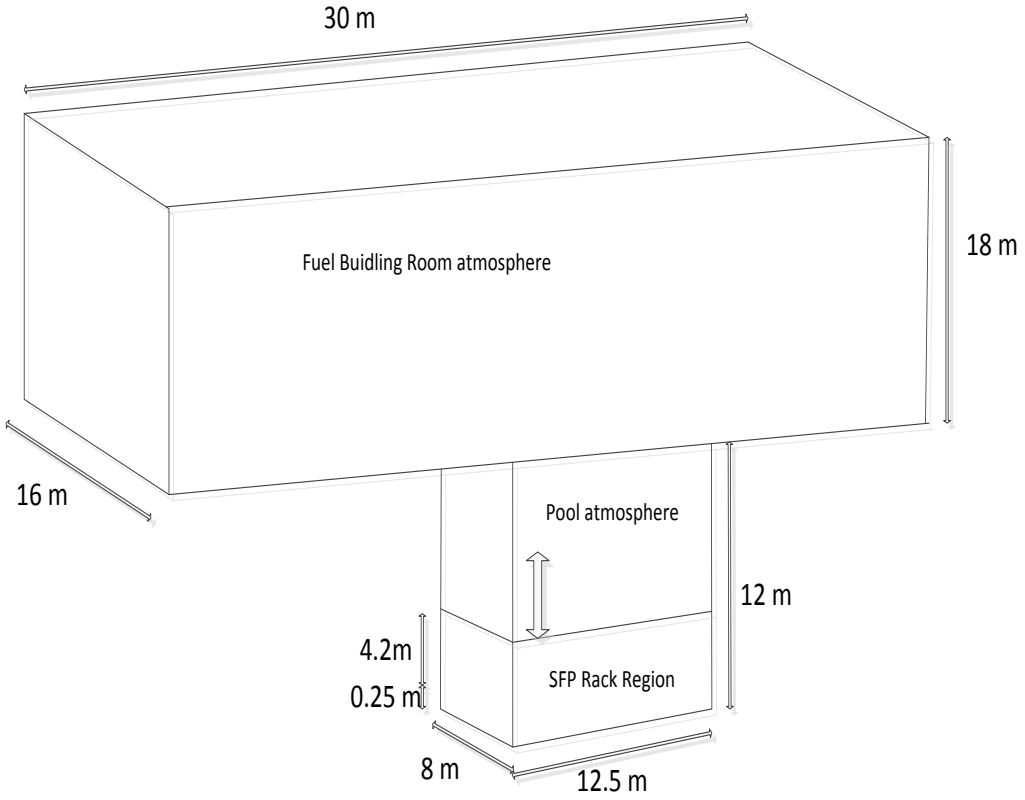

Figure 7: Simplified Representative Geometric Model of the SFP and FB

The SFP view area to the FB roof surface areas are circa 100m^2 and 480 m^2 respectively, similarly the SFP view area to the FB wall surface areas are circa 100m^2 and 414 m^2 respectively, assuming only 25% of the FB wall is visible. The thickness of the FB roof is assumed to be 250 mm [16] with a thermal conductivity of 1.4 W/m.K [8]. The FB walls are assumed to be 800 mm thick. Both roof and walls are made of reinforced concrete. The concrete floor and walls of the SFP are also made

of reinforce concrete (assumed to be 1.5 m thick). The inside stainless steel SFP liner is typically 6.4 mm thick for most PWR spent fuel pools [16].

Figure 8 below shows the top view of the SFP, with Zone 1 at the left bottom corner.

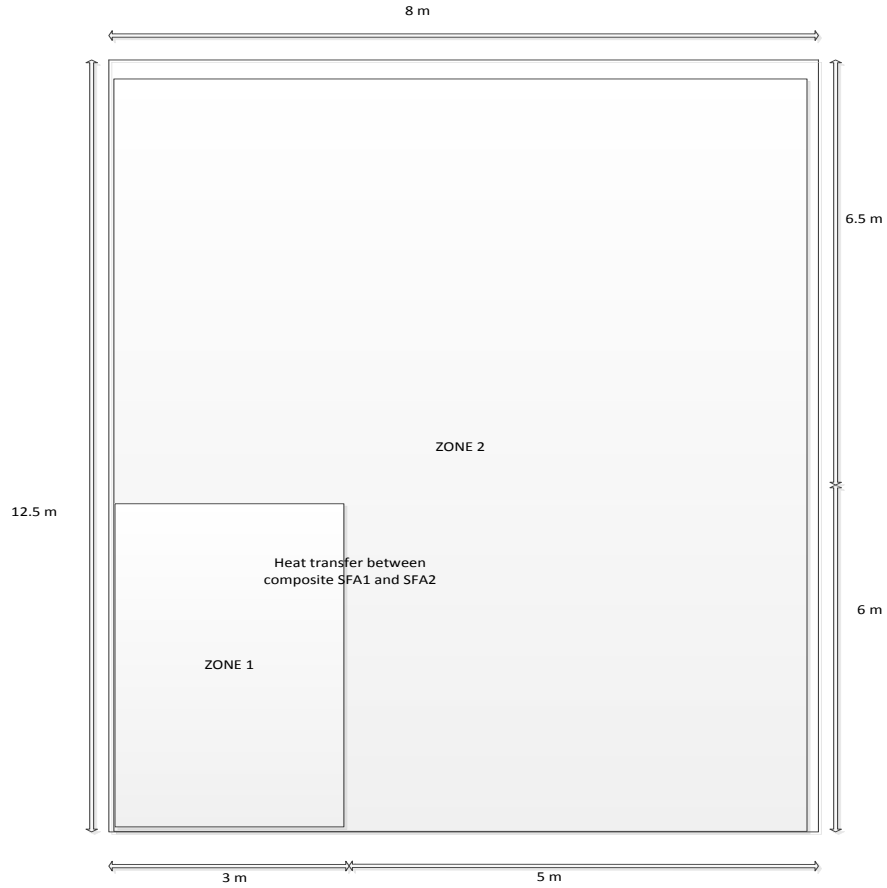

Figure 8: Top view of loading of the SFP and composite SFAs under consideration

From figure 8, the overall dimensions are 8.0m in width, 12.5m in length and 12.0 m in height. Zone 1 consists of 160 SFAs and Zone 2 consists of 710 SFAs respectively (Figure 8 also depicts the zone dimensions). The racks are constructed of austenitic stainless steel with borated stainless as neutron absorbing material (see Figure 9 below).

Figure 9 shows the overall physical dimensions of the storage rack cells used for the SFP network model. The active fuel length used in the SFP network model is 3.69m.

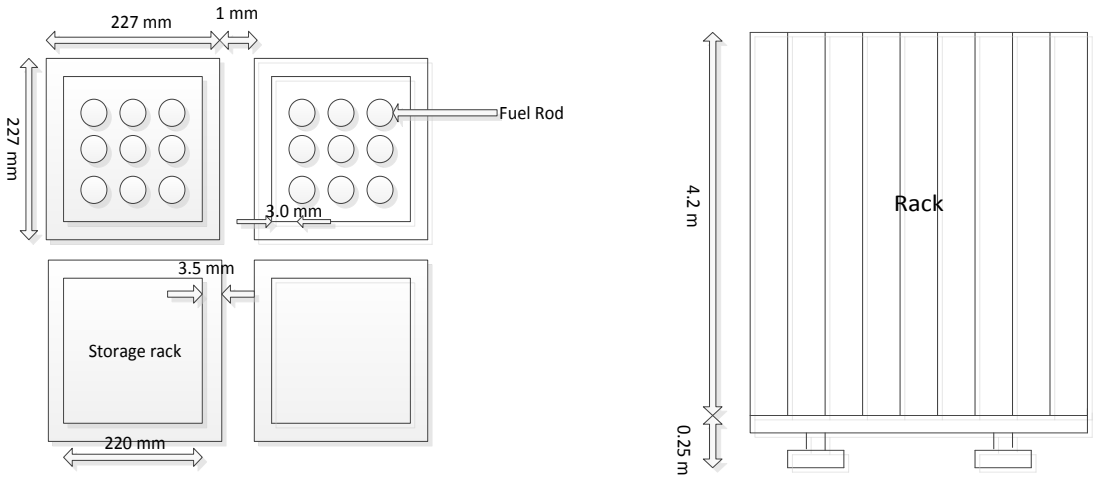

Figure 9: Top and front view of typical PWR spent fuel pool storage rack cells with dimensions

Figure 10 shows the cross section of a Fuel Assembly (FA) pitch and dimensions of a single Fuel Rod (FR).

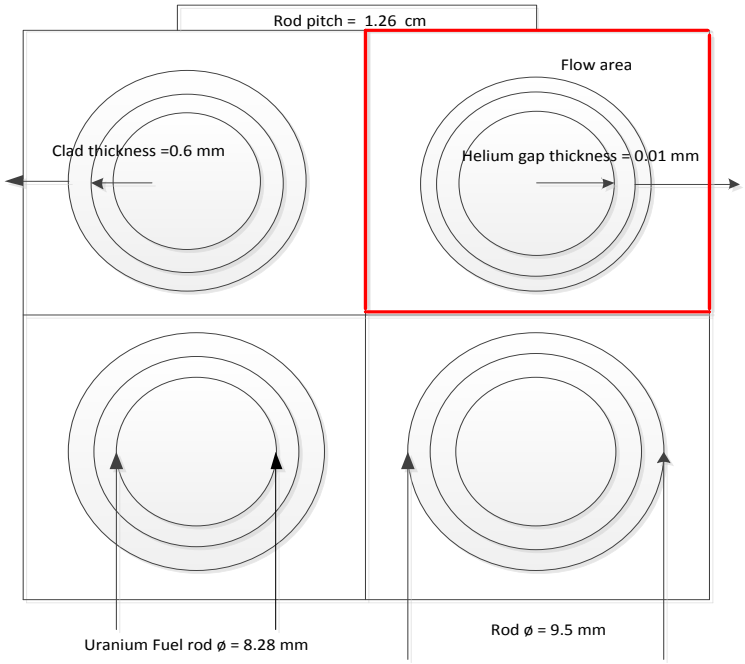

Figure 10: Cross section of a Fuel Rod Assembly pitch and dimensions

The fuel dimensions characteristics [8] are summarised in Table 3. These are used as inputs to the Flownex network model.

Typical Fuel Dimensions	
Outside diameter	9.5mm
Clad thickness	0.6mm
Cladding material	Zirconium
Radial gap	0.01 mm
Pellet diameter	8.28 mm
Rod pitch	12.6 mm
Number of active rods per fuel assembly	264

Table 3: Typical Pressurised Water Reactor SFA dimensions

2.2 Heat Modes

To simulate the severe accident scenario discussed in section 1.1, the various heat modes that are considered when constructing the Flownex network model is discussed next.

Air above the SFAs is modelled as a well-mixed adiabatic control volume. Heat is transferred to the heat sink represented by the FB. Convective heat flow includes the heat transfer path through the channel walls of the composite SFAs and from the SFP room atmosphere to the FB room atmosphere. The conductive and radiative heat transfer flow path is from the spent fuel to the FB roof surface and side walls.

Figure 11 shows a cross-sectional front view of the SFP and FB, assuming that the spent fuel sees the inside surface of the FB roof and a quarter of the FB side wall inside surface. Further, it is also assumed that the SFP has a view factor of 1.

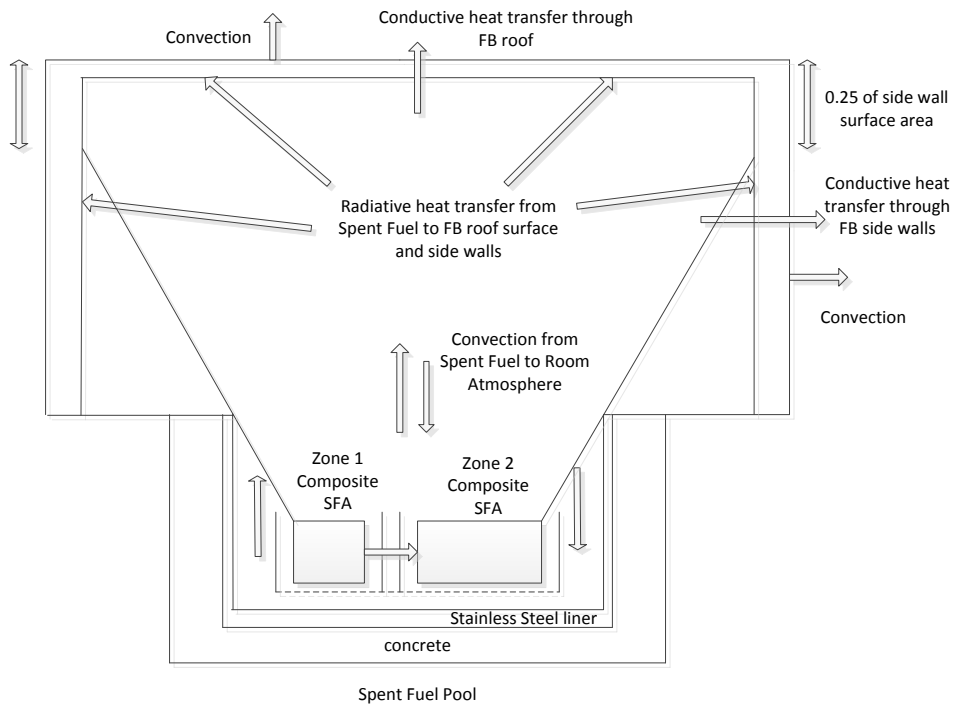

Figure 11: Heat modes considered in Flownex network model

From Figure 11, there is natural convective heat transfer through the composite SFA channel walls between the two composite SFAs, conductive heat transfer along the SFAs and through the inner and outer rack wall as well as through the FB roof and side wall. There is convective heat transfer from the SFP air to the FB air atmosphere. The radiative heat transfer flow path is from the cladding of the composite SFAs to the FB roof and side walls.

Figure 12 shows a front view of the composite SFAs representing Zone 1 (discharged core) and Zone 2 (older SFAs) in the SFP rack region.

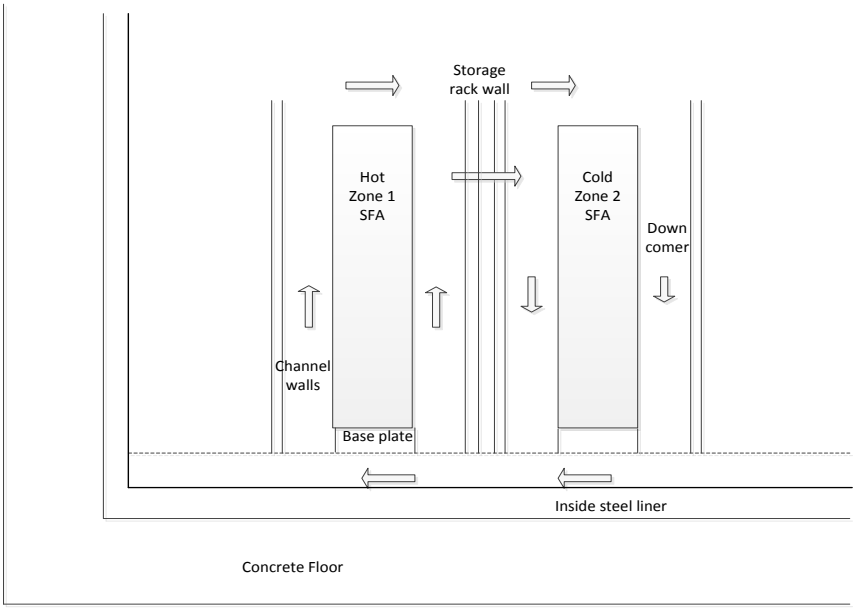

Figure 12: Front view of two composite SFAs representing Zone 1 and Zone 2 respectively, under induced natural convection conditions

From Figure 12 above, the induced natural convective air flow will be through the down-comer next to the edge of the pool, entering the fuel assemblies through the base plate. It will then flow upwards through the channel walls between the fuel rods and inside walls of the storage racks.

Figure 13 depicts the various heat transfer modes between two adjacent composite SFAs with Zone 1 having a higher heat load then Zone 2.

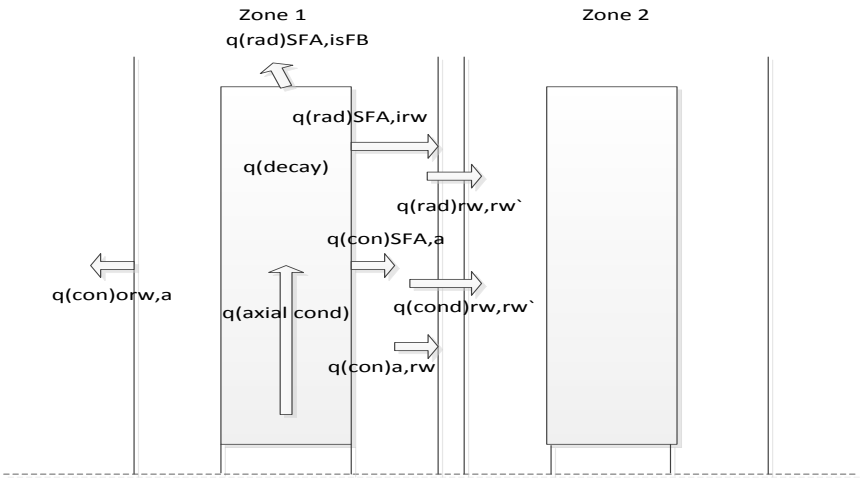

Figure 13: Heat transfer modes around a composite SFA representing Zone 1

The nomenclature in Figure 13 denotes:

$q_{(decay)}$ = Decay heat from SFA

$q_{(axial\ cond)}$ = Heat axially conducted along the vertical axis of SFA

$q_{(con)\ SFA,\ a}$ = Heat convected from the SFA to the air stream

$q_{(con)\ a,\ irw}$ = Heat convected from the air stream to the inside rack wall

$q_{(rad)\ SFA,\ isFB}$ = Heat radiated from the SFA to the inside surface of the Fuel Building

$q_{(rad)\ SFA,\ irw}$ = Heat radiated from the SFA to the inside rack wall

$q_{(con)\ orw,\ a}$ = Heat convected from the outside rack wall to the air stream

$q_{(rad)\ rw,\ rw`}$ = Heat radiated from the rack wall to the adjacent rack wall

$q_{(cond)\ rw,\ rw`}$ = Heat conducted from the rack wall to the adjacent rack wall

2.3 Main Simplifying Assumptions for Flownex Network Model

A number of simplifying assumptions are made in modelling the overall heat transfer of the SFP under consideration. These follow:

- Pool drains instantaneously with an inability to maintain level.
- The geometry of the fuel assemblies and the storage racks remains intact.
- The decay heat is produced only by the fuel rods and is distributed from the fuel rod centreline to the cladding surface.
- Air flow patterns depicted in the geometric model are locally and 1-dimensional.
- Only conduction for the fuel rods in the vertical direction is considered.
- Air spaces between the SFA holders are closed to air flow.
- No air gap exists between the spent fuel pellets in the SFAs and cladding.
- Physical models for clad chemistry are not considered.
- All spent fuel rods (SFRs) in the composite SFA of the respective zones have the same vertical temperature distribution. This is reasonable as all the SFAs of the respective zones are assumed to have the same average decay heat.

- Heat conducted between SFAs of the same decay heat load can be neglected.
- Radiative heat transfer from the composite SFAs to the SFP floor is not considered.

All the assumptions listed above were taken into account during the development of the Flownex network model. The governing equations to predict the cladding temperatures in the severe accident scenario using the Flownex network model will be discussed in the next chapter.

3. Thermal-Hydraulic Theory

This chapter explains the governing equations used to model the physics of heat transfer from the SFAs in the SFP. It commences with the basic conservation laws and concludes with the heat transfer modes considered. All the conservation equations were solved using the Flownex code.

3.1 Conservation laws

Section 2.3 detailed the primary assumptions with regards to the heat transfer modes accounted for in the SFP and FB. The governing equations is presented and described below. This conservation of mass, momentum and energy equations are solved using the Flownex code.

Conservation of Mass

The law of the conservation of mass is defined as the rate of change of mass through a control volume. Equation (3.1.1) provides this in its simplified form [29].

$$\frac{dm_{cv}}{dt} + \dot{m}_e - \dot{m}_i = 0 \tag{3.1.1}$$

where $\frac{dm_{cv}}{dt}$ denotes the time rate of change of mass within the control volume boundaries. Further, $\dot{m}_i$ and $\dot{m}_e$ refer to the total rates of mass flow into and out of the control volume.

Conservation of Momentum

Equation (3.1.2) provides the conservation of momentum law [5].

For incompressible flow,

$$\rho L \frac{\partial v}{\partial t} + (P_{oe} - P_{oi}) + \rho g\,(z_{outlet} - z_{inlet}) + \Delta P_{o,losses} = 0 \tag{3.1.2}$$

where $\rho L \frac{\partial v}{\partial t}$ denotes the rate of change of momentum over time (v being flow velocity) and $P_{oe} - P_{oi}$ refers to the difference in total pressure between the inlet and outlet of the control volume. Further, the term $\rho g\,(z_{outlet} - z_{inlet})$ refers to the gravitational force, and $\Delta P_{o,losses}$ refers to the total pressure losses through the control volume.

Conservation of Energy

Equation (3.1.3) describes the conservation of energy within a control volume [5].

$$\dot{Q} + \dot{W} = \forall \frac{\partial}{\partial t}(\rho h_{0-} p) + \dot{m}_e h_{oe} - \dot{m}_i h_{oi} + \dot{m}_e g z_e - \dot{m}_i g z_i \tag{3.1.3}$$

where $\dot{Q}$ denotes the energy generated, and $\dot{W}$ the work done in the control volume. Further, $\forall \frac{\partial}{\partial t}(\rho h_{0-} p)$ refers to the rate change of energy over time (with $\forall$ being the control volume and

p being the density) plus the losses of energy throughout the control volume. Equation 3.1.3 is used in Flownex to calculate the total energy lost in the control volume. Further, h and p respectively denote enthalpy and pressure.

The heat transfer equations (in its simplistic form) governing the heat transfer modes will be discussed next.

3.2 Heat Transfer

There are three modes of heat transfer that are accounted for; conduction, convection and radiation [30] . All three modes will be taken into account in the Flownex network model (see Figure 14 below).

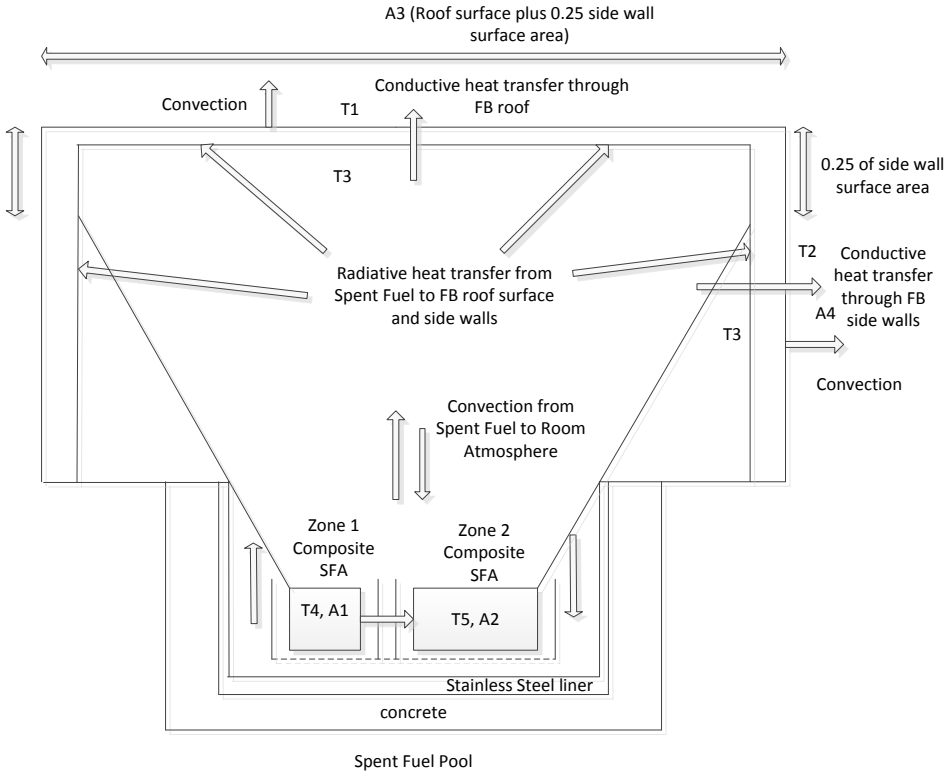

Figure 14: Heat Transfer flow paths from SFP to FB

From Figure 14, Temperature (T_1) denotes the outside roof surface temperature and Temperature (T_2) the outside FB side wall temperature. The inside FB roof surface temperature is assumed to be the same as the inside FB wall surface temperature (T_3). Temperature (T_4) denotes the peak cladding temperature of Zone 1. Temperature (T_5) denotes peak cladding temperature of Zone 2. A1 to A4 denote the respective surface areas. It is further assumed that the total decay heat from the SFP is transferred to the FB.

Conduction is heat transfer through molecular diffusion or interaction in fluids or solids. The rate of heat transfer by conduction is given by [30]:

$$q_{conduction} = -kA\ \frac{\Delta T}{\Delta x} \tag{3.2.1}$$

where A denotes the cross-sectional area through which the heat is conducting and ΔT refers to the temperature difference across a finite distance, Δx. Further k refers to the thermal conductivity of the material.

In Flownex [31], the heat transfer through conduction is given by the schematic in Figure 15 below

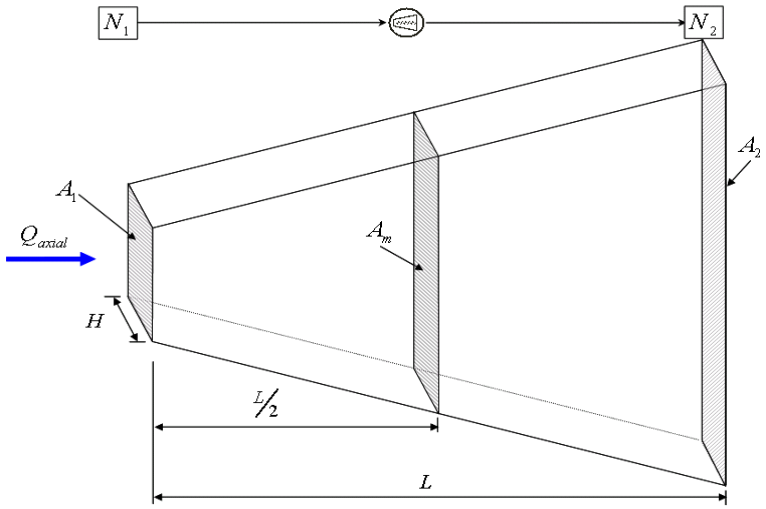

Figure 15: Typical Heat Transfer conduction element layout in Flownex [31]

where L refers to the length of the conduction element and H, refers to the height of the conduction element. A_1 and A_2 refer to the upstream and downstream surface areas respectively across which the heat transfer occurs.

Conduction heat transfer will be accounted for in the Flownex network model to determine the total heat transfer between the uranium fuel and the zirconium cladding in the representative composite SFAs.

The decay heat is caused only by the fuel rods and conduction is only considered in the vertical direction, the transient conduction heat transfer equation yields [31].

$$\frac{\partial\ (\mathrm{p}\forall c_p\ T_0)}{\partial_t} = \Sigma\ (\bar{Q}_{convection} + \bar{Q}_{conduction} + \bar{Q}_{radiation})_{in} - \Sigma(\bar{Q}_{convection} + \bar{Q}_{conduction} + \bar{Q}_{radiation})_{out} + \Sigma S_d \tag{3.2.2}$$

where $\frac{\partial\,(\mathrm{p}\forall c_p\ T_0)}{\partial_t}$ denotes the rate of energy storage (with p being the density and c_p the specific heat capacity. $\bar{\mathrm{Q}}_{convection}$, $\bar{\mathrm{Q}}_{conduction}$,and $\bar{\mathrm{Q}}_{radiation}$ refer to heat transfer contributed by convection, conduction and radiation respectively. Further, S_d is the source term which refers to the decay heat. T refers to the control volume temperature and ∀ refers to the control volume.

In the Flownex network model, Equation (3.2.2) will be discretized into six control volumes along the length of the SFRs (represented by a composite SFA since the vertical temperature distribution in all the rods of the respective zones is the same). The cladding surface temperature is calculated at each control volume (see mathematical derivation for each cladding temperature in Appendix B).

Conduction heat transfer through the inner stainless steel rack wall (IRW) between the SFAs will also be accounted for. Furthermore, conduction heat transfer will also be assessed through the FB roof and side walls, including conduction through the SFP outer stainless steel rack walls (ORW) from the respective zones.

Convection is heat transfer through the motion of fluids. The rate of heat transfer from a surface by convection is given by [30]:

$$q_{convection} = -h_c A_s \left(T_{surface} - T_\infty\right) \tag{3.2.3}$$

where A_s denotes the surface area of the object and $T_{surface}$ refers to the surface temperature. Further, T_∞ refers to the ambient or fluid temperature and h_c denotes the convective heat transfer coefficient.

Convective heat transfer is accounted for in the Flownex network model to model heat transfer between the air and the zirconium cladding of the representative composite SFAs in order to determine the surface cladding temperatures along the SFAs under various heat load scenarios.

The air flow field is in the laminar flow regime since only natural convection was under consideration. The calculated Reynolds number was below 2300 and Flownex automatically evaluated the simulation under laminar flow regime conditions (see hand calculation in Appendix C).

The Reynolds number is calculated in Flownex using the following equation:

$$Re = \frac{\mathrm{p}\,V\,D_H}{\mu} = \left|\frac{\dot{\mathrm{m}}\,D_H}{\mu}\right| \tag{3.2.4}$$

where p denotes the density of the fluid and V denotes to the velocity of the fluid. Further, D_H denotes the hydraulic diameter, μ the viscosity of the fluid and ṁ, denotes the mass flow of the fluid.

Also, D_H is calculated using the following equation:

$$D_H = \frac{4A}{P} \tag{3.2.5}$$

where A refers to the total flow area and P refers to the total wetted perimeter

Radiative heat transfer occurs when the emitted radiation strikes another body and is absorbed. The amount of radiation given off by an object is given by [30]:

$$q_{emitted} = \varepsilon \sigma A_s T^4 \tag{3.2.6}$$

where A_s denotes the surface area of the object and *T* refers to the temperature of the body. Further, σ refers to the Stefan-Boltzmann constant, equal to 5.67x10^{-8} W/m^{2}K^4 and ε refers to the emissivity of the material.

The radiative heat transfer considered in this work includes that between the cladding surfaces of the respective zones to the FB roof and walls and Equation (3.2.8) can be expanded to give [30]:

$$Q_{decay\ (Zone\ 1)} = \frac{\sigma\ (T^4_{zone\ 1} - T^4_{3}\ )}{\frac{1-\varepsilon_1}{\varepsilon_1 A_1} + \frac{1}{A_1 F_{12}} + \frac{1-\varepsilon_2}{\varepsilon_2 A_3}} \tag{3.2.7}$$

where, A_1 (Figure 14) denotes the SFP surface area (surface area of Zone 1). Further, A_3 denotes the FB roof surface area (including a quarter of the FB side wall surface areas). ε_1 and ε_2 refer to the emissivity values from A_1 (Zone 1 cladding) and A_3 (FB concrete roof and walls) respectively, assumed to be 0.7 [16] and 0.95 [32]. F_{12} refers to the form or view factor.

Similarly, for Zone 2, [30].

$$Q_{decay\ (Zone\ 2)} = \frac{\sigma\ (T^4_{zone\ 2} - T^4_{3}\ )}{\frac{1-\varepsilon_1}{\varepsilon_1 A_2} + \frac{1}{A_2 F_{12}} + \frac{1-\varepsilon_2}{\varepsilon_2 A_3}} \tag{3.2.8}$$

The governing equations discussed above will be solved numerically using the Flownex network model to predict the peak cladding temperatures along the vertical axis of the respective composite SFAs under the severe accident heat load scenario.

View factors and assumptions used

View factors can be defined as the fraction of the radiation leaving the upstream surface that is intercepted by the downstream surface [31]. Van Antwerpen, 2008 indicated that when overall heat loss from an integrated system is considered, good accuracy can be obtained by linking only directly opposing surfaces with a view factor of one. He also indicated that for system simulation codes that focus on transient response, it is not considered worthwhile to use a detailed radiation model, as the gain in accuracy does not justify the increased solution time or the implementation

and verification effort [33]. Hence in the Flownex network, view factors of 1 are assumed from the respective zones to the fuel building roof and side walls; as well as between SFA surfaces.

The development and construction of the Flownex network model will be discussed next.

4. Flownex Network Model

This chapter provides detail on the development of the Flownex network model.

4.1 Construction of Flownex Network Model

In the Flownex network model, the natural air flow conditions are established through the buoyancy driven convection as a result of the temperature variation between the fuel and the remainder of the spent fuel building. Pipe elements were used to simplify the complex modelling of the air flow channels in the fuel assembly and primary losses were calculated in Flownex using Darcy Weisbach with a pipe roughness of 30 micron. As such one composite pipe was created for Zone 1 (representing the discharged core, higher heat load) and another for Zone 2 (representing the older SFAs with lower heat load) as depicted in Figure 16. For the air volume directly above the SFAs, a reservoir is used to represent a well-mixed adiabatic control volume at atmospheric conditions.

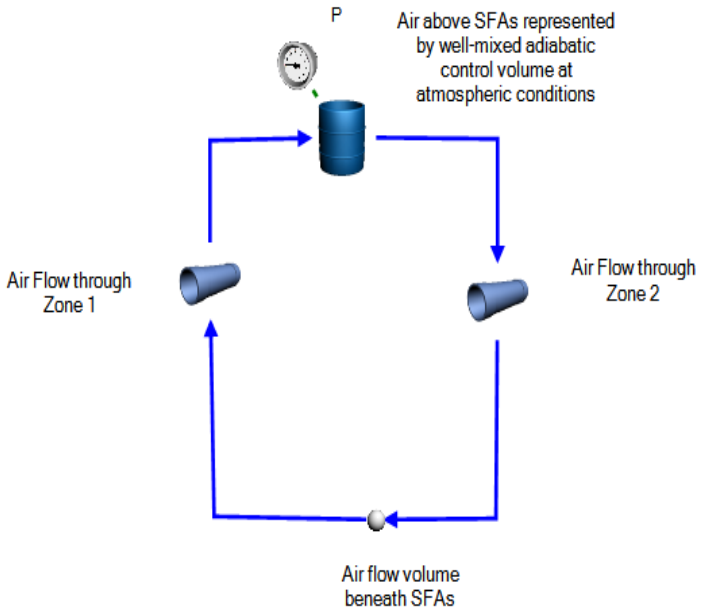

Figure 16: Air flow represented by Flownex pipe elements

Flownex Spent Fuel Assembly and Air Flow Channel Representation

Figure 17 depicts an incremental layer of the composite Flownex SFAs for the respective zones.

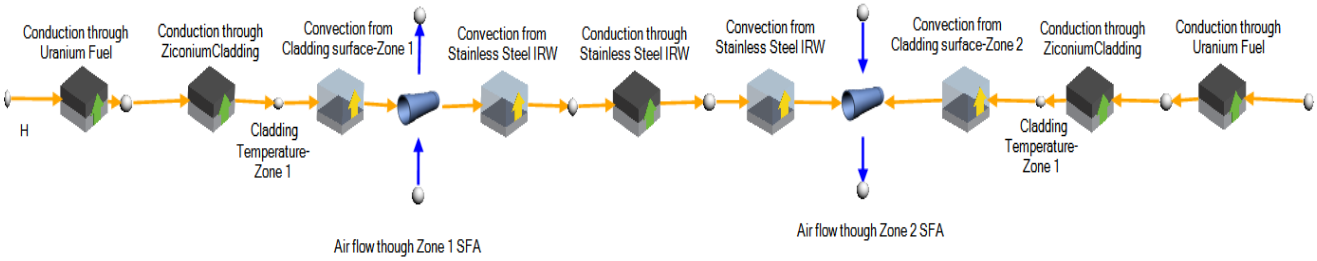

Figure 17: Incremental layer of the Flownex composite SFAs and Air Flow

From Figure 17, the composite SFAs representing Zones 1 and 2 of the SFP are constructed in Flownex using elementary conductive heat transfer elements (representing the uranium fuel, zirconium cladding and the stainless steel rack walls between the SFAs respectively). The dimensions detailed in Chapter 2 were used as input values.

Convection from the cladding to the ORW and conduction through the ORW of the respective zones were added to the incremental layer given in Figure 17 above (see below):

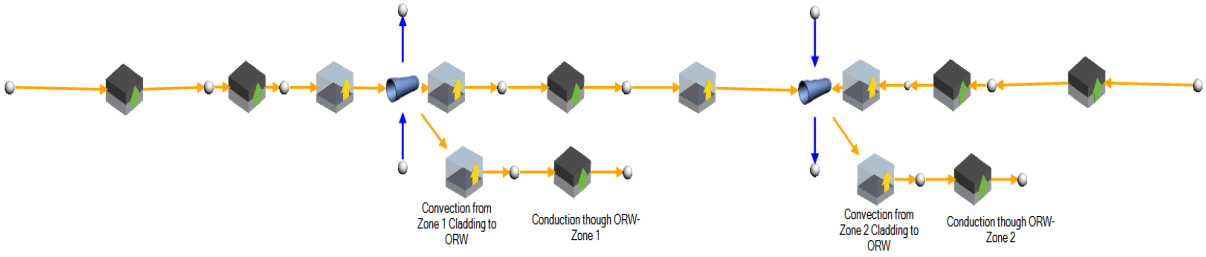

Figure 18: Complete incremental layer of the Flownex composite SFAs and Air Flow

Figure 18 represents the complete incremental layer, and in the Flownex network model, six of these incremental layers were constructed axially to represent composite SFAs for Zones 1 and 2 (see Figure 19 below).

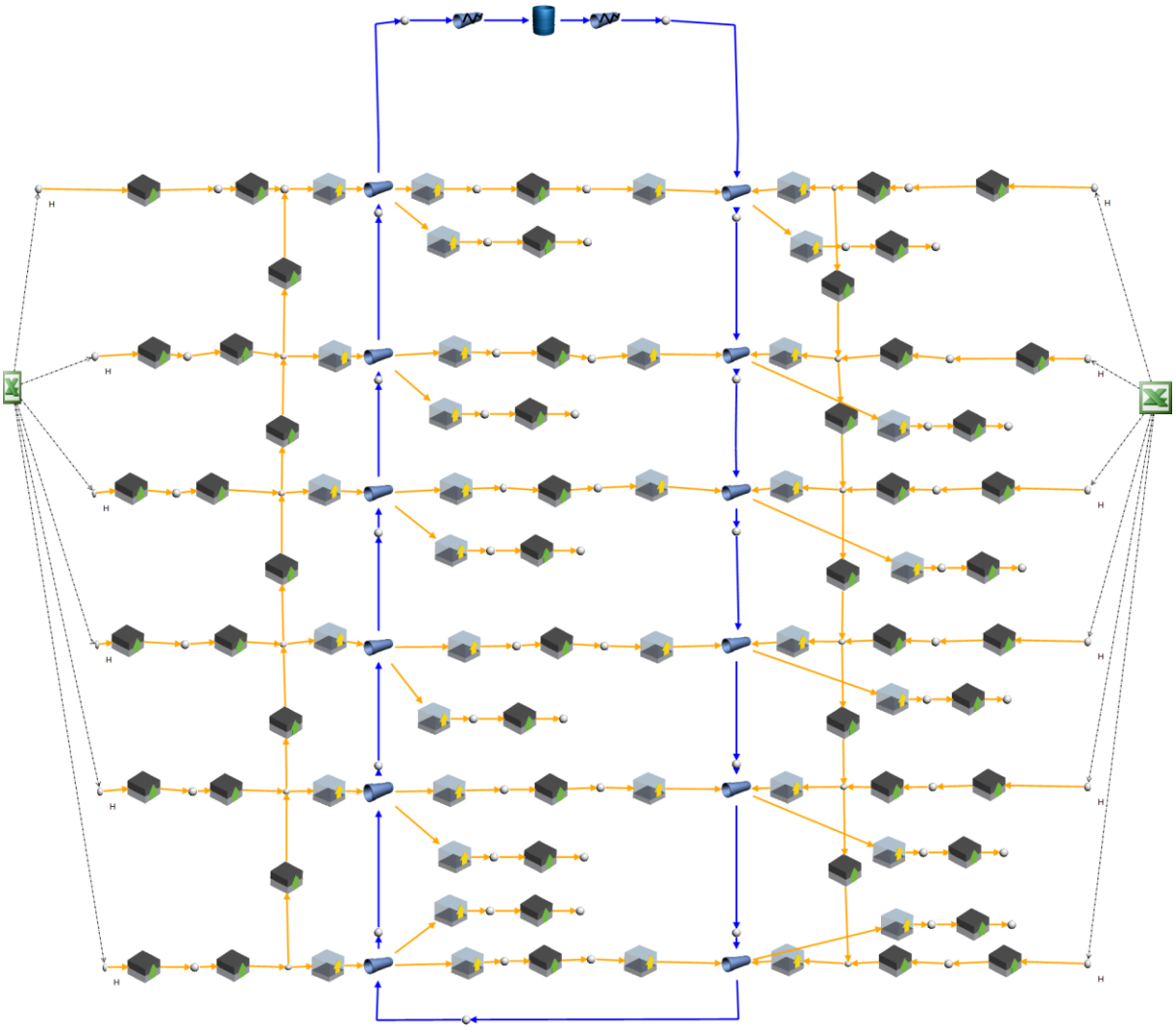

Figure 19: Six Incremental layers that axially represent the full composite SFAs of Zones 1&2

Figure 19 shows 6 incremental layers that make up the total active length of the respective composite SFAs.

Radiation was also modelled axially along the cladding of the composite SFAs by using conduction heat transfer elements between the incremental layers. By modelling radiation this way, there is no need to include view factors and areas; as a result these elements carry no thermal capacity and therefore the density and specific heat input values were close to zero. An excel link was also established to distribute the heat load to the incremental layers of the respective zones.

The complete Flownex network model is shown in Figure 20 below. Details of input parameters used in the Flownex network model are documented in Appendix D to account for the various layers of materials used. Further simplification to the model to note is that the convection coefficient used was chosen as fixed inputs, hence the results obtained for convection are based on the coefficient used.

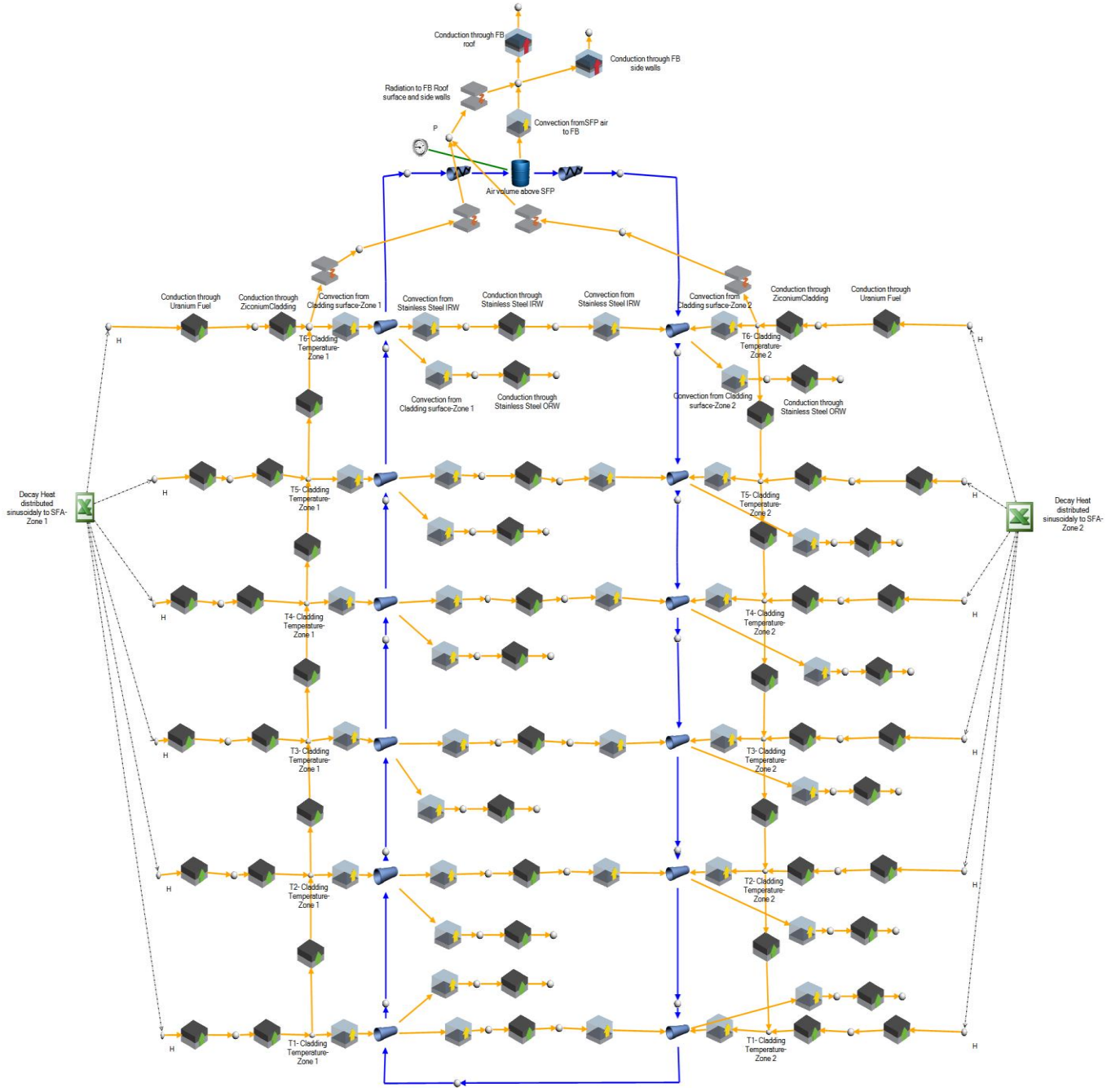

Figure 20: Full Flownex network model between Zones 1 and 2 composite SFAs

Figure 20 depicts the complete Flownex network model. Radiation heat transfer elements are added from the upper ends of the composite SFAs to the inside roof surface of the FB from Zones 1 and 2 respectively. Conduction through the FB roof and side walls is represented by composite heat transfer elements (CHTEs). The reservoir at the top of the model is used as a spacing element with a very high admittance which represents a well-mixed adiabatic control volume at atmospheric conditions, hence there will be a near zero pressure drop through this component. The flow resistors were added in order to use the opening input of these components to enforce zero flow for the steady state calculation.

In order to assess the model under the severe accident scenario conditions, an order of magnitude comparison as obtained using the 3-D CFD work of Boyd C.F.2000 [24]. Boyd employed FLUENT (version 5) to predict fuel heat-up and natural circulation flow paths throughout the SFP and the upper containment building. The order of magnitude comparison results obtained will be discussed next.

4.2 Order of Magnitude comparison of the Flownex Network Model

A 3-D FLUENT CFD code was used by Boyed C.F. 2000 [24] to predict fuel heat-up and natural circulation flow paths throughout a SFP and the upper containment building of a BWR. For the purposes of this study, spent fuel with a 4 year decay time was used. Boyed C.F, 2000 [24] identified four zones in the SFP with the hottest load along the left edge of the pool and cooler zones progressively outwards. These inputs were fed into the Flownex network model developed in this work (with similar total heat load). This resulted in Zone 2 having the higher heat load (summation of the heat load from all the cooler zones) and consequently the heat transfer flow path was amended to be from Zone 2 to Zone 1. Further, as the code was applied to a BWR plant, the changes in SFA geometries, SFP and FB dimensions were taken into account in the Flownex network model. Additional changes included the addition of a forced ventilation system to remove heat from the FB, and the removal of radiative components. The latter is to enable evaluation of the peak cladding temperatures as a result of natural convection (see Figure 18 below). Details of input parameters used in the Flownex network model are documented in Appendix E (project data files of the Flownex network models developed in this dissertation are available from the author on request).

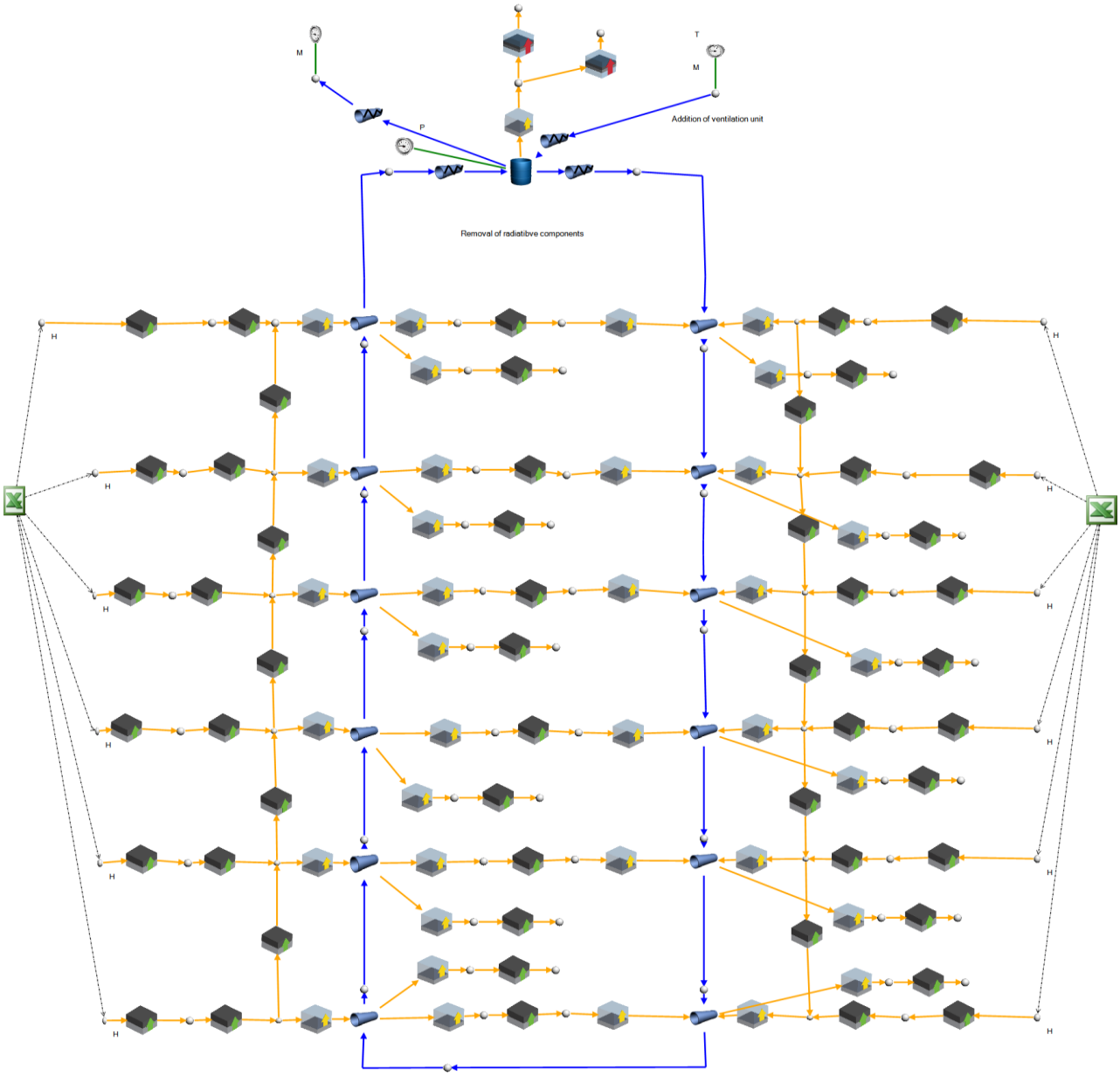

Figure 21: Flownex Network Model used for comparison with 3-D CFD FLUENT (version 5)

Assumptions used in the FLUENT Code

- The external pool walls are adiabatic, only heat transfer from the upper building and ceiling are considered.
- Uniform heat generation in fuel, with axial fuel peaking being ignored.
- Radiation is neglected, though Boyd C.F. 2000 [24] indicated that it can be important at elevated temperatures.
- Clad oxidation chemistry is neglected, though Boyd C.F. 2000 [24] states that oxidation chemistry considerations may be important at elevated temperatures.
- Only steady state results were shown.

FLUENT Model vs Flownex Network Model Results

Table 4 compares the steady-state results achieved via the Flownex network FLUENT models for the stated heat load scenario. Geometries and heat load data were extracted from the FLUENT model (Boyd C.F. 2000) and used in the Flownex Network Model in Figure 21 (see geometry detail in Appendix E). From the given data it showed that the cladding temperatures predicted by the FLUENT model compare favourable to when the same geometrical data was used in the Flownex network model. Favourable results were achieved in the order of magnitude comparison and the basic Flownex network model (Figure 20), it is now applied to simulate the spent fuel building described in Section 1 under the severe accident scenario conditions. This is done to identify the dominant heat transfer modes, and will be discussed next.

	Decay Time (48 months) Base Case (Forced ventilation)		**Peak air temperatures in the channels**	**Temperature above the SFP**
Heat Load	Zone 1 0.37 MW	Zone 2 0.733 MW		
FLUENT Model Peak Cladding Temperature (Zone 1)	540°C +/- 20°C		500°C	200°C
Flownex Model Peak Cladding Temperature (Zone 1)	484°C		474°C	147°C

Table 4: Steady state Flownex network model results vs FLUENT model results (using the FLUENT model geometrical detail)

4.3 Assessment of the Flownex Network Model

The Flownex network model (Figure 20) was used to assess the severe accident scenario discussed in Section 1.1. Due to the high heat loads of the respective zones (5.44MW in Zone 1 and 1.065MW in Zone 2), lower heat loads were first used and progressively increased. The heat loads were progressively increased in Zone 1 from 100 kW to 500 kW (see Figure 22 below). Key simulation results are shown in Figures 22 and 23. From these results, it is clear that the radiative heat transfer component quickly becomes the dominant mode above heat loads of 250 kW in Zone 1.

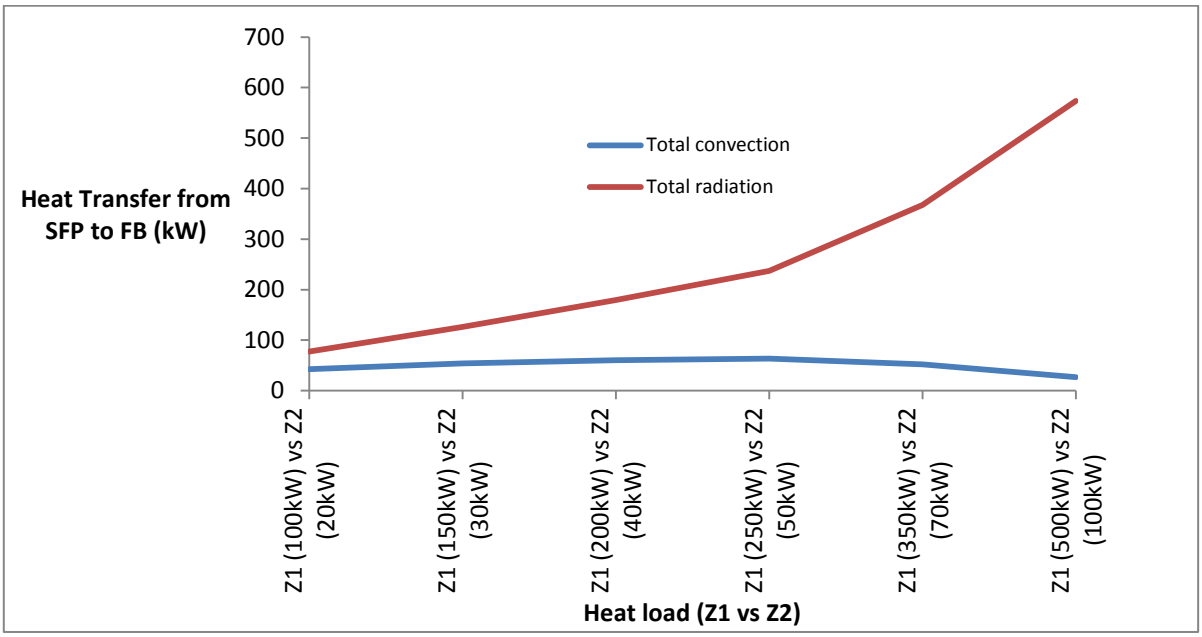

Figure 22: Total convective vs Total radiative heat transfer using the Flownex network model for heat loads below 500 kW in Zone 1

Figure 23 shows a corresponding decrease in air flow and air density as a result of increasing heat load in Zone 1. These point to the excessive dominance of radiative heat transfer over convection at the heat loads of interest to this study (Boyed C.F.2000 also indicated that models for radiation and clad chemistry become important at T>600°C). This is further enforced by the Flownex network model not taking into account any forced ventilation with exhaust air from the FB and no heat loss from the spent fuel pool walls.

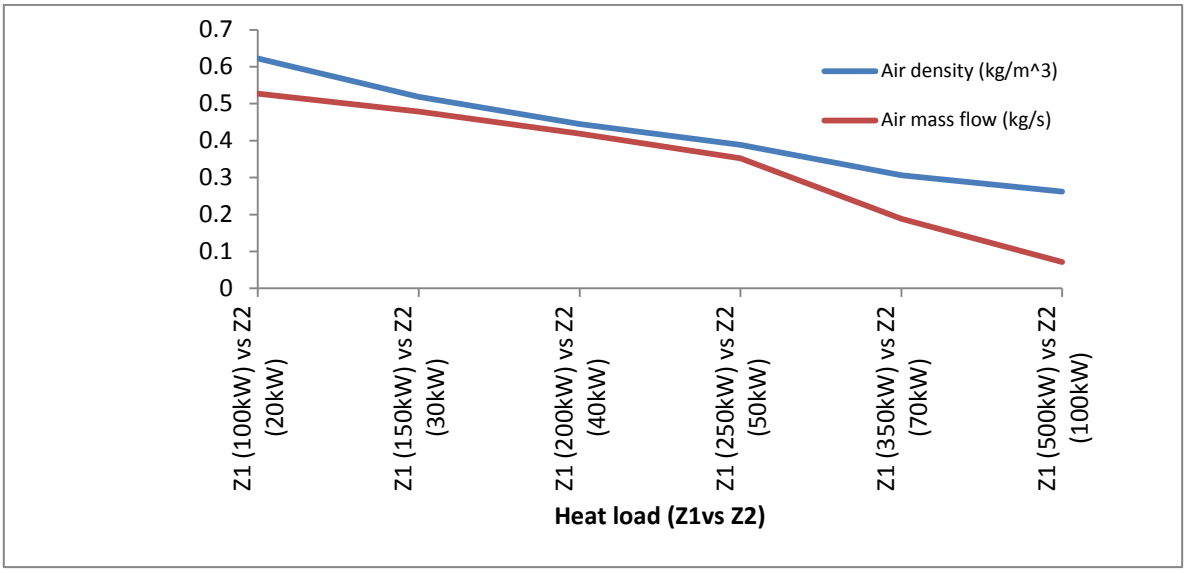

Figure 23: Air density and air mass flow vs various heat loads in Zone 1 below 500 kW

Figure 24 shows the peak cladding temperatures at various heat loads in Zone 1 below 500kW.

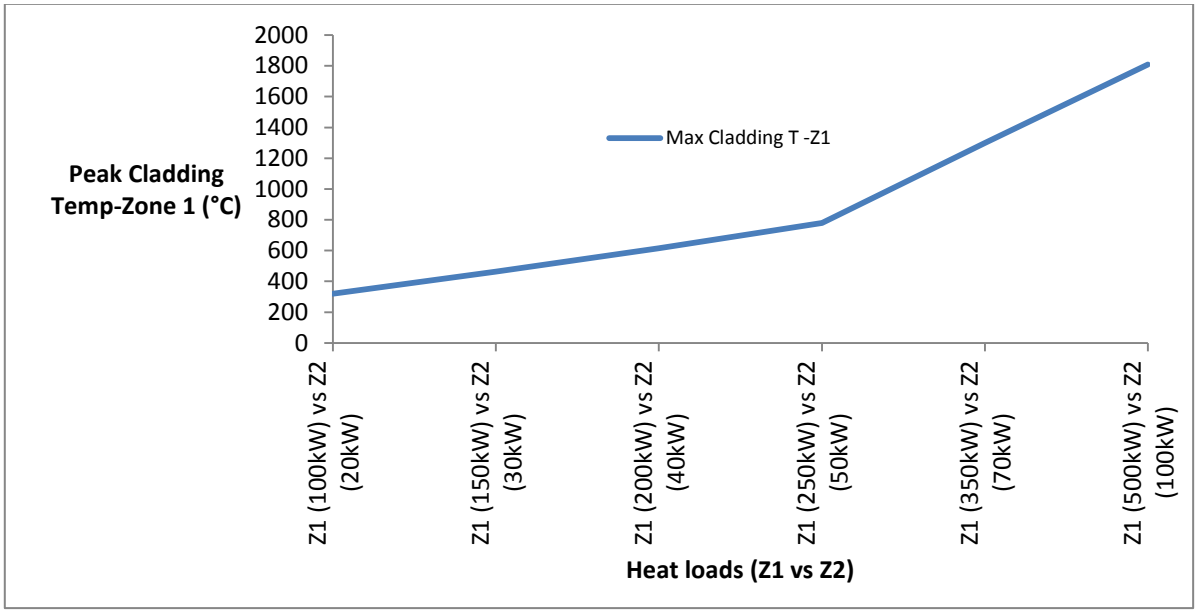

Figure 24: Peak Cladding temperatures at various heat loads in Zone 1 below 500 kW

From Figure 24, for heat loads above 250 kW, the cladding temperatures are seen to increase excessively (perhaps unrealistically so). This may have to do with numerical complexities with modelling gas flows at these extreme conditions. Fortunately, as described above, the radiative component is by far the dominant mode and a modified Flownex network was developed (See chapter 5) for higher heat load predictions. This model focussed largely on conductive and radiative heat transfer elements to simulate the severe accident scenario and to determine the average cladding/Fuel zone temperatures that can be expected under the scenario.

The development of the modified Flownex network model will be discussed next.

5. Modified Flownex 2-D Network Model of SFP

The modified Flownex 2-D network model excludes the effect of air flow through the channel walls of the spent fuel assemblies. The exclusion is motivated from the results obtained in Section 4.3 (dominance of radiative heat transfer) and supported by the literature, Boyed C.F.2000. This permits the building of a simplified network model to simulate the SFP under high heat load scenarios (where natural convective heat transfer plays a small role).

From the literature survey [34] conducted and the Flownex network modelling performed on SFAs, it became evident that thermal analysis of spent fuel assemblies required detailed modelling of individual rod sections to more accurately represent the different heat loads in the SFP. In the modified 2-D Flownex network model, a coarsely discretized model of the 2-D layout of the spent fuel zone was therefore developed using conduction and radiative elements in the X and Y directions (top view is the X-Y plane), see Figure 25 below.

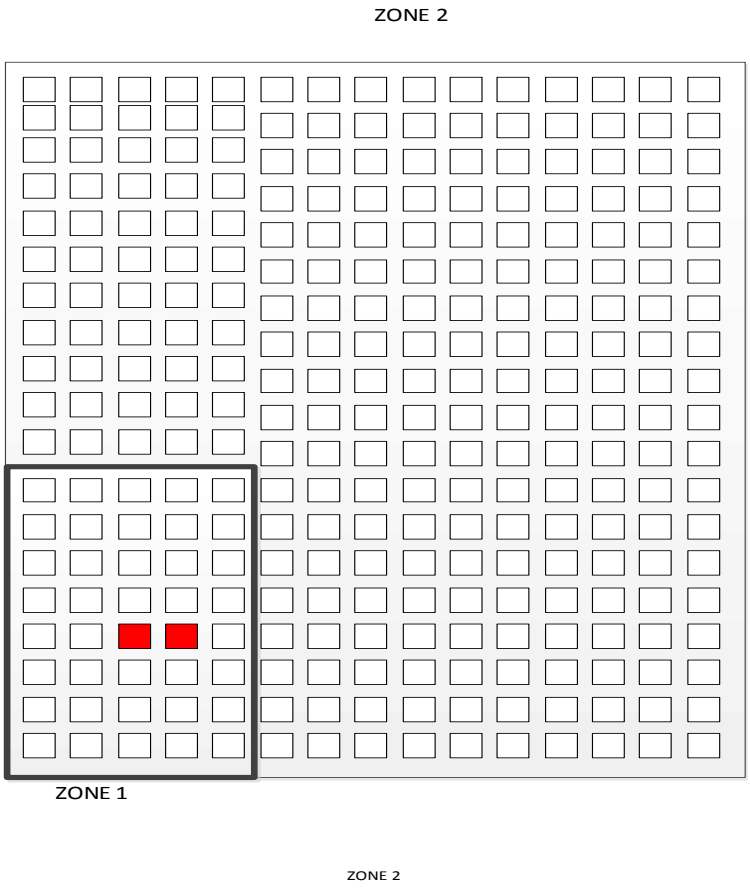

Figure 25: 2-D Schematic layout of the SFA arrangement in the SFP in the X-Y direction (Top view)

The main mode of heat transfer between the SFRs, SFAs and the fuel rack considered therefore is via conduction and radiative heat transfer only. In order to assess the average Fuel zone temperature evolution within the SFP, the effective thermal conductivity through a cross section of the fuel region of the fuel assemblies is calculated. This is a simple and practical alternative which describes the SFP as a homogeneous but non-isothermal medium. This method involves developing an empirical correlation for the effective thermal conductivity. This approach will be discussed in the next session by magnifying the two FAs highlighted in red above. This effective conductivity model will then be scaled-up to assess the heat transfer in the SFP and the average Fuel zone temperatures.

The development of the effective thermal conductivity empirical correlation will be discussed next.

5.1 Constructing a 1-D Flownex model for calculating the effective thermal conductivity

An effective thermal conductivity for the fuel volume is highly dependent on temperature. This is established via an empirical correlation for the Fuel zone by creating a detail 1-D model of the "conduction" path from one fuel rod to an adjacent one between two FAs (see Figure 26 below).

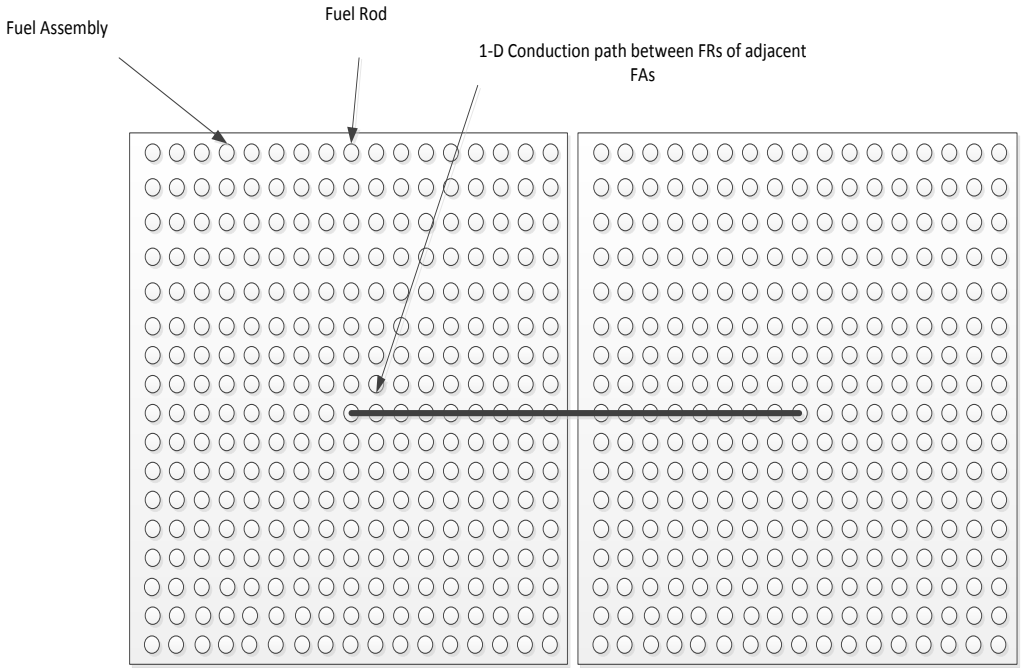

Figure 26:1-D Conduction path between two SFAs

From Figure 26, the 1-D model displays the conduction through the UO2 and cladding (centre FR from one FA to centre FR of adjacent FA, including radiative heat transfer between FRs and the fuel racks of the respective FAs). The effective thermal conductivity is used to model the heat transfer by radiation and conduction between the fuel rods, between the fuel rods and the fuel racks in which the fuel assemblies reside and between the fuel racks of respective zones [35]. Figure 27 below shows the 1-D Flownex model representing the 1-D heat flow path between the adjacent FRs of the two FAs.

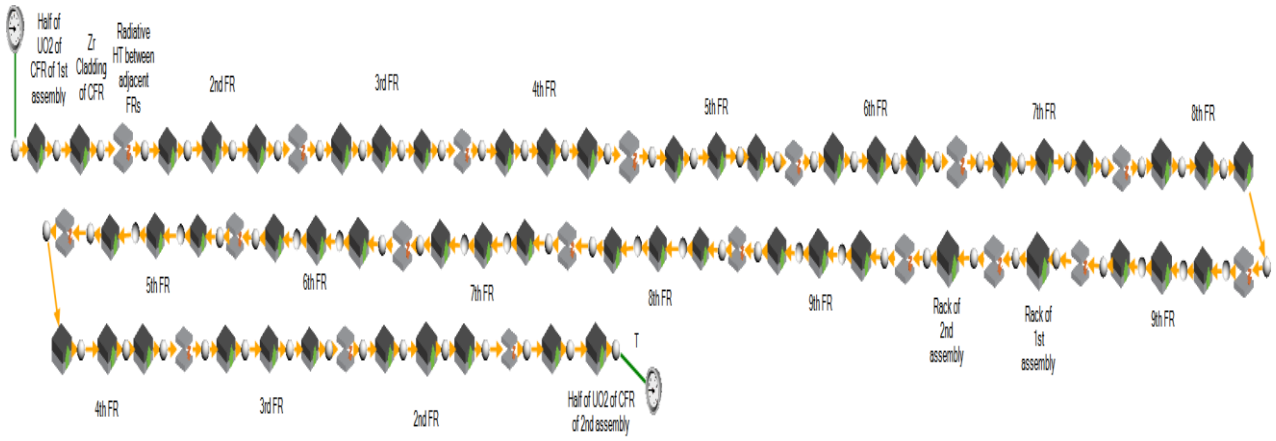

Figure 27: 1-D Flownex Conduction model

The 1-D Flownex conduction model depicted in Figure 27 is used to generate the values for Keff at various temperatures (using temperature as boundary condition) in order to develop the empirical Keff correlation (this is discussed in section 5.3). The main simplifying assumptions for the 1-D Flownex conduction model are discussed in section 5.2 below.

5.2 Main Simplifying Assumptions for the 1-D Flownex Model

A number of simplifying assumptions are made in computing the effective thermal conductivity in the 1-D Flownex model. These follow:

- Pool drains instantaneously with an inability to maintain level.
- The geometry of the SFRs, SFAs and the storage racks remains intact.
- Conduction in the Z direction is ignored, assuming temperature along a rod is relatively uniform. This is motivated by the rods containing a uniform heat source along their length, with the heat source varying per FA only and convection being small.
- All rods are assumed to be FRs.
- The thermal conductivity is not dependant on the decay heat but rather on the temperature at which the heat is generated.

- Physical models for clad chemistry are not included.
- The helium gaps between the fuel pellets in the FRs are assumed to be filled with fuel pellet material because the gaps between the fuel pellets and their cladding are too small compared to the size of the FR.

5.3 Generating the empirical K_{eff}

The discretized general conduction equation is given by

$$q_{conduction} \approx -kA\,\frac{\Delta T}{\Delta x}$$

where A denotes the cross-sectional area through which the heat is conducting and ΔT refers to the temperature difference across a finite distance, Δx. Further k refers to the thermal conductivity of the material.

For the effective thermal conductivity (K_{eff}), k can be re-written in the following form

$$\mathrm{k}\frac{\partial \mathrm{T}}{\partial \mathrm{x}} \approx \mathrm{K_{eff}}(T_{ave})\,\frac{\Delta \mathrm{T}}{\Delta \mathrm{x}} \qquad 5.3.1$$

where $\mathrm{K_{eff}}(\mathrm{T})$ denotes the thermal conductivity as a function of average temperature.

Similarly, Equation 5.3.1 can be re-written as,

$$\mathrm{q} \approx \mathrm{K_{eff}}(T_{ave})A\,\frac{\partial \mathrm{T}}{\partial \mathrm{x}} \approx \mathrm{K_{eff}}\,(T)A\,\frac{T_2-T_1}{\mathrm{x}_2-x_1} \qquad 5.3.2$$

Hence,

$$\mathrm{K_{eff}}(T_{ave}) = \frac{q\,(x_2-x_1)}{\mathrm{A}(\,\mathrm{T}_2-T_1)} \qquad 5.3.3$$

From Equation 5.3.3, the empirical correlation for $\mathrm{K_{eff}}(\mathrm{T})$ was generated for the Fuel zone (Figures 25 and 26 above) by plotting $\mathrm{K_{eff}}(\mathrm{T})$ vs average temperatures (see Appendix F for data input to excel graph below) and is shown in Figure 28.

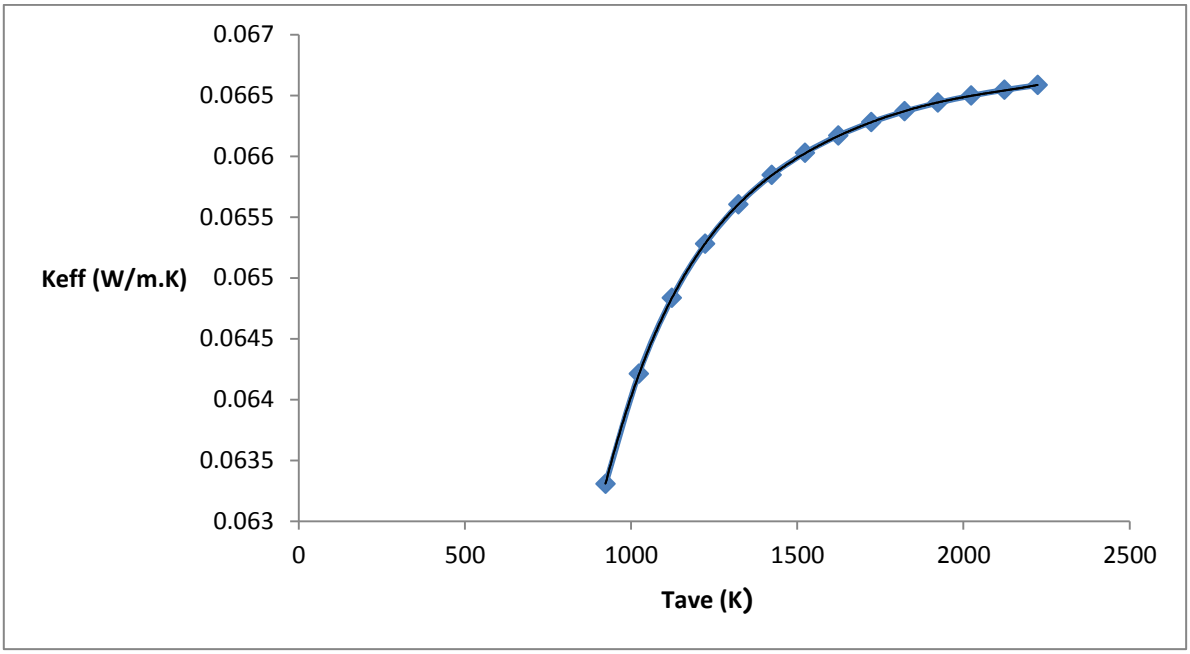

Figure 28: K_{eff} vs T_{ave}

The following empirical correlation for $\mathrm{K_{eff}}(T_{ave})$ was obtained from Figure 28.

$$K_{eff}\,(T_{ave}) = 2.297E^{-18}T^5 - 2.074E^{-14}T^4 + 7.528E^{-11}T^3 - 1.384E^{-07}T^2 + 0.0001305T + 0.01508 \quad 5.3.4$$

Where $K_{eff}\,(T_{ave})$ refers to the effective thermal conductivity (W/m.K) and T_{ave} refers to the average cladding temperature (K) (see appendix F for the curve fit data).

The top view of the SFP layout will be discussed next in more detail, with specific focus to the SFAs configuration and number of SFAs in the respective zones.

5.4 Detailed Spent Fuel Pool Layout (top view)

For the beyond design base accident scenario, the unloaded core (discharged core) SFAs are represented by red squares and the “older” SFAs are represented by the blue squares (see Figure 29 below). The white squares represent empty spent fuel racks.

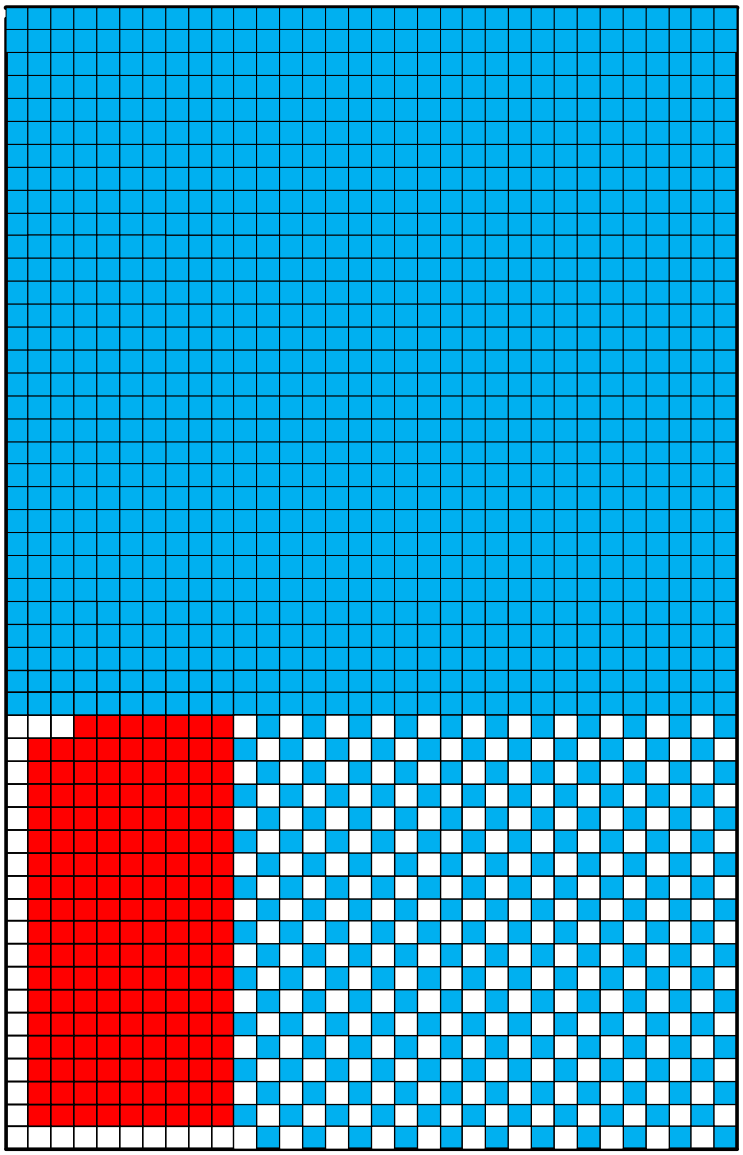

Figure 29: Detailed 2-D layout of the SFA arrangement in the SFP in the X-Y direction (Top view)

Table 5 below, depicts the total heat load and number of SFAs respectively.

	Total heat load (kW)	**Total no of SFAs**
Red squares (unloaded core)	5440	160
Blue squares ("older" SFAs)	1065	1201

Table 5: Total heat load

Figure 29 is discretized into 22 respective Fuel zones as shown in Figure 30 below:

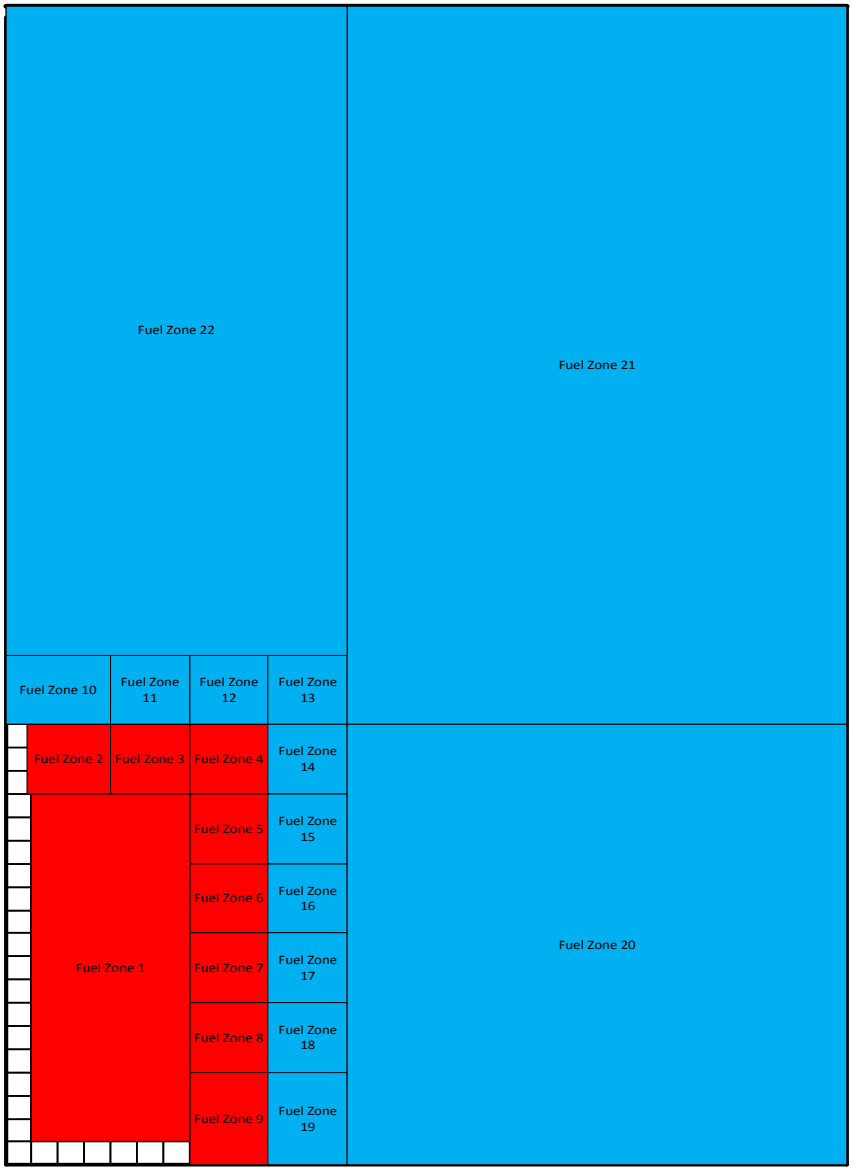

Figure 30: SFP discretized into 22 respective Fuel zones

From Figure 30, the heat loads depicted in table 5 are further distributed in four main Fuel zones as shown in table 6 below.

	Fuel zone	**Total heat load (kW)**	**Total no of SFAs**
Red squares (unloaded core)	Zone 1	5440	160
Blue squares ("older" SFAs)	Zone 20	185.33	209
Blue squares ("older" SFAs)	Zone 21	522.30	589
Blue squares ("older" SFAs)	Zone 22	357.36	403

Table 6: Heat load distribution in the main Fuel zones

Table 6 depicts the heat load distribution and number of SFAs in the four main Fuel zones. Heat loads for Fuel zones 20 to 22 were calculated by multiplying the average heat load per SFA of the entire "older" Fuel zone (Table 5) with the total number of SFAs in the respective zones.

From Figure 30, each Fuel zone will be connected in the X-Y direction with conductive heat transfer elements which represents the effective thermal conductivity developed in section 5.3, see Figure 31 below (also see Appendix G for the number of SFAs represented by the respective Fuel zones).

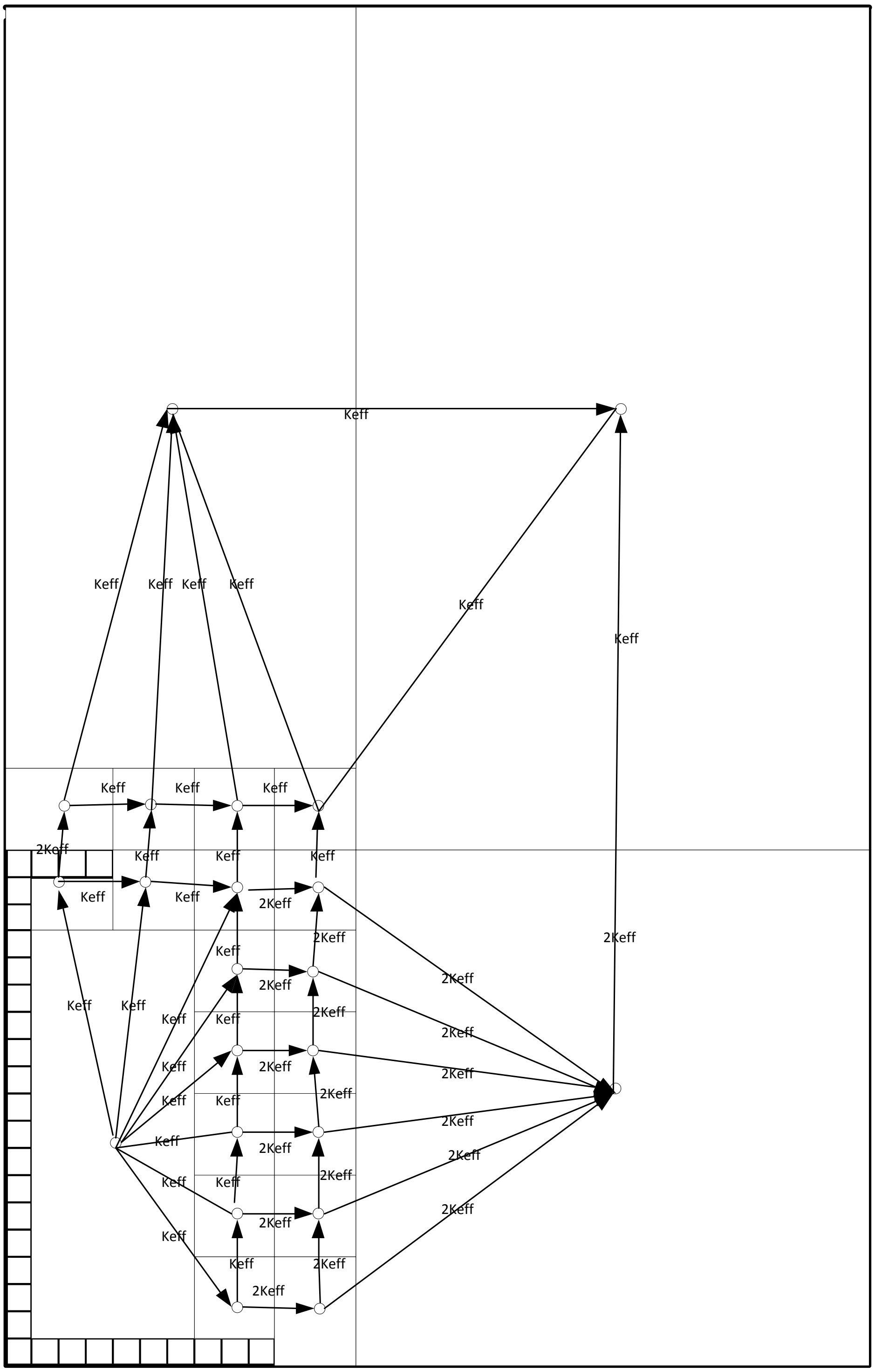

Figure 31: Effective thermal conductivity linkages between the various Fuel zones in the X-Y direction

From Figure 31, the actual heat flux areas and lengths through the respective Fuel zones were determined by the conversion of actual measurements (see Appendix H). Also for Fuel zones 14 to 20 the thermal conductivity is given as 2Keff due to the checker board arrangements of the SFAs. This is as the empty spaces do not increase the conductivity of the material but reduces the effective conduction length by halve which makes the homogeneous medium appear to have

better conductivity (also see heat flow derivation through checker box arrangement of SFAs in Appendix I). Conductive and radiative heat transfer elements were also added in the X-Y direction to represent heat loss through the SFP walls (see red arrows in Figure 32, below).

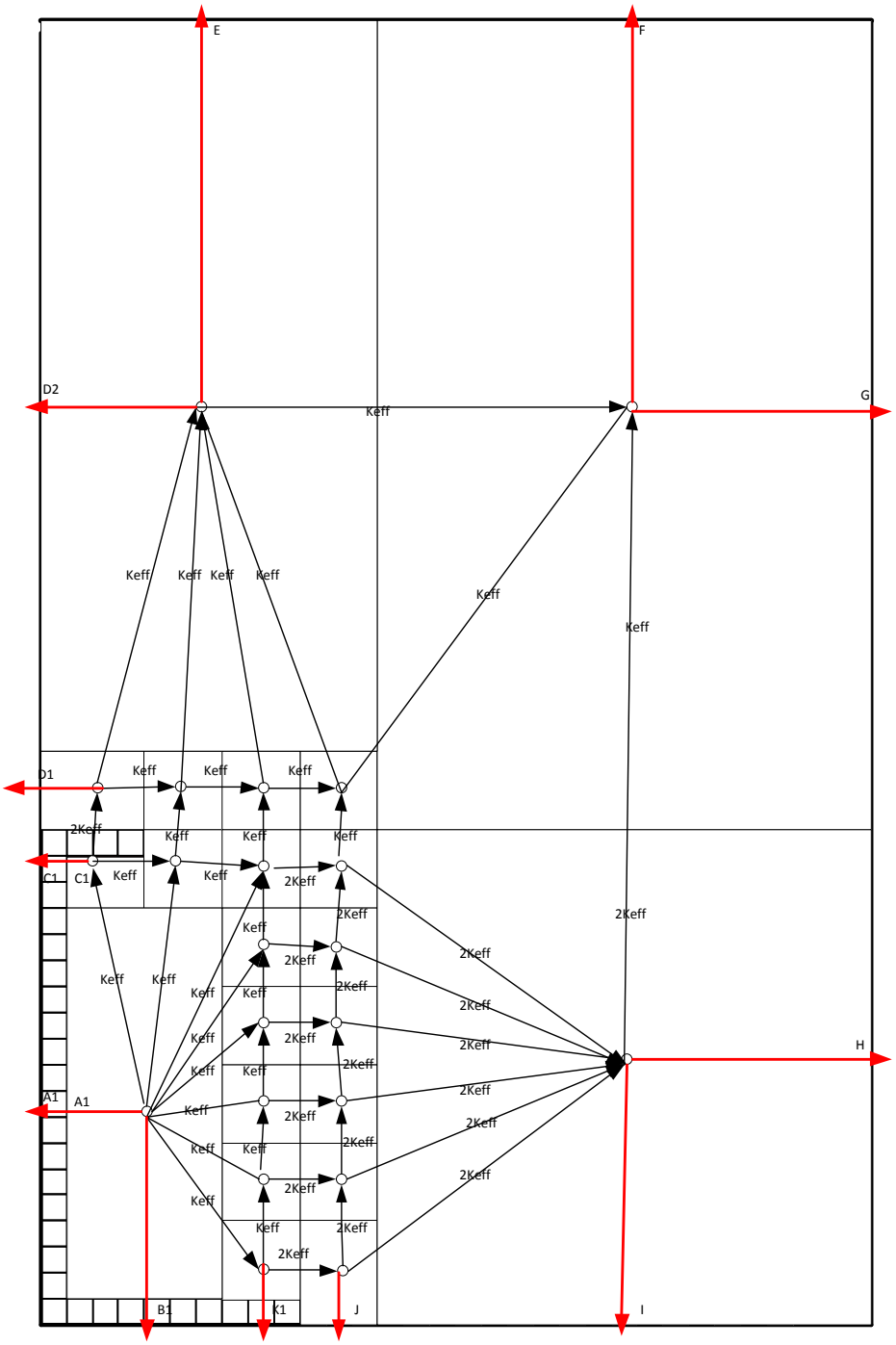

Figure 32: Heat loss through the SFP walls (X-Y direction)

The construction of the modified Flownex 2-D network model of the SFP will be discussed next.

5.5 Construction of the Modified 2-D network model in Flownex

The effective thermal conductivity is constructed in Flownex using conductive heat transfer elements (see Appendix F for table input values used for the effective thermal conductivity). No values for density and specific heat were given as input to these components hence carrying no thermal capacity.

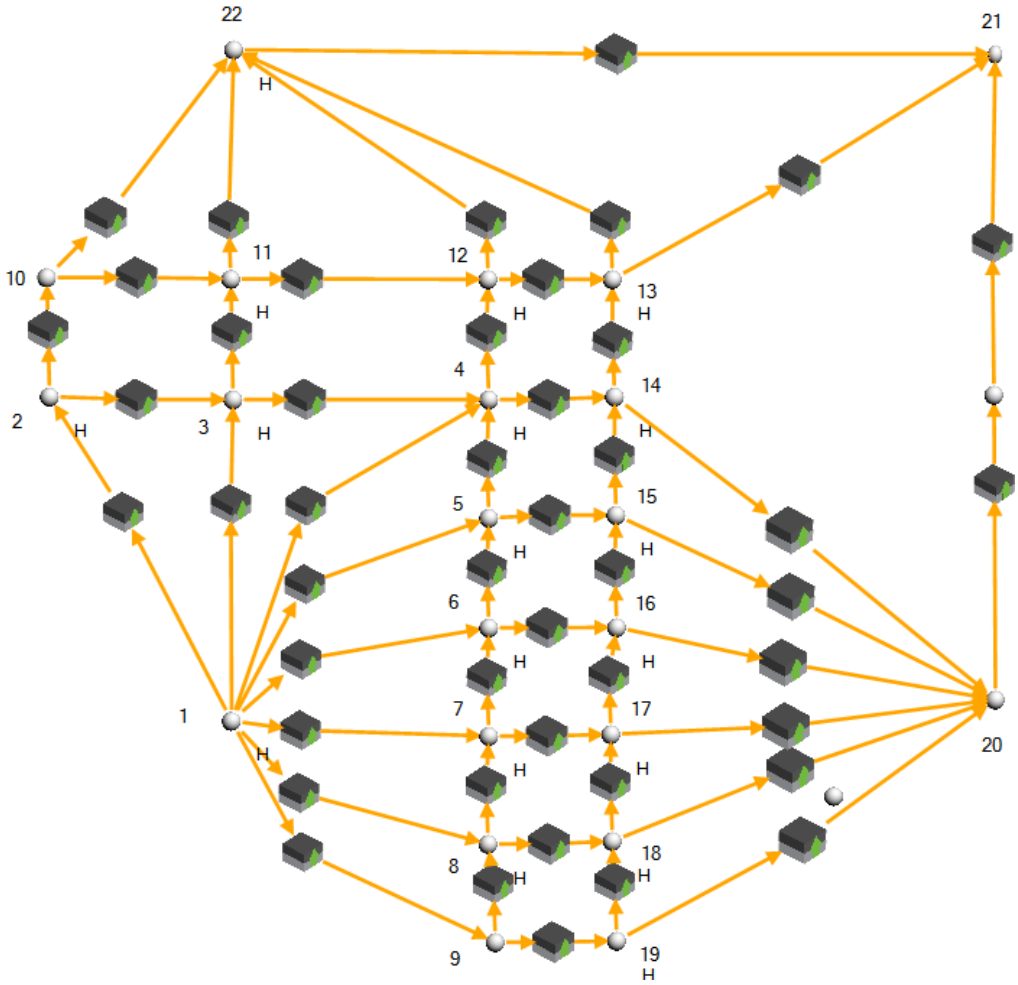

Figure 33: SFP discretized into 22 Fuel zones using Flownex solid nodes and conduction elements

From Figure 33, solid nodes were used to represent the respective Fuel zones and were interconnected with the effective thermal conductivity heat transfer elements. Conductive flow areas (upstream and downstream) and conductive lengths were used as input values in the respective effective conductivity elements between the various Fuel zones (see input values in Appendix H). The next step was to add thermal capacity as well as radiative heat transfer to each Fuel zone. Radiative heat transfer coming from each of the respective discretized Fuel zones was connected to the inside of the FB roof and side walls (see Figure 34 below).

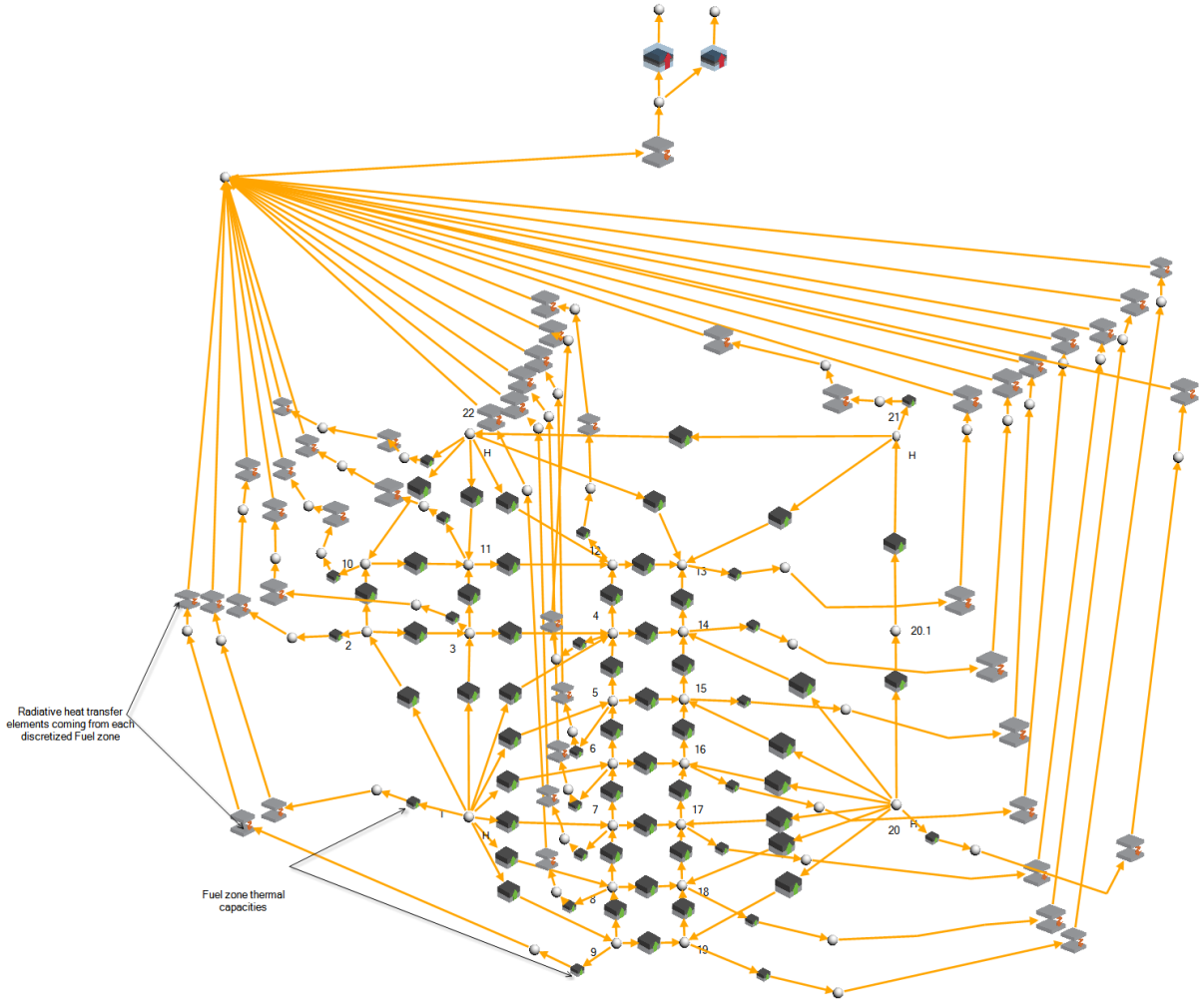

Figure 34: SFP in Flownex with radiative heat transfer and thermal capacity from each discretized Fuel zone

From Figure 34, conductive heat transfer elements were used to represent the thermal capacity of each Fuel zone. The lengths were made small such that the top and bottom of the Fuel zones are at the same respective temperatures. The sum of all the uranium oxide, zirconium and stainless steel of each Fuel zone were determined in order to calculate the respective thermal capacities of each Fuel zone (see Appendix K for input values used). Each radiative heat transfer element from each discretized Fuel zone was then projected to the FB roof and side walls (see radiative heat transfer areas from the respective Fuel zones in Appendix L). The same FB roof and side wall geometrical detail were used as discussed in section 2.1. The next and final step was to add radiative and conductive heat transfer elements to represent heat loss through the SFP walls (see Figure 35 below).

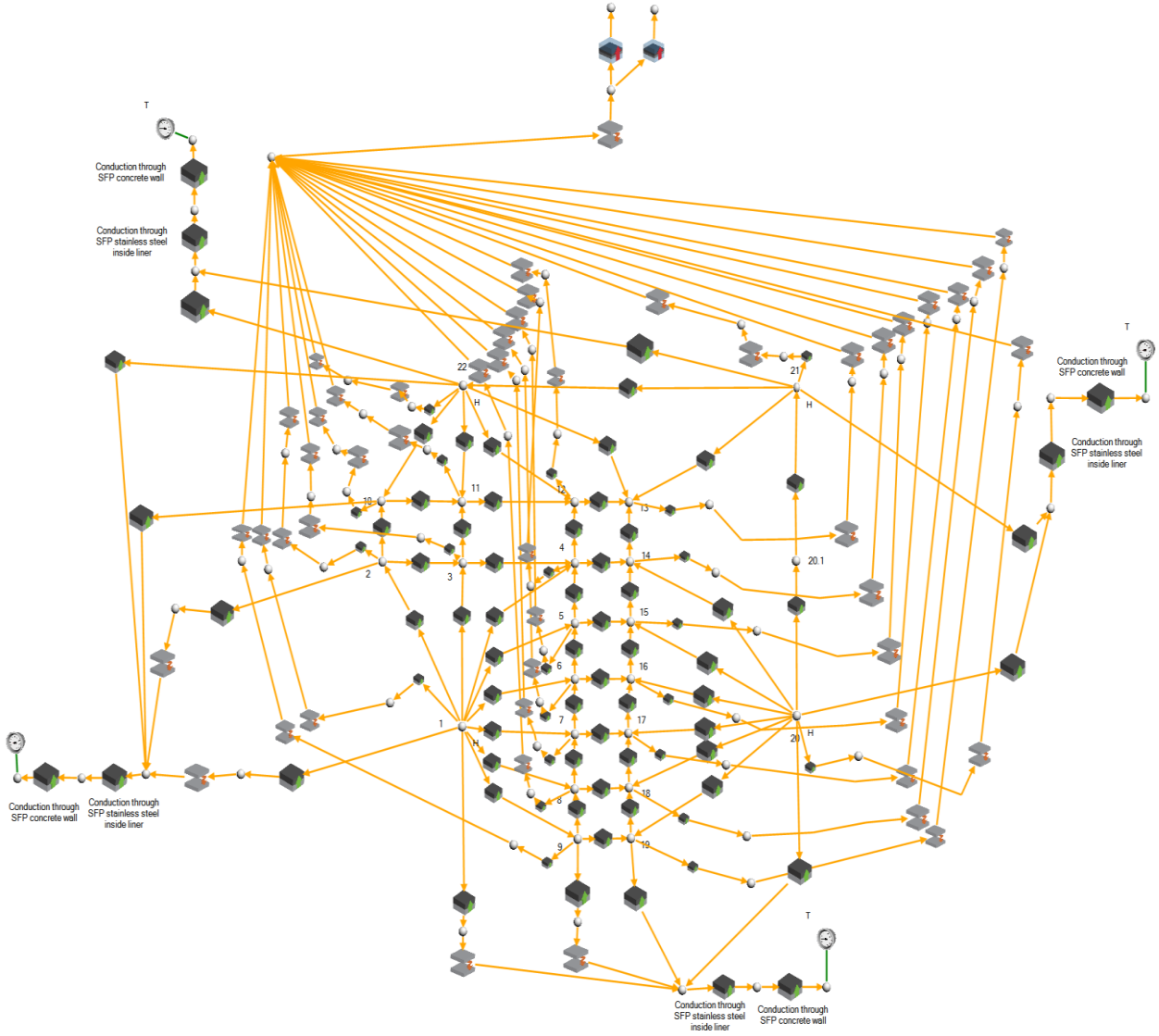

Figure 35: Complete modified Flownex 2-D network model of SFP

From Figure 35, heat losses through the SFP walls are represented by radiative and conduction heat transfer elements. Conductive heat transfer through the inner stainless steel SFP liner and then through the concrete wall to the environment are represented for all four walls respectively (see Appendix J for the input values). The network constructed in Figure 35 is analysed under the transient accident scenario to determine the average Fuel zone temperature increase during fuel uncovery to determine which Fuel zone will reach zirconium cladding oxidation temperatures in the shortest time period.

Assessment of the modified Flownex 2-D network model is discussed next.

6. Assessment of the Modified Flownex 2-D Network Model

The network model (Figure 35) is assessed next under transient conditions (see a summary of input data and sample calculations in Appendix L). This analysis will be discussed next.

Transient Analysis

The transient analysis for the severe accident was set-up in the modified 2-D Flownex network model to run from initial conditions of 60°C (normal operating temperature in SFP, as maintained by water cooling). It is further assumed that during complete loss of inventory, the cladding surface (i.e. Fuel zone) temperatures in all the discretized zones and the inner SFP walls are at 60°C and the FB roof and side walls are at 20°C respectively.

6.1 Temperature evolution analysis in the SFP

Figure 36 provides insight into the average temperature evolution of the respective discretized Fuel zones in the SFP up to 12 hrs after a complete loss of inventory.

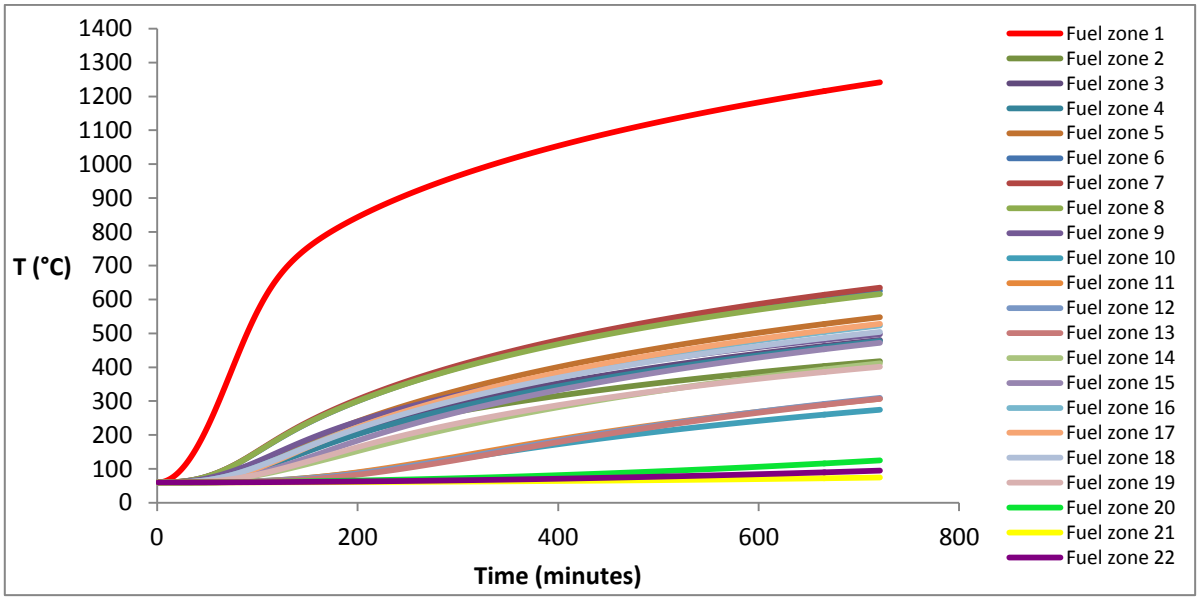

Figure 36: Average Temperature evolution of all Fuel zones up to 12 hrs after a complete loss of inventory

From Figure 36, Fuel zone 1 reached zirconium cladding oxidation temperature of 1204°C within circa 10.5 hours, following a complete loss of inventory. The rest of the Fuel zones are at relatively lower average temperatures. As expected, Fuel zone 1 reached zirconium cladding oxidation temperatures first due to the high heat load of the unloaded (discharged) core. It can also be observed that the Fuel zones closest to Fuel zone 1 (Fuel zone 6,7 and 8) having higher

temperatures (heating up much faster) than those further away, with Fuel zone 21 having the lowest temperature. See Figure 37 below for the average temperature evolution of the four main Fuel zones up to 12 hours after complete loss of inventory.

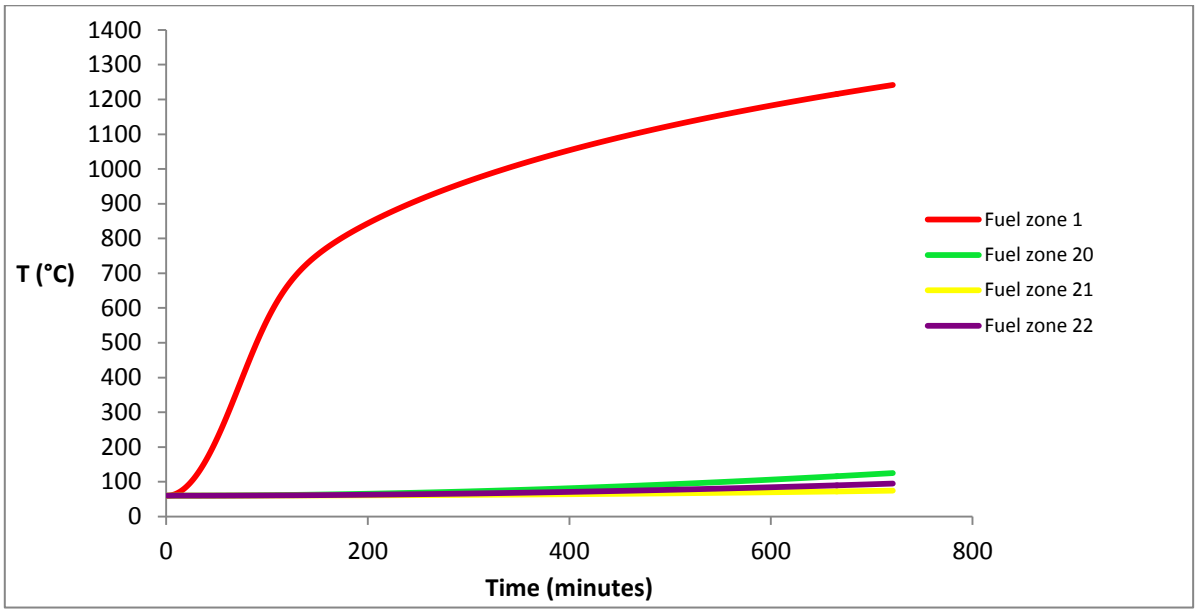

Figure 37: Average Temperature evolution of the main Fuel zones up to 12 hours after complete loss of inventory

From Figure 37, it can be observed that the average Fuel zone temperatures for Fuel zones 20 to 22 remain relatively low in comparison with Fuel zone 1, with Fuel zone 20 having the highest temperature and Fuel zone 21 the lowest of the three main neighbouring zones.

A temperature distribution analysis of each of the main Fuel zones (Unloaded core, Fuel zone 20, 21 and 22) in the SFP is discussed next.

6.2 Temperature evolution analysis in the four main Fuel zones

Unloaded (discharged) core -Fuel zones 1 to 9

Figure 38 below, depicts the average Fuel zone temperature evolution in the unloaded (discharged) core up to 12 hours after a complete loss of inventory.

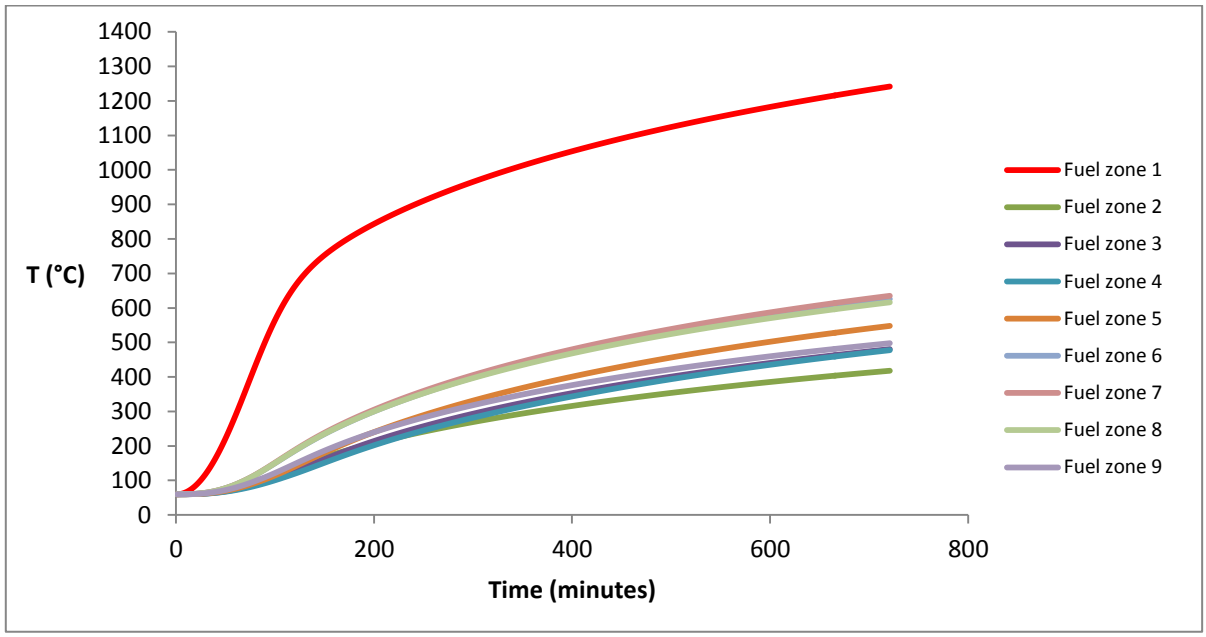

Figure 38: Average Temperature evolution of Fuel zones 1 to 9 unloaded (discharged) core up to 12hrs after complete loss of inventory

From Figure 38, it can be observed that Fuel zone 1 heats up the fastest and reach zirconium oxidation temperature within circa 10.5 hours. Fuel zones 2 to 9 heats up due to the higher heat load of Fuel zone 1. These zones lose heat to the other cooler zones, which is why they are cooler than Fuel zone 1.

Figure 39 below depicts the average temperatures of Fuel zones 2-9, 12 hrs after complete loss of inventory.

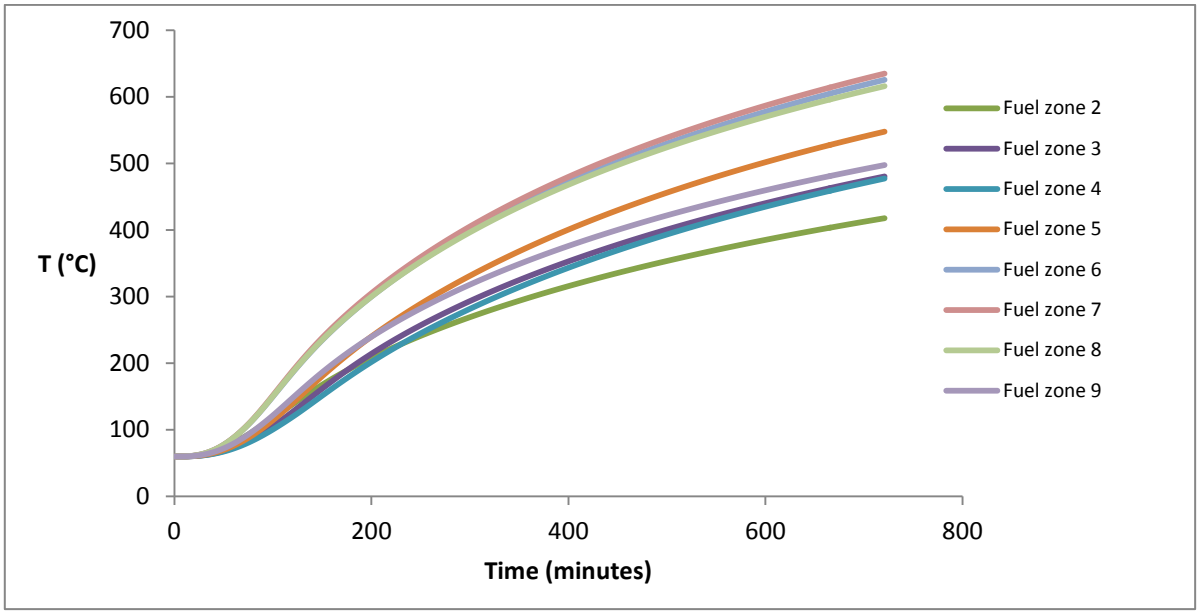

Figure 39: Average Temperature evolution of Fuel zones 2 to 9 up to 12 hrs after complete loss of inventory

From Figure 39, it can be observed that Fuel zone 7 of the unloaded (discharged) core reached the second highest temperature with Fuel zone 2 the lowest.

Fuel zones 14 to 20

Figure 40, below depicts the average Fuel zone temperature evolution around Fuel zone 20 up to 12 hours after a complete loss of inventory.

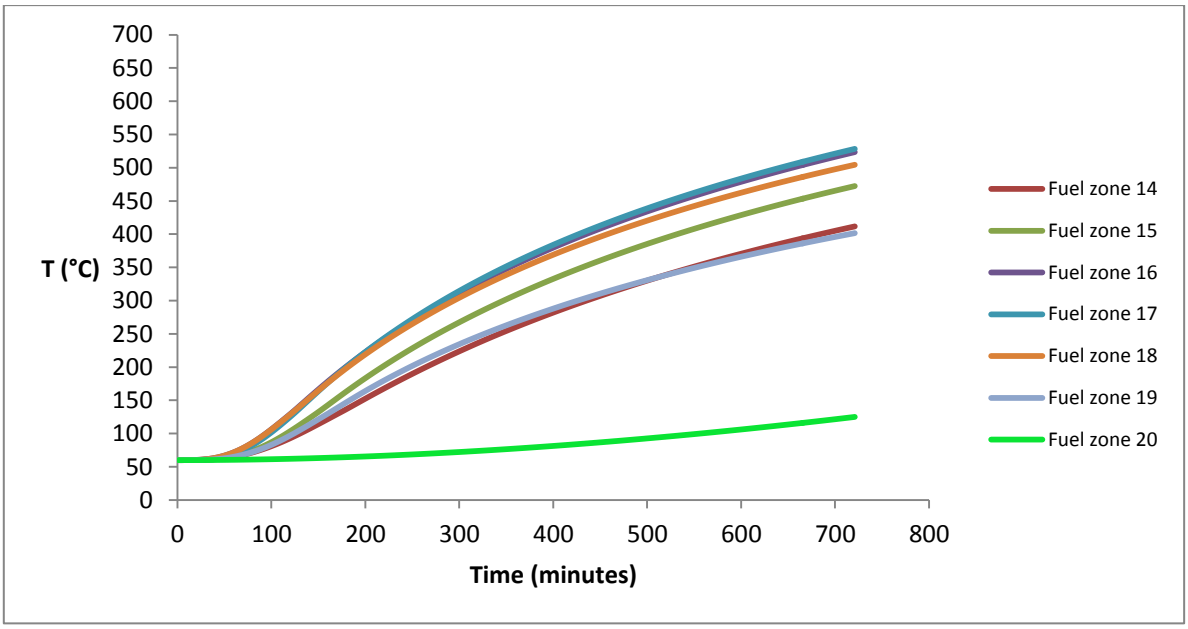

Figure 40: Average Temperature evolution of Fuel zones 14 to 20 up to 12 hrs after complete loss of inventory

From Figure 40 it can be observed that the heat transfer through conduction from Fuel zones 14 to 19 is giving rise to the heat up of Fuel zone 20.

Fuel zones 20 to 22

Figure 41, below depicts the average Fuel zone evolution in the Fuel zones 20 to 22 up to 12 hours after a complete loss of inventory.

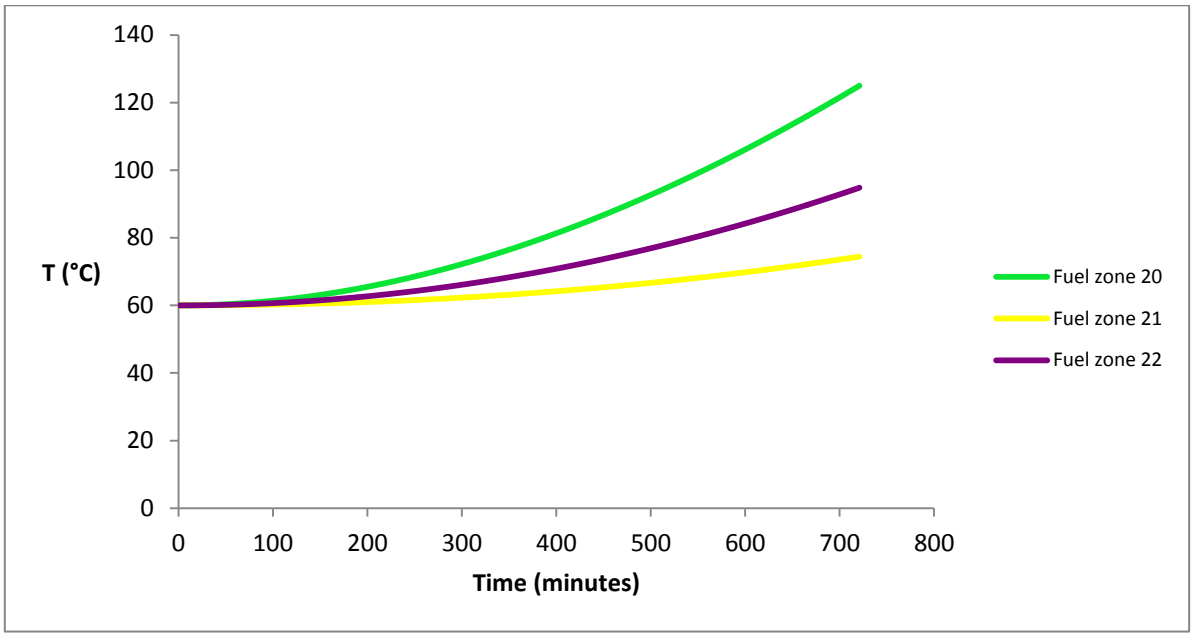

Figure 41: Average Temperature evolution of Fuel zones 20 to 22 up to 12 hrs after complete loss of inventory

From Figure 41, it can be observed that Fuel zone 21 has the lowest temperature increase as expected, since it is the furthest away from Fuel zone 1 (unloaded core) with the highest thermal capacity (see Table 6, for total number of SFAs/zone). The increase in temperature of Fuel zone 21 is primarily due to the conductive heat transfer from Fuel zones 20 and 22.

Conductive heat transfer between the respective Fuel zones will be discussed next.

6.3 Conductive heat transfer analysis in the SFP

Figure 42 provides insight into the total conductive heat transfer distribution between the four main Fuel zones in the SFP up to 12 hrs after a complete loss of inventory.

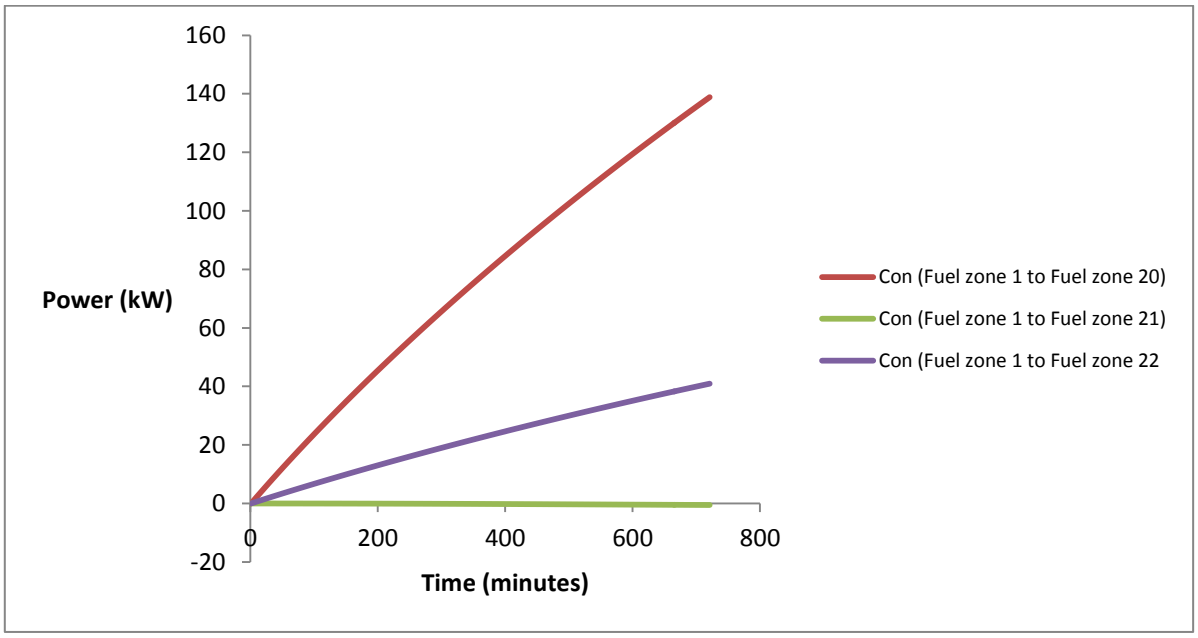

Figure 42: Conductive heat transfer distribution from Fuel zone 1 (unloaded core) to Fuel zones 20 to 22 respectively

From Figure 42, it can be observed that the highest amount of conductive heat transfer from Fuel zone 1 is to Fuel zone 20. This is due to the shorter heat flow distances and higher total heat flow area. As a result, Fuel zones 4 to 9, more specifically Fuel zones 6, 7 and 8 reached the highest temperatures of the periphery Fuel zones (also refer to Figure 39). The observation from Figure 42 also justifies why Fuel zone 20 reached a higher temperature than Fuel zones 21 and 22 (also see Figure 41).

Radiative heat transfer analysis will be discussed next.

6.4 Radiative heat transfer analysis in the SFP

Figure 43 provides insight into the radiative heat transfer distribution from the four main Fuel zones in the SFP up to 12 hrs after a complete loss of inventory.

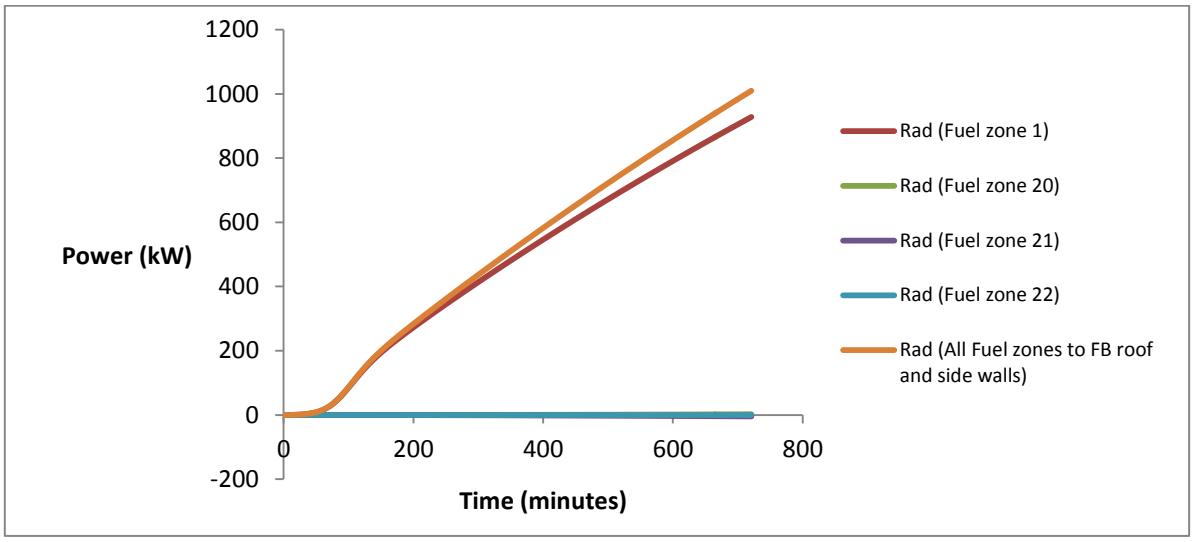

Figure 43: Radiative heat transfer distribution from the four main Fuel zones up to 12 hrs after a complete loss of inventory

From Figure 43, it can be observed that radiative heat transfer from Fuel zone 1 (unloaded core) is the dominant contributor of radiative heat transfer from all the Fuel zones to the FB roof and side walls. The high radiative heat transfer from Fuel zone 1 is a result of the rapid increase in Fuel zone temperature (see Figures 36 to 38). Radiative heat transfer from other Fuel zones is relatively small in comparison with Fuel zone 1 (see Figure 44 below).

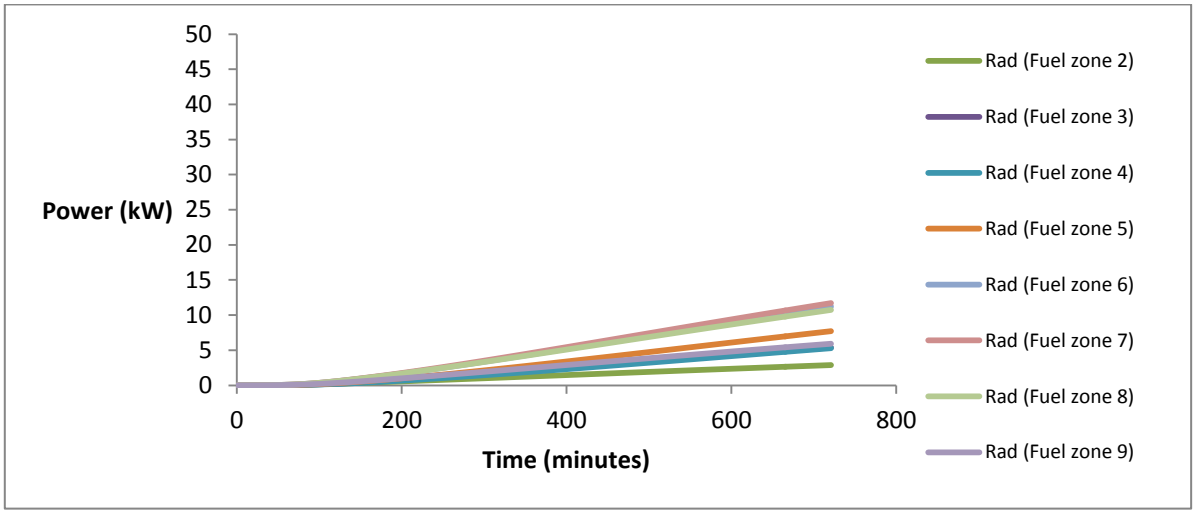

Figure 44: Radiative heat transfer from Fuel zones 2 to 9 up to 12 hrs after a complete loss of inventory

From Figure 44 above, it can be observed that radiative heat transfer from Fuel zones 2 to 9 are relatively small in comparison with the radiated heat transfer from Fuel zone 1.

An analysis of the SFP inside wall temperatures will be discussed next and the heat up of the FB roof and side walls up to 12 hrs after a complete loss of inventory.

6.5 SFP wall, FB roof and side wall inside temperatures

Figure 45 below provides a schematic of heat losses through the SFP walls; the walls are assigned as follows for easy reference:

Spent Fuel Wall- Left side: SFP-LS

Spent Fuel Wall- Top side: SFP-TS

Spent Fuel Wall- Right side: SFP-RS

Spent Fuel Wall- Bottom side: SFP-BS

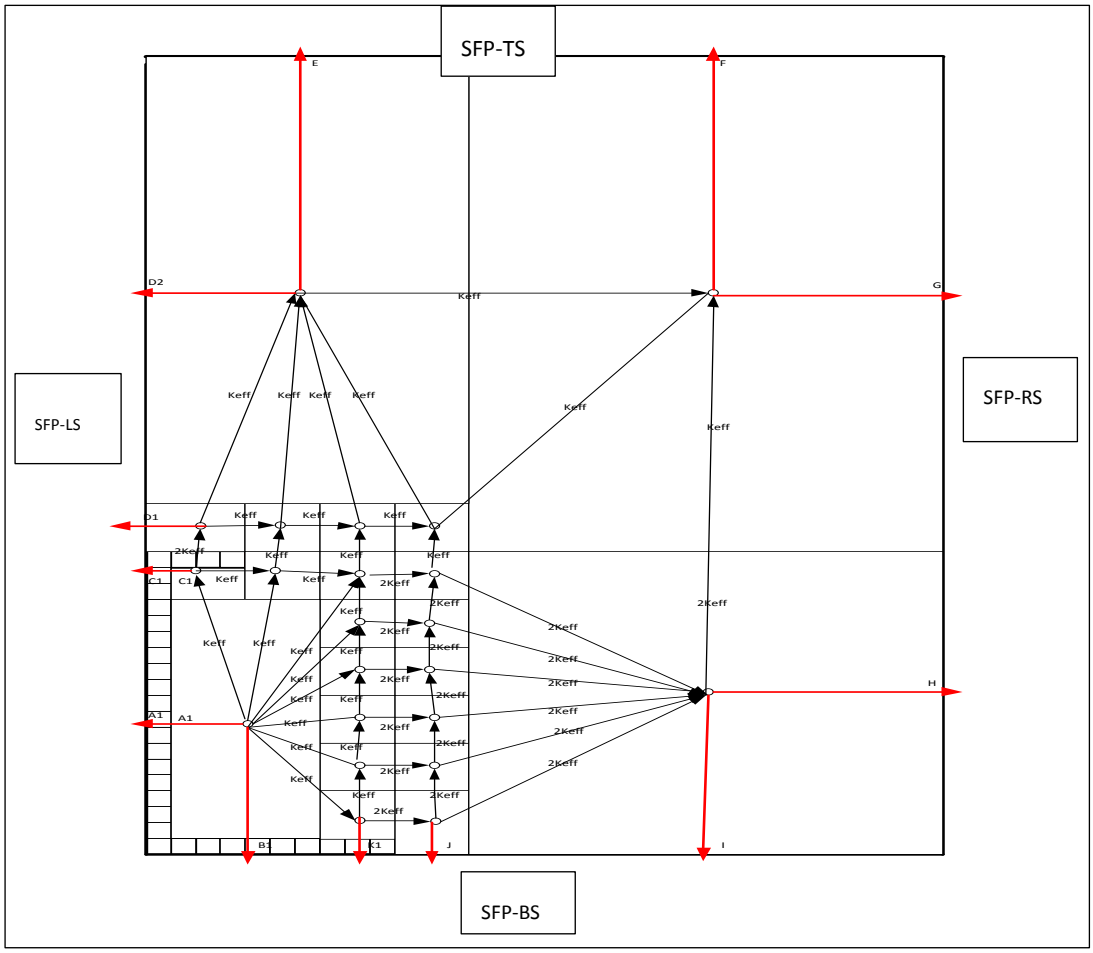

Figure 45: SFP side walls

Figure 46 below, depicts the temperature evolution of the inside SFP walls including the FB roof up to 12 hrs after a complete loss of inventory.

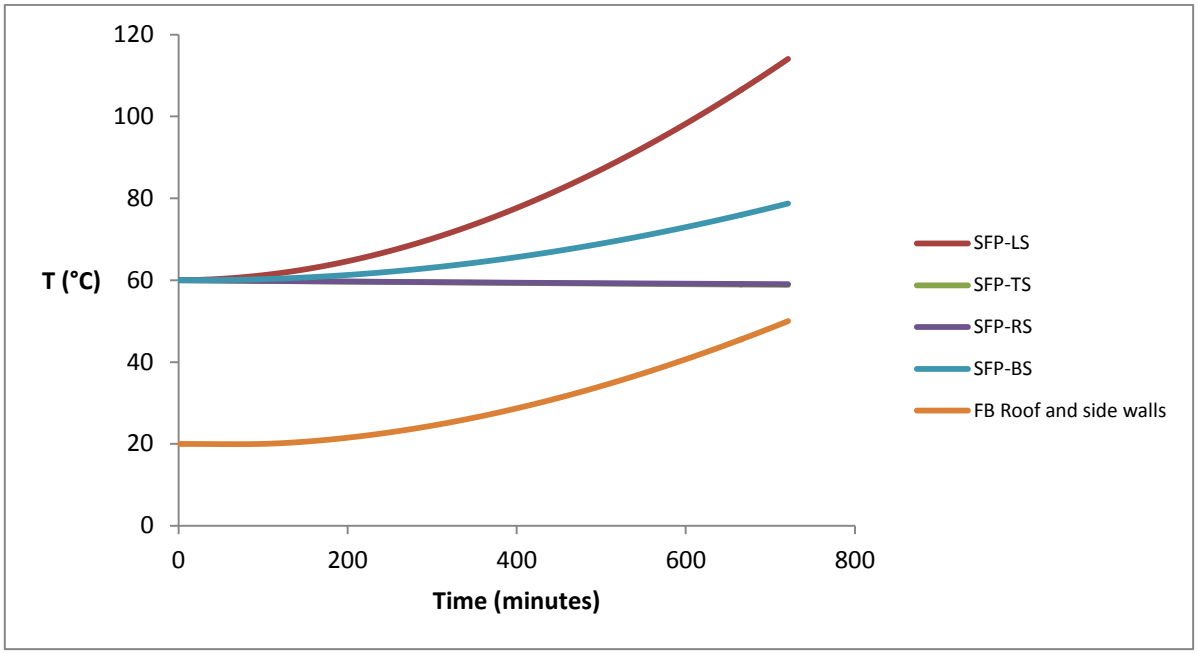

Figure 46: SFP walls and FB roof inside temperatures evolution up to 12 hrs after a complete loss of inventory

From Figure 46 above, it can be observed that the SFP-LS heat up faster than the rest of the SFP walls. This temperature increase is as a result of the heat conducted and radiated from Fuel zone 1. Also, it is expected that the SFP-LS and SFP-BS will heat up faster than the rest because it is directly heated up through Fuel zone 1. It is also expected that SFP-TS and SFP-RS will not heat up as rapid as SFP-LS and SFP-BS because of its relatively longer heat flow distances away from Fuel zone 1. The increase in inside temperature of the FB roof and side walls is attributed to the high radiative heat transfer from Fuel zone 1 as observed in Figure 43.

6.6 Conclusions

The modified 2-D Flownex network model provided valuable insight into the heat transfer from the discretized Fuel zones of the SFP and from the SFP to the SFP inside walls and FB roof, subsequent to the complete loss of inventory. Fuel zone 1 will reach zirconium cladding temperature (1204°C) within circa 10.5 hours after a complete loss of inventory. This is as expected due to the far higher heat load in the freshly unloaded (discharged) zone. In contrast, the more aged Fuel zone (20) only reached 125°C after 12 hours. The rapid increase in temperature from Fuel zone 1, resulted in a much larger radiative heat transfer to the FB roof and side walls.

7. Overall Conclusions and Recommendations

The Flownex code [31] proved to be a valuable tool to gain insight into the heat transfer modes in a SFP and FB during a complete loss of inventory. The Flownex network model that was developed initially offered a crude insight into the heat transfer modes especially the attempt made to include convective heat transfer in a quite complex geometrical scenario. However this model shows favourable results when compared to 3-D CFD studies by Boyd C.F (2000). It showed that radiative heat transfer becomes dominant as compared to natural convection at cladding temperatures above 600°C. This phenomenon is also supported by previous studies, viz. Benjamin *et al.*, 1979 [16] and Boyd C.F, 2000 [24].

The modified 2-D Flownex network model provided valuable insight into the heat transfer within the respective Fuel zones of the SFP and from the SFP to the SFP walls and FB roof and side walls. The model highlighted the strong variation in temperature with-in the SFP subsequent to the severe accident scenario. This is due to the large difference in heat generation between freshly unloaded and the more aged Fuel zones. By assessing the severe accident scenario, transient results showed that Fuel zone 1 will reach cladding oxidation temperature within circa 10.5 hours after a complete loss of inventory. This time period estimates obtained from this study can be used in developing appropriate coping strategies for preventing the onset of cladding oxidation and/or mitigating the consequences thereof. The model provided valuable insight into the heat-up characteristics of the respective Fuel zones as a result of the SFA layout in the SFP. It showed that under the severe accident scenario investigated with the given SFA layout in the SFP that Fuel zones at the periphery of the unloaded core within smaller heat flow distances and larger heat flow areas will heat up faster than those situated further from the unloaded (discharged) core with smaller heat flow areas.

For future research into the heat transfer phenomenon during severe accidents it is recommended that more sophisticated 3-D modelling software be used that also include the effect of cladding oxidation chemistry in order to provide more accurate predictions of average Fuel zone temperatures under high heat load scenarios in the SFP. The quantification of the amount of hydrogen accumulation during these scenarios could then also be predicted with more certainty.

The effect of forced ventilation on the Fuel zone heat-up characteristics was beyond the scope of this investigation. However, literature reveals that it plays an important role on Fuel zone temperatures which could be explored further in providing mitigation strategies for optimum cooling solutions during such scenarios.

8. Bibliography

[1] R.N. Jayaraj., C.Ganguly, “Recent Developments in Design and Manufacture of Uranium Dioxide Fuel Pellets for PHWRs in India,” in *Advanced fuel pellet materials and designs for water cooled reactors (IAEA-TECDOC-1416)*, Belgium, 2004.

[2] Nuclear Waste- San Onofre Safety, [Online]. Available: http://sanonofresafety.org. [Accessed 15 January 2016].

[3] US Nuclear Regulatory Commission- Technical Training Center, “Pressurized Water Reactor Systems (Reactor Concepts Manual),” [Online]. Available: http://www.nrc.gov. [Accessed 18 January 2016].

[4] E.E.Lewis, “Fundamentals of Nuclear Reactor Physics , Chapter 8- Energy Transport,” Academic Press, 2008.

[5] R.Slabbert, “Thermal-hydraulics simulation of a benchmark case for a typical Materials Test Reactor using FLOWNEX,” Master's thesis, North West University, Potchefstroom, 2011.

[6] U.S Nuclear Regulatory Commission, “Potential Safety Enhancements To Spent Fuel Pool Storage,” NRC Information Notice 2014-14, Washington, DC, 2014.

[7] International Atomic Energy Agency, “The Fukushima Daiichi Accident, Technical Volume 2/5 Safety Assesment,” Vienna, 2015.

[8] H.P.Nourbakhsh., G.Miao., and Z. Cheng, “Analysis of Spent Fuel Heatup Following Loss of Water in a Spent Fuel Pool (NUREG/CR-6441),” U.S. Nuclear Regulatory Commission, Washington, DC, 2002.

[9] A.Katliaka., V.Ognerubov., V.Vileiniskis and E.Uspuras, “Analysis of the Processes in Spent Fuel Pools in Case of Loss of Heat Removal due to Water Leakage,” Hindawi Publishing Corporation, Lithuania, 2013.

[10] M.Bales, “Regulatory Guide 1.224- Establishing Analytical Limits for Zirconium-Alloy Cladding Material,” U.S Nuclear Regulatory Commission, Washington D.C, March, 2014.

[11] V.L. Sailor., K.R. Perkins., J.R. Weeks and H.R. Connell, “Severe Accidents in Spent Fuel Pools in Support of Generic Safety Issue 82,” Department of Nuclear Energy, Upton, New York, 1987.

[12] Zirconium, “Oxidation of zirconium by steam,” [Online]. Available: https://en.wikipedia.org. [Accessed 18 January 2016].

[13] L. Perryman, “Severe Accident Management Guides (SAMGs) Training slides: Fukushima Daiichi Accident-NEP (rev1) ppt (Koeberg Internal Training),” 2013.

[14] Tokyo Electric Power Company, Inc, “"Fukushima Nuclear Accident Analysis Report",” TEPCO, 2012.

[15] R.M.Springman, “"Hi-Cool: An Autonomous Spent Fuel Cooling System",” *Holtec Technical Bulletin ,* vol. 1, p. p3, 2011.

[16] A.S. Benjamin., D.J. McCloskey., D.A. Powers and S.A. Dupree, “Spent Fuel Heatup Following Loss of Water During Storage (NUREG/CR-0649),” Sandia Laboratories, New Mexico, 1979.

[17] A.Kaliatka., V.Ognerubov., V.Vileiniskis and E.Uspuras, “Analysis of the Processes in Spent Fuel Pools in Case of Loss of Heat Removal due to Water Leakage,” *Hindawi Publishing Corporation, Science and Technology of Nuclear Installations,* vol. 2013, p. 12, 2013.

[18] F.Nimander, “Master Thesis " Investigation of Spent Nuclear Fuel Pool Coolability",” Sweden

Royal Institute of Technology, Sweden, 2011.

[19] Spent Nuclear Fuel, [Online]. Available: https://en.wikipedia.org. [Accessed August 2015].

[20] U.S.Nuclear Regulatory Commission, “Spent Fuel Storage in Pools and Dry Casks,” April 2015. [Online]. Available: http://www.nrc.gov/waste. [Accessed August 2015].

[21] Spent Fuel Pool, [Online]. Available: https://en.wikipedia.org. [Accessed August 2015].

[22] American Nuclear Society (ANS), “Decay heat power in light water reactors,” Illinois, USA, 2005.

[23] American Nuclear Society (ANS), “American National Standard for Decay Heat Power in Light Water Reactors (ANSI/ANS-5.1),” Illinois, USA, 1979.

[24] C.F. Boyd, “Predictions of Spent Fuel Heatup After a Complete Loss of Spent Fuel Pool Coolant (NUREG-1726),” Office of Nuclear Regulatory Research, Washington, 2000.

[25] Fuel Pool, [Online]. Available: https://en.wikipedia.org. [Accessed January 2016].

[26] M.Kennedy, “Modeling of the Spent Fuel Pool During Severe Accident Using the MAAP Code,” [Online]. Available: https://www.fauske.com. [Accessed March 2016].

[27] E.R.Lindgren and S.G.Durbin, “"Characterization of Thermal Hydraulic and Ignition Phenomena in Prototypic,Full Lenght Boiling Water Reactor Spent Fuel Assemblies After a Postulated Complete Loss-of-Coolant Accident",” US National Regulatory Commission, Washington, DC, 2013.

[28] J.Cardoni, “MELCOR Model for an Experimental 17x17 Spent Fuel PWR Assembly,” Sandia National Laboratories, New Mexico, 2010.

[29] Y.A.Cengel and M.A.Boles, “Thermodynamics an Engineering Approach (7th Edition),” McGraw-Hill, 2011.

[30] F.P.Incropera and D.P.De Witt, Introduction to Heat Transfer, Second Edition, New York: Wiley & Sons, 1990.

[31] FLOWNEX, “Flownex Simulation Environment- Libary Manual,” 2015.

[32] C.K.Wang.,C.G.Solomon and J.A.Pincheira, “Reinforced Concrete Design,” John Wiley and Sons, Inc, 2006.

[33] H.J.van Antwerpen, G.P.Greyvenstein, “Evaluation of a detailed radiation heat transfer model in a high temperature reactor systems simulation model,” *Nuclear Engineering and Design,* pp. 2985-2994, February 2008.

[34] Mahini, R.T., “The Effective Thermal Conductivity of a Fuel Assembly in a Storage Canister,” NUTECH Engineers, INC., San Jose, California 95119.

[35] Sung-Hwan Chung, Kyoung-Myoung Chae, Byung-I1 Choi and Heung-Young Lee, “Calculation of the Effective Thermal Conductivity for PWR Spent Fuel Assembly,” in *Nuclear Environment Technology Institute (NETEC)*, Korea.

[36] “The Engineering Toolbox,” [Online]. Available: http://www.engineeringtoolbox.com/dry-air-properties-d_973.html. [Accessed 3 05 2017].

[37] M.Bahrami, “Simon Frazer University,” [Online]. Available: http://www.sfu.ca/~mbahrami/ENSC%20388/Notes/Natural%20Convection.pdf. [Accessed 11 July 2017].

[38] B. Stephens, “CAE 331/513 Building Science Fall 2015, Week 2: Heat Transfer in buildings: Convection,” Built Environment Research, 3 September 2015. [Online]. Available: www.built-

envi.com. [Accessed 2 March 2016].

[39] F. Incropera, Fundamentals of Heat and Mass Transfer, New York: Wiley & Sons, 2002, 5th Edition.

[40] W.G.Geelhood and K.J. Luscher, “Material Property Correlations: Comparisons between FRAPCON-3.5, FRAPTRAN-1.5, and MATPRO,” U.S Nuclear Regulatory Comission, Washington, DC, 2014.

[41] Lecture slides, “One Dimensional, Steady-State Conduction with Thermal Energy Generation, chapter 3,” [Online]. Available: http://me.queensu.ca/Courses/MECH346/Notes.html . [Accessed May 2016].

[42] H.J.Van Antwerpen, “Modelling a pebble bed High Temperature Gas-cooled Reactor using a system-CFD approach (PhD-thesis),” North West University, 2009.

[43] Lecture slides (Lesson 34), “Cooling and Heating Load Calculations- Heat Transfer through Buildings Fabric Heat Loss/Gains,” [Online]. Available: http://nptel.ac.in/courses. [Accessed 20 January 2016].

Appendix A. Typical Core Heat Load Distribution

Decay Period (days)	Batch 1 1 Assembly (W)	Batch 2 4 Assemblies (W)	Batch 3 8 Assemblies (W)	Batch 4 40 Assemblies (W)	Batch 5 48 Assemblies (W)	Batch 6 56 Assemblies (W)	Average heat load per Assembly (160 FAs) (W)	Total Decay heat (W)
10	4.0E+04	1.0E+05	3.0E+05	1.0E+06	2.0E+06	2.0E+06	34E+03	5.44E+06

Table 7: Core discharge decay heat load (Watts) distribution-10days after shutdown

Batch #	Number of Fuel Assemblies	Average Uranium oxide mass per Fuel Assembly (tons)	Total Mass (tons)
1	1	0.46	0.46
2	4	0.458	1.832
3	8	0.46	3.68
4	40	0.464	18.56
5	48	0.464	22.272
6	56	0.464	25.984
Total uranium mass from core discharged			72.788

Table 8: Average uranium oxide mass per Spent Fuel Assembly in Zone 1

Number of Fuel Assemblies (Zone 2)	**Assuming average Uranium oxide Mass per Fuel Assembly (tons)**	**Total Mass (tons)**
710	0.462	328

Table 9: Average uranium oxide mass per Spent Fuel Assembly in Zone 2

Appendix B. Mathematical Derivation for Cladding Temperatures

Figure 47 below shows a SFR that is discretized into six segments (control volumes)

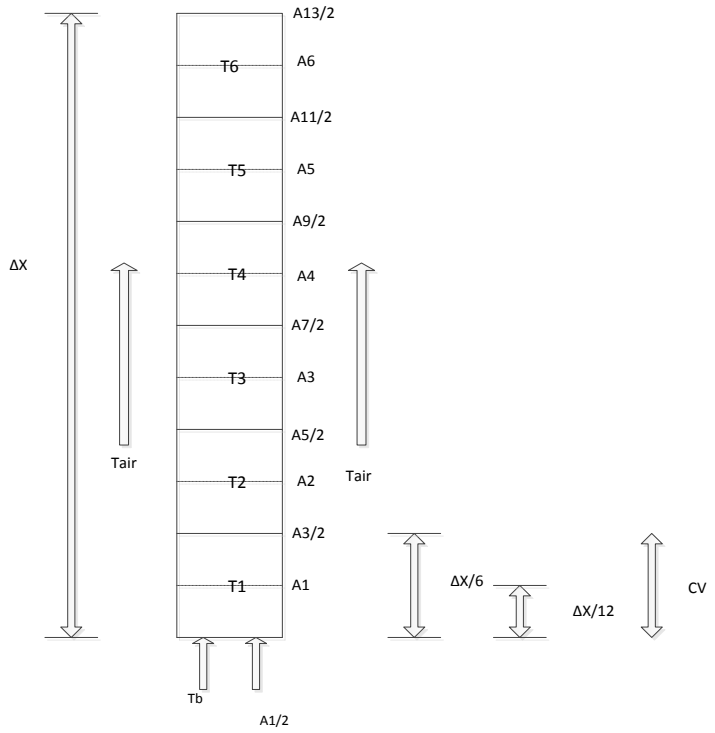

Figure 47: Discretization of transient conduction heat transfer through Spent Fuel Rod (6 control volumes)

where, T_b denotes the temperature at the base of the spent fuel rod and T_1 to T_6 denotes the temperatures along the vertical axis. Further, Δx denotes to the length of the spent fuel rod, T_{air} denotes the air temperature and $A_{1/2}$ to $A_{13/2}$ denotes the heat transfer areas. Each control volume (CV) is calculated by (A x).

From section 3.2, by discretizing the transient conduction Equation (3.2.2), the cladding temperatures T_1 to T_6 can be calculated as follows (considering only conduction and convection along the vertical axis of the SFRs),

For T_1 at control volume 1:

$$\mathrm{p}c_p A\Delta x \left[\frac{\left[T_1\,(t+\Delta t)-\,T_1(t)\right)}{\Delta t}\right] = \int_{A_{1/2}} k\,\frac{\partial T}{\partial x}\,nx\,(-)\,\partial \mathrm{A} + \int_{A_{3/2}} k\,\frac{\partial T}{\partial x}\,nx\,(+1)\,\partial \mathrm{A} - \mathrm{h}A_0\,(T_1(t) - \,T_{air})$$

$$= \,-kA\,\frac{T_1(t)-\,T_{\frac{1}{2}}\,(t)}{x_1-\,x_{1/2}} + kA\,\frac{T_2(t)-\,T_1\,(t)}{x_2-\,x_1} - \mathrm{h}A_0\,(T_1(t) - \,T_{air})$$

$$= -kA\frac{T_1(t)-T_{\frac{1}{2}}(t)}{\frac{\Delta x}{12}} + kA\frac{T_2(t)-T_1(t)}{\frac{\Delta x}{6}} - \mathrm{h}A_0\,(T_1(t) - T_{air})$$

$$T_1(t+\Delta t) = \left[-\frac{12kA}{\Delta x}\frac{\left[T_1(t)-T_{\frac{1}{2}}(t)\right]}{\mathrm{p}c_pA\Delta x}\right]\Delta t + \left[\frac{6kA}{\Delta x}\frac{[T_2(t)-T_1]}{\mathrm{p}c_pA\Delta x}\right]\Delta t - \left[\frac{hA_0[T_1(t)-T_{air}]}{\mathrm{p}c_pA\Delta x}\right]\Delta t + T_1$$

Where,

The term on the left-hand side refers to the peak cladding temperature over the first incremental length/ control volume of SFR as a function of time. The right-hand side terms refers to the heat transfer due to conduction and convection in the control volume over the specific increment at the specific time interval.

Similarly,

For CV2 (conduction and convection only)

$$\mathrm{p}c_pA\Delta x\left[\frac{[T_2(t+\Delta t)-T_2(t)]}{\Delta t}\right] = \int_{A_{3/2}} k\frac{\partial T}{\partial x}\,nx\,(-)\,\partial\mathrm{A} + \int_{A_{5/2}} k\frac{\partial T}{\partial x}\,nx\,(+1)\,\partial\mathrm{A} - \mathrm{h}A_0\,(T_2(t) - T_{air})$$

$$= -kA\frac{T_2(t)-T_1(t)}{x_2-x_1} + kA\frac{T_3(t)-T_2(t)}{x_3-x_2} - \mathrm{h}A_0\,(T_2(t) - T_{air})$$

$$= -kA\frac{T_2(t)-T_1(t)}{\frac{\Delta x}{6}} + kA\frac{T_3(t)-T_2(t)}{\frac{\Delta x}{6}} - \mathrm{h}A_0\,(T_2(t) - T_{air})$$

$$T_2(t+\Delta t) = \left[-\frac{6kA}{\Delta x}\frac{[T_2(t)-T_1(t)]}{\mathrm{p}c_pA\Delta x}\right]\Delta t + \left[\frac{6kA}{\Delta x}\frac{[T_3(t)-T_2]}{\mathrm{p}c_pA\Delta x}\right]\Delta t - \left[\frac{hA_0[T_2(t)-T_{air}]}{\mathrm{p}c_pA\Delta x}\right]\Delta t + T_2$$

For CV3 (conduction and convection only)

$$\mathrm{p}c_pA\Delta x\left[\frac{[T_3(t+\Delta t)-T_3(t)]}{\Delta t}\right] = \int_{A_{5/2}} k\frac{\partial T}{\partial x}\,nx\,(-)\,\partial\mathrm{A} + \int_{A_{7/2}} k\frac{\partial T}{\partial x}\,nx\,(+1)\,\partial\mathrm{A} - \mathrm{h}A_0\,(T_3(t) - T_{air})$$

$$= -kA\frac{T_3(t)-T_2(t)}{x_3-x_2} + kA\frac{T_4(t)-T_3(t)}{x_4-x_3} - \mathrm{h}A_0\,(T_3(t) - T_{air})$$

$$= -kA\frac{T_3(t)-T_2(t)}{\frac{\Delta x}{6}} + kA\frac{T_4(t)-T_3(t)}{\frac{\Delta x}{6}} - \mathrm{h}A_0\,(T_3(t) - T_{air})$$

$$T_3(t+\Delta t) = \left[-\frac{6kA}{\Delta x}\frac{[T_3(t)-T_2(t)]}{\mathrm{p}c_pA\Delta x}\right]\Delta t + \left[\frac{6kA}{\Delta x}\frac{[T_4(t)-T_3]}{\mathrm{p}c_pA\Delta x}\right]\Delta t - \left[\frac{hA_0[T_3(t)-T_{air}]}{\mathrm{p}c_pA\Delta x}\right]\Delta t + T_3$$

For CV4 (conduction and convection only)

$$\mathrm{p}c_p A\Delta x\left[\frac{[T_4\,(t+\Delta t)-T_4(t)]}{\Delta t}\right] = \int_{A_{7/2}} k\frac{\partial T}{\partial x}\,nx\,(-)\,\partial \mathrm{A} + \int_{A_{9/2}} k\frac{\partial T}{\partial x}\,nx\,(+1)\,\partial \mathrm{A} - \mathrm{h}A_0\,(T_4(t) - T_{air})$$

$$= -kA\frac{T_4(t)-T_3\,(t)}{x_4-x_3} + kA\frac{T_5(t)-T_4\,(t)}{x_5-x_4} - \mathrm{h}A_0\,(T_4(t) - T_{air})$$

$$= -kA\frac{T_4(t)-T_3\,(t)}{\frac{\Delta x}{6}} + kA\frac{T_5(t)-T_4\,(t)}{\frac{\Delta x}{6}} - \mathrm{h}A_0\,(T_4(t) - T_{air})$$

$$T_4\,(t+\Delta t) = \left[-\frac{6kA}{\Delta x}\frac{[T_4\,(t)-T_3\,(t)]}{\mathrm{p}c_p A\Delta x}\right]\Delta t + \left[\frac{6kA}{\Delta x}\frac{[T_5(t)-T_4]}{\mathrm{p}c_p A\Delta x}\right]\Delta t - \left[\frac{hA_0[T_4(t)-T_{air}]}{\mathrm{p}c_p A\Delta x}\right]\Delta t + T_4$$

For CV5 (conduction and convection only)

$$\mathrm{p}c_p A\Delta x\left[\frac{[T_5\,(t+\Delta t)-T_5(t)]}{\Delta t}\right] = \int_{A_{9/2}} k\frac{\partial T}{\partial x}\,nx\,(-)\,\partial \mathrm{A} + \int_{A_{11/2}} k\frac{\partial T}{\partial x}\,nx\,(+1)\,\partial \mathrm{A} - \mathrm{h}A_0\,(T_5(t) - T_{air})$$

$$= -kA\frac{T_5(t)-T_4\,(t)}{x_5-x_4} + kA\frac{T_6(t)-T_5\,(t)}{x_6-x_5} - \mathrm{h}A_0\,(T_5(t) - T_{air})$$

$$= -kA\frac{T_5(t)-T_4\,(t)}{\frac{\Delta x}{6}} + kA\frac{T_6(t)-T_5\,(t)}{\frac{\Delta x}{6}} - \mathrm{h}A_0\,(T_5(t) - T_{air})$$

$$T_5\,(t+\Delta t) = \left[-\frac{6kA}{\Delta x}\frac{[T_5\,(t)-T_4\,(t)]}{\mathrm{p}c_p A\Delta x}\right]\Delta t + \left[\frac{6kA}{\Delta x}\frac{[T_6(t)-T_5]}{\mathrm{p}c_p A\Delta x}\right]\Delta t - \left[\frac{hA_0[T_5(t)-T_{air}]}{\mathrm{p}c_p A\Delta x}\right]\Delta t + T_5$$

For CV6 (conduction and convection only)

$$\mathrm{p}c_p A\Delta x\left[\frac{[T_6\,(t+\Delta t)-T_6(t)]}{\Delta t}\right] = \int_{A_{11/2}} k\frac{\partial T}{\partial x}\,nx\,(-)\,\partial \mathrm{A} + \int_{A_{13/2}} k\frac{\partial T}{\partial x}\,nx\,(+1)\,\partial \mathrm{A} - \mathrm{h}A_0\,(T_6(t) - T_{air})$$

$$= -kA\frac{T_6(t)-T_5\,(t)}{x_6-x_5} + kA\frac{T_{\frac{13}{2}}(t)-T_6\,(t)}{x_{\frac{13}{2}}-x_6} - \mathrm{h}A_0\,(T_6(t) - T_{air})$$

$$= -kA\frac{T_6(t)-T_5\,(t)}{\frac{\Delta x}{6}} + kA\frac{T_{\frac{13}{2}}(t)-T_6\,(t)}{\frac{\Delta x}{12}} - \mathrm{h}A_0\,(T_6(t) - T_{air})$$

$$T_6\,(t+\Delta t) = \left[-\frac{6kA}{\Delta x}\frac{[T_6\,(t) - T_5\,(t)]}{\mathrm{p}c_p A\Delta x}\right]\Delta t + \left[\frac{12kA}{\Delta x}\frac{\left[T_{\frac{13}{2}}(t) - T_6\right]}{\mathrm{p}c_p A\Delta x}\right]\Delta t - \left[\frac{hA_0[T_6(t) - T_{air}]}{\mathrm{p}c_p A\Delta x}\right]\Delta t + T_6$$

Appendix C. Flownex Network Model-Calculation of Reynolds Number

From equation 3.2.5, the Reynolds number is given as:

$$Re = \frac{\mathrm{p}\, V\, D_H}{\mu} = \left|\frac{\dot{\mathrm{m}}\, D_H}{\mu}\right|$$

From equation 3.2.6, the hydraulic diameter is given as

$$D_H = \frac{4A}{P}$$

Table 10 depicts the geometrical values used in one Fuel Assembly (dimensions as depicted in Figures 9 and 10)

X1	Flow area available to Flownex model	$(0.227)^2$ = 0.051529 m^2
X2	Inside Fuel assembly flow area (no rods)	$(0.220)^2$ = 0.0484 m^2
X3	Inside Fuel Assembly perimeter	4 x 0.220 = 0.88 m
X4	Cross-section area of rods (264 *πd^2 /4)	0.018712896 m^2
X5	Cross-section area of control rods (25*πd^2 /4)	0.001772054 m^2
X6	Perimeter of all rods (289*πd)	8.62524263 m
X7	Total wetted perimeter (X3 +X6)	9.50524263 m
X8	Total flow area (X2-X4-X5)	0.02791505 m^2
X9	Hydraulic diameter (4A/P) = 4*X8/X7	0.011747222 m

Table 10: Geometrical values used in one Fuel Assembly

From the heat load scenarios assessed in section 4.3, the following mass flows and densities were obtained. Dynamic viscosities for air were obtained using viscosity tables in reference [36]. The Reynolds numbers were calculated for each heat load scenario in Table 11 below.

Z1 (heat load - kW)	Air density (kg/m^3)	Air mass flow (kg/s)	Max Cladding T	Dynamic viscosity (kg/m.s)*10^-05	Re
Z1 (100kW) vs Z2 (20kW)	0.622795156	0.527067745	319.5542434	3.017	205.233
Z1 (150kW) vs Z2 (30kW)	0.51883838	0.478371301	463.0752724	3.482	161.388
Z1 (200kW) vs Z2 (40kW)	0.445011766	0.418671404	615.9473877	3.897	126.205
Z1 (250kW) vs Z2 (50kW)	0.388732845	0.35221852	780.1993171	4.153	99.629
Z1 (350kW) vs Z2 (70kW)	0.306657287	0.188178536	1299.30543	5.457	40.509
Z1 (500kW) vs Z2 (100kW)	0.262099821	0.071075535	1809.495112	6.008	13.897

Table 11: Calculation of Reynolds numbers for the respective heat load scenarios

From Table 11 above, the Reynolds numbers for all the heat load scenarios were assessed, and confirms that the Flownex Network Model operated under laminar flow (Re <2300) conditions.

Appendix D. Input Parameters Used in the Flownex Network Model

The geometric values used for input to the Flownex network model are depicted in section 2.1

Sample input data to the respective HTEs for a single layer as depicted in Figure 48 will be given below. The input data will be the same for all six respective layers (as depicted in Figure 18).

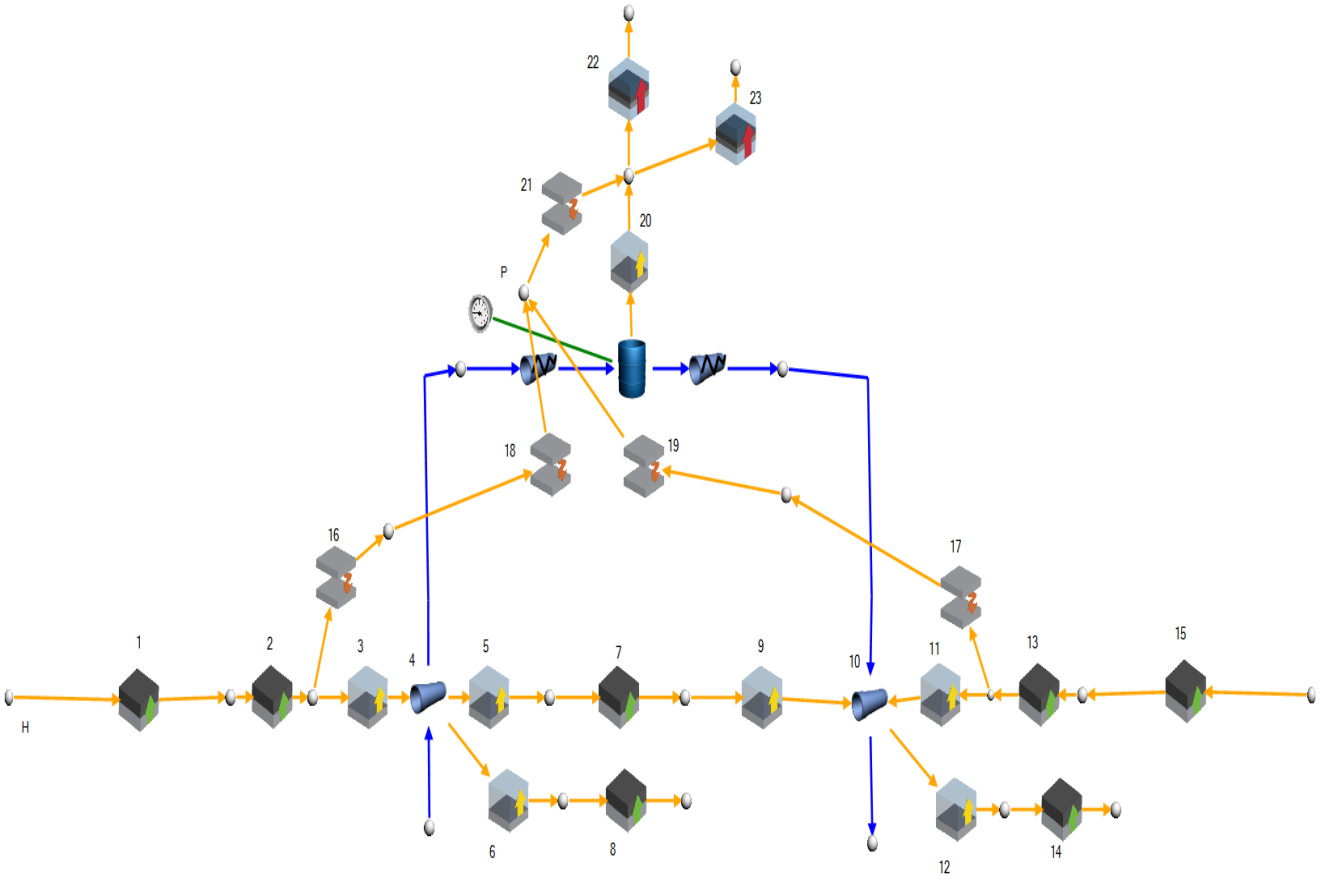

Figure 48: Top incremental layer of the Flownex Network Model

HTE 1- Conduction[1] Through Uranium in Zone 1		
Material	Uranium oxide	
Geometry		
Length	0.00415	
Height	0.0083	
Inlet area specification	Specify area	
Area	2πrh*No of FRs	
	0	m^2
Outlet area specification	Specify area	
Area	2πrh*No of FRs	
	675.84	m^2

HTE 2- Conduction[1] Through Zirconium Cladding in Zone 1		
Material	Zirconium	
Geometry		
Length	0.0006	
Height	0.0095	
Inlet area specification	Specify area	
Area	2πrh*No of FRs	
	675.84	m^2
Outlet area specification	Specify area	
Area	2πrh*No of FRs	
	777.2	m^2

HTE 3- Convection from Zone 1 Cladding		
Upstream area specification	Specify area	
Area	777.2	m^2
Convection		
Laminar Nusselt number[2]	4	

Note 1- Refer to Figure 15 that illustrate input parameters to Conduction heat transfer elements (CHTEs). All linear geometry is given in meters.

Note 2-The value for Nusselt number, N_u, depends on the heat transfer regime (forced convection, natural convection or mixed convection) flow condition (Turbulent vs Laminar) and geometry. Nourbakhsh et al, 2001, indicated that for laminar fully developed forced convection along rod bundles (inside FAs) the Nusselt number is taken as a constant 8 [8]. For the purpose of this analysis where laminar air flow and natural convection is assumed a value of 4 was used.

Element 4- Air Flow Area- Zone 1		
Geometry		
Geometry option	Specify geometry	
Wall thickness	0	m
Length	0.615	m
Options		
Cross sectional option	Circumference and area	
Variable area	No	
Inlet		
Circumference	29.8	mm
[3]Area	87.9	mm^2
Losses		
Roughness option	Specify manually	
Primary loss type	Darcy Weisbach	
Roughness	30	µm
Discretisation		
Number of increments	1	
Number in parallel	42240	

HTE 5- Convection from Zone 1 Cladding to IRW		
Upstream area specification	Specify area	
Area	6.3	m^2
Convection[4]		
Convection coefficient option	Constant	
h	1	W/ m^2.K

HTE 6- Convection from Zone 1 Cladding to ORW		
Upstream area specification	Specify area	
Area	6.3	m^2
Convection[4]		
Convection coefficient option	Constant	
h	1	W/ m^2.K

Note 3: $A_{Pitch(FR)} = (1.26 *10^{-2})^2 = 0.00015876\ m^2$

$A_{Cross\ section\ (FR)} = \Pi d^2/4 = 7.088*10^{-5}\ m^2$

$A_{Flow\ (per\ FR)} = A_{Pitch(FR)} - A_{Cross\ section\ (FR)} = 0.00008788\ m^2 = 87\ mm^2$

Note 4: Since the fluid velocity associated with natural convection is relatively low, the heat transfer coefficient encountered in natural convection is also low, hence a heat transfer coefficient of 1 $W/m^2.K$ was assumed [37].

HTE 7- Conduction Through IRW		
Material	Stainless Steel	
Geometry		
Length	0.007	
Height	9	
Inlet area specification	Specify area	
	6.3	m^2
Outlet area specification	Specify area	
Area		
	6.3	m^2

HTE 8- Conduction Through ORW-Zone 1		
Material	Stainless Steel	
Geometry		
Length	0.0035	
Height	9	
Inlet area specification	Specify area	
	6.3	m^2
Outlet area specification	Specify area	
Area		
	6.3	m^2

HTE 9- Convection from IRW		
Upstream area specification	Specify area	
Area	6.3	m^2
Convection		
Convection coefficient option	Constant	
h	1	$W/ m^2.K$

Element 10- Air Flow area-Zone 2		
Geometry		
Geometry option	Specify geometry	
Wall thickness	0	m
Length	0.615	m
Options		
Cross sectional option	Circumference and area	
Variable area	No	
Inlet		
Circumference	29.8	mm
Area	87.9	mm^2
Losses		
Roughness option	Specify manually	
Primary loss type	Darcy Weisbach	
Roughness	30	µm
Discretisation		
Number of increments	1	
Number in parallel	187440	

HTE 11- Convection from Zone 2 Cladding		
Upstream area specification	Specify area	
Area	3448.9	m^2
Convection		
Laminar Nusselt number	4	

HTE 12- Convection to Zone 2 -ORW		
Upstream area specification	Specify area	
Area	22.4	m^2
Convection		
Convection coefficient option	Constant	
h	1	$W/ m^2.K$

HTE 13- Conduction Through Zirconium Cladding-Zone 2		
Material	Zirconium	
Geometry		
Length	0.0006	
Height	0.0095	
Inlet area specification	Specify area	
Area		
	2999	m^2
Outlet area specification	Specify area	
Area		
	3448.9	m^2

HTE 14- Conduction Through ORW-Zone 2		
Material	Stainless Steel	
Geometry		
Length	0.0035	
Height	32	
Inlet area specification	Specify area	
Area		
	22.4	m^2
Outlet area specification	Specify area	
Area		
	22.4	m^2

HTE 15- Conduction Through Uranium in Zone 2		
Material	Uranium oxide	
Geometry		
Length	0.00415	
Height	0.0083	
Inlet area specification	Specify area	
Area	2πrh*No of FRs	
	0	m^2
Outlet area specification	Specify area	
Area	2πrh*No of FRs	
	2999	m^2

HTE 16- Radiation from SFP –Zone 1[5]		
Radiation type	Surface radiation only	
Emissivity	0.7	
Area specification	Specify area	
Area	18	m^2

HTE 17- Radiation from SFP –Zone 2		
Radiation type	Surface radiation only	
Emissivity	0.7	
Area specification	Specify area	
Area	82	m^2

HTE 18- Spatial Radiation from Zone 1		
Radiation type	Spatial radiation only	
Form Factor F12	1	
Area specification	Specify area	
Area	18	m^2

HTE 19- Spatial Radiation from Zone 2		
Radiation type	Spatial radiation only	
Form Factor F12	1	
Area specification	Specify area	
Area	82	m^2

HTE 20- Convection from SFP TO FB		
Upstream area specification	Specify area	
Surface area	100	m^2
Convection coefficient option	Constant	
h	4	$W/ m^2.K$

HTE 21- Surface Radiation to FB		
Radiation type	Surface radiation only	
Emissivity	0.95	
Area specification	Specify area	
Area	894	m^2

Note 5: Complete plan view is assumed to be at the same temperature (refer to the main assumptions in section 2.3; zones 1 & 2 are treated as respective composite SFAs

HTE 22- Composite Element-Conduction Through FB Roof		
Conduction		
Area Upstream surface	480	m^2
Thickness in element direction	0.25	m
Area downstream surface	480	m^2
Material	Specify locally	
Capacitance	1637	kJ/ m^3.K
Conductivity in element direction	1.4	W/m.K
Conductivity in element cross direction	1.4	W/m.K
Convection/Radiation and wall Flux		
Upstream	Adiabatic	
Downstream	Convection	
Convection option	To ambient	
Convection area option	Specify area	
Convection area	480	m^2
h[6]	5	W/ m^2.K
T(ambient) convection	20	°C

HTE 23- Composite element-Conduction through FB walls		
Conduction		
Area Upstream surface	414	m^2
Thickness in element direction	0.8	m
Area downstream surface	1656	m^2
Material	Specify locally	
Capacitance	1637	kJ/ m^3.K
Conductivity in element direction	1.4	W/m.K
Conductivity in element cross direction	1.4	W/m.K
Convection/Radiation and Wall Flux		
Upstream	Adiabatic	
Downstream	Convection	
Convection option	To ambient	
Convection area option	Specify area	
Convection area	1656	m^2
h[6]	5	W/ m^2.K
T(ambient) convection	20	°C

Note 6: Magnitude of convective heat transfer coefficients from building roofs depends largely on surface roughness and air velocity and ranges between 5-30 W/m^2K, for this scenario a conservative value of 5 W/m^2K was assumed [38].

Appendix E. Fluent (version 5) Code Input Parameters Used in the Flownex Network Model

Sample input data to the respective HTEs for a single layer as depicted in Figure 49 will be given below. The input data will be the same for all six layers respectively (as depicted in Figure 21).

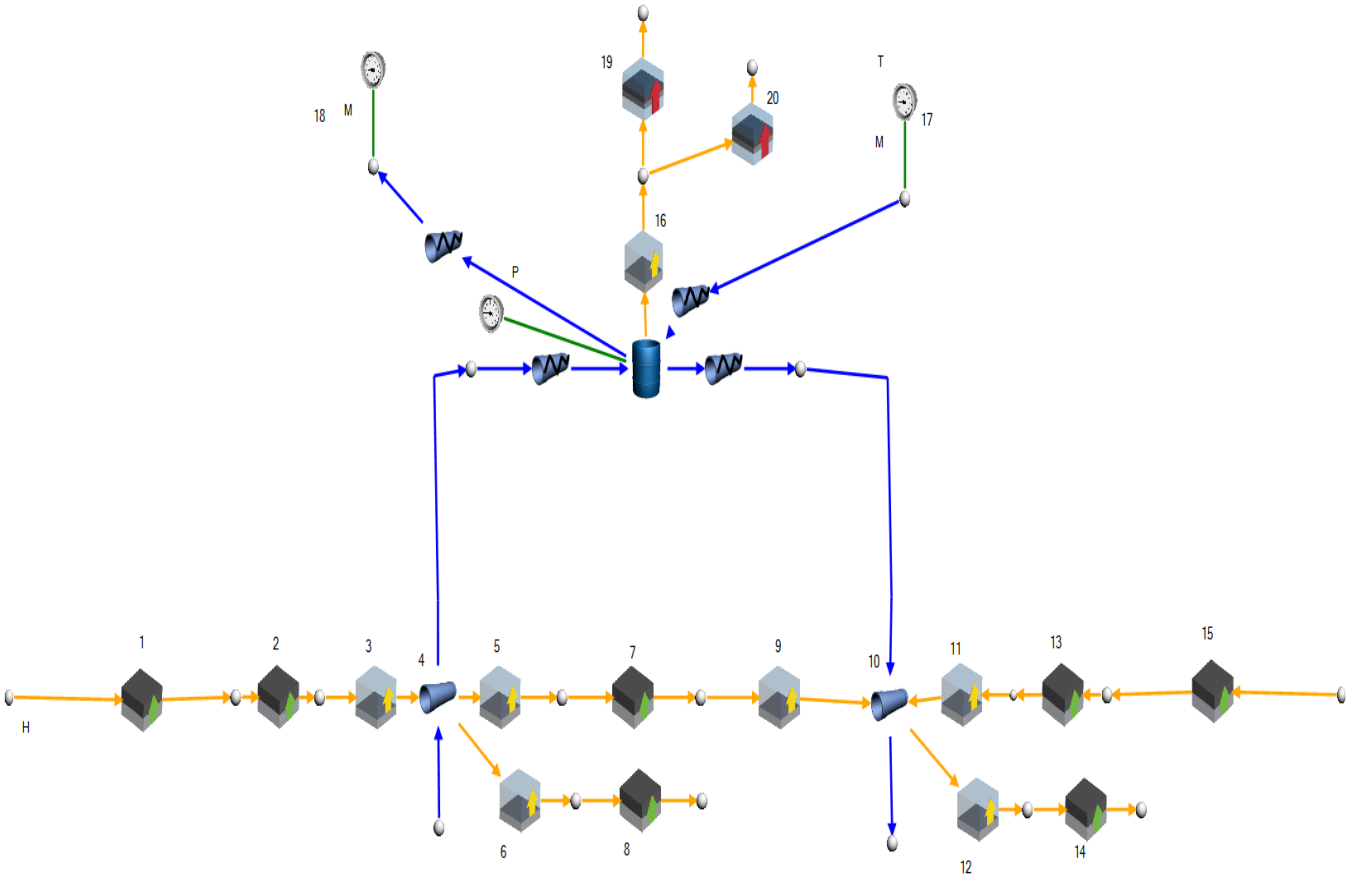

Figure 49: Top incremental layer of the FLUENT (version 5) model

Input Data and Sample Calculations to HTE in Flownex Network Model (Using the FLUENT CODE Geometries)									
Input Parameters									
					Stainless Steel			**Concrete**	
	Zone 1	**Zone 2**	**Uranium oxide**	**Zirc Clad**	**IRW**	**ORW-Z1**	**ORW-Z2**	**FB Roof**	**FB Side Walls**
Density (ρ,kg/ m^3)			10970	6500	7800	7800	7800	1860	1860
Thermal Conductivity (k, W/m.K)			3.6	13	23	23	23	2	2
Specific Heat capacity (cp, kJ/kg.K)			0.247	0.33	0.58	0.58	0.58	0.88	0.88
Emissivity				0.7	0.2	0.2	0.2	0.95	0.95
Thickness (L,m)			0.009976	0.0006	0.039728	0.019864	0.019864	0.25	0.8
Inside radius - (m)			0.004988	0.004988					
Outside Radius-(m)			0.004988	0.005588					
Capacitance (kJ/ m^3.K)			2709.59	2145				1636.8	1636.8
Height (m)				0.011176	0	0	0	31.36	40.35
Number of Fuel Rods	64800	275400							
Fuel Rod Outside Diameter (m)			0.009976	0.011176					
Total Active Length (z, m)			3.8	3.8	4.3	4.3	4.3	40.35	12.4
Area on Top of SFP (m^2)	19.5	80.634							
Inside Area (m^2)					46.354	61.49	110.682	1265.376	444.602
Outside Area (m^2)					46.354	61.49	110.682	1265.376	1778.408
Heat Input (MW)	0.370	0.733							

	FA	FRs per bundle	Watts/FA	Total Heat load	Total FRs
			48 months	48 months	
				MW	
f1,hot	800	81	462	0.3696	64800
f2, Med hot	267	81	360	0.09612	21627
f3, ,Med Cold	267	81	304	0.081168	21627
f4, cold	2866	81	194	0.556004	232146
	3400			0.733292	275400

HTE 1- Conduction Through Uranium in Zone 2		
Material	Uranium oxide	
Geometry		
Length	0.004988	
Height	0.009976	
Inlet area specification	Specify area	
Area	2πrh*No of FRs	
	0	m^2
Outlet area specification	Specify area	
Area	2πrh*No of FRs	
	5452.92	m^2

HTE 2- Conduction Through Zirconium Cladding in Zone 2		
Material	Uranium oxide	
Geometry		
Length	0.0006	
Height	0.011176	
Inlet area specification	Specify area	
Area	2πrh*No of FRs	
	5452.92	m^2
Outlet area specification	Specify area	
Area	2πrh*No of FRs	
	6120.7	m^2

HTE 3- Convection from Zone 2 Cladding		
Upstream area specification	Specify area	
Area	6120.7	m^2
Convection		
Laminar Nusselt number	4	

Element 4- Air Flow Area		
Geometry		
Geometry option	Specify geometry	
Wall thickness	0	m
Length	0.633	m
Options		
Cross sectional option	Circumference and area	
Variable area	No	
Inlet		
Circumference	35.09	mm
Area	108.7	mm^2
Losses		
Roughness option	Specify manually	
Primary loss type	Darcy Weisbach	
Roughness	30	µm
Discretisation		
Number of increments	1	
Number in parallel	275400	

HTE 5- Convection from Zone 2 Cladding to IRW		
Upstream area specification	Specify area	
Area	7.73	m^2
Convection		
Convection coefficient option	Constant	
h	1	$W/ m^2.K$

HTE 6- Convection from Zone 2 Cladding to ORW		
Upstream area specification	Specify area	
Area	18.45	m^2
Convection		
Convection coefficient option	Constant	
h	1	W/ m^2.K

HTE 7- Conduction through IRW		
Material	Stainless Steel	
Geometry		
Length	0.0397	
Height	10.78	
Inlet area specification	Specify area	
	7.73	m^2
Outlet area specification	Specify area	
Area		
	7.73	m^2

HTE 8- Conduction through ORW-Zone 2		
Material	Stainless Steel	
Geometry		
Length	0.01986	
Height	25.74	
Inlet area specification	Specify area	
	18.45	m^2
Outlet area specification	Specify area	
Area		
	18.45	m^2

HTE 9- Convection from IRW		
Upstream area specification	Specify area	
Area	7.73	m^2
Convection		
Convection coefficient option	Constant	
h	1	W/ m^2.K

Element 10- Air Flow area		
Geometry		
Geometry option	Specify geometry	
Wall thickness	0	m
Length	0.633	m
Options		
Cross sectional option	Circumference and area	
Variable area	No	
Inlet		
Circumference	35.09	mm
Area	108.7	mm^2
Losses		
Roughness option	Specify manually	
Primary loss type	Darcy Weisbach	
Roughness	30	µm
Discretisation		
Number of increments	1	
Number in parallel	64800	

HTE 11- Convection from Zone 1 Cladding		
Upstream area specification	Specify area	
Area	1440.2	m^2
Convection		
Laminar Nusselt number	4	

HTE 12- Convection to ORW		
Upstream area specification	Specify area	
Area	7.73	m^2
Convection		
Convection coefficient option	Constant	
h	1	W/ m^2.K

HTE 13- Conduction through Zirconium Cladding-Zone 1		
Material	Zirconium	
Geometry		
Length	0.0006	
Height	0.011176	
Inlet area specification	Specify area	
Area		
	1283.04	m^2
Outlet area specification	Specify area	
Area		
	1440.2	m^2

HTE 14- Conduction through ORW-Zone 1		
Material	Stainless Steel	
Geometry		
Length	0.01986	
Height	10.78	
Inlet area specification	Specify area	
Area		
	10.25	m^2
Outlet area specification	Specify area	
Area		
	10.25	m^2

HTE 15- Conduction through uranium in Zone 1		
Material	Uranium oxide	
Geometry		
Length	0.004988	
Height	0.009976	
Inlet area specification	Specify area	
Area	2πrh*No of FRs	
	0	m^2
Outlet area specification	Specify area	
Area	2πrh*No of FRs	
	1283.04	m^2

HTE 16- Convection from SFP TO FB		
Upstream area specification	Specify area	
Area	100.134	m^2
Convection		
Convection coefficient option	Constant	
h	4	W/ m^2.K

HTE 17- Inlet Air Mass flow to FB (2 Building volumes /hr, Air ρ = 1)		
Boundary Conditions		
Temperature boundary condition	Fix on user value	
Temperature	27	°C
Mass source boundary condition	8.72	kg/s

HTE 18- Outlet Air Mass flow from FB (2 Building volumes /hr, Air ρ = 1)		
Boundary Conditions		
Temperature boundary condition	Fix on user value	
Temperature	27	°C
Mass source boundary condition	(-)8.72	kg/s

HTE 19- Composite element-Conduction through FB roof		
Conduction		
Area Upstream surface	1265.38	m^2
Thickness in element direction	0.25	m
Area downstream surface	1265.38	m^2
Material	Specify locally	
Capacitance	1637	kJ/ m^3.K
Conductivity in element direction	2	W/m.K
Conductivity in element cross direction	2	W/m.K
Convection/Radiation and wall Flux		
Upstream	Adiabatic	
Downstream	Convection	
Convection option	To ambient	
Convection area option	Specify area	
Convection area	1265.38	m^2
h	2	W/ m^2.K
T(ambient) convection	27	°C

HTE 20- Composite element-Conduction through FB wall		
Conduction		
Area Upstream surface	1778.41	m^2
Thickness in element direction	0.8	m
Area downstream surface	1778.41	m^2
Material	Specify locally	
Capacitance	1637	kJ/ m^3.K
Conductivity in element direction	2	W/m.K
Conductivity in element cross direction	2	W/m.K
Convection/Radiation and wall Flux		
Upstream	Adiabatic	
Downstream	Convection	
Convection option	To ambient	
Convection area option	Specify area	
Convection area	1778.41	m^2
h	2	W/ m^2.K
T(ambient) convection	27	°C

Appendix F. Input Data Derived from 1-D Flownex Conduction Model for Calculating Keff

Developing Keff Emperical Correlation														
Keff=	Q*ΔX/(TL-TR)*A		Tave =	(TL +TR)/ 2	K	273.15		A	0.11012853			ΔX	0.2225	
Flownex obtained Q (W)	**Q*ΔX**	**Delta T**	**TLeft (DegC)**	**Tright (DegC)**	**TAVE (DegC)**	**TL (K)**	**TR (K)**	**TAVE (K)**	**TAVE (K)**	**Keff (W/mK)**	**Delta T*A**	**Tave (K)**		**Keff x2 (W/mK)**
3.13342	0.697186	100	700	600	650	973.15	873.15	923.15	923.15	0.063306578	11.01285305	923.15		0.12661316
3.178134	0.707135	100	800	700	750	1073.2	973.15	1023.15	1023.15	0.064209965	11.01285305	1023.15		0.12841993
3.20905	0.714014	100	900	800	850	1173.2	1073.15	1123.15	1123.15	0.064834572	11.01285305	1123.15		0.12966914
3.231039	0.718906	100	1000	900	950	1273.2	1173.15	1223.15	1223.15	0.06527883	11.01285305	1223.15		0.13055766
3.247068	0.722473	100	1100	1000	1050	1373.2	1273.15	1323.15	1323.15	0.065602676	11.01285305	1323.15		0.13120535
3.259011	0.72513	100	1200	1100	1150	1473.2	1373.15	1423.15	1423.15	0.06584396	11.01285305	1423.15		0.13168792
3.268073	0.727146	100	1300	1200	1250	1573.2	1473.15	1523.15	1523.15	0.06602706	11.01285305	1523.15		0.13205412
3.275082	0.728706	100	1400	1300	1350	1673.2	1573.15	1623.15	1623.15	0.066168661	11.01285305	1623.15		0.13233732
3.280581	0.729929	100	1500	1400	1450	1773.2	1673.15	1723.15	1723.15	0.066279757	11.01285305	1723.15		0.13255951
3.284947	0.730901	100	1600	1500	1550	1873.2	1773.15	1823.15	1823.15	0.066367966	11.01285305	1823.15		0.13273593
3.288476	0.731686	100	1700	1600	1650	1973.2	1873.15	1923.15	1923.15	0.066439261	11.01285305	1923.15		0.13287852
3.291343	0.732324	100	1800	1700	1750	2073.2	1973.15	2023.15	2023.15	0.066497186	11.01285305	2023.15		0.13299437
3.293701	0.732848	100	1900	1800	1850	2173.2	2073.15	2123.15	2123.15	0.066544825	11.01285305	2123.15		0.13308965
3.295642	0.73328	100	2000	1900	1950	2273.2	2173.15	2223.15	2223.15	0.066584042	11.01285305	2223.15		0.13316808

*Note: TL and TR refers to left and right hand side temperatures of the 1-D model respectively

$$A = A_{Fuel\ rod} = 2\pi rL$$

Δx = Sum of all thickness from centre FR to adjacent centre FR between two SFAs

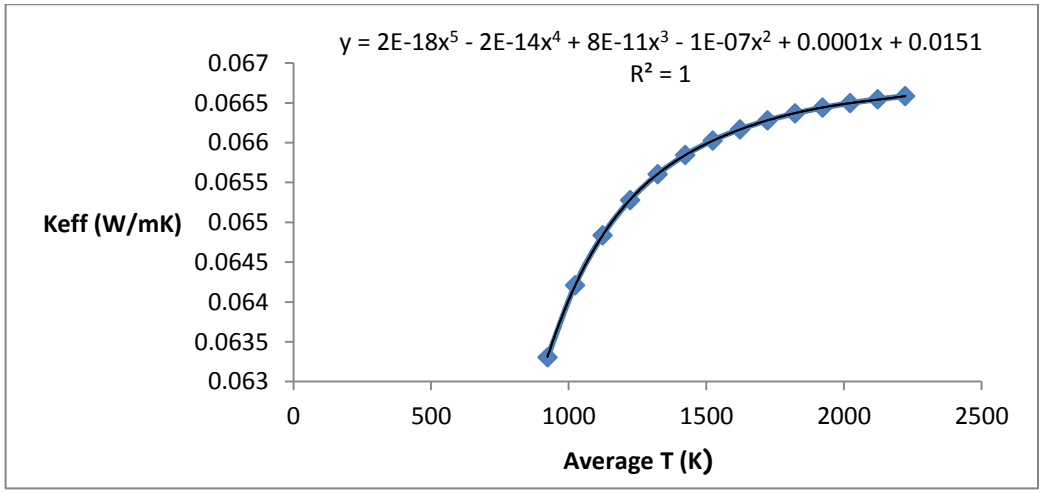

$$k_{eff}(T) = 2 * 10^{-18}T^5 - 2 * 10^{-14}T^4 + 8 * 10^{-11}T^3 - 1 * 10^{-07}T^2 + 0.0001T + 0.0151 \quad (1)$$

Tave	Keff (Data)	Keff (Polinomial-uncorrected) *eq-1*	Keff (Polinomial-corrected)* *eq-2*
923.15	0.063306578	0.071947305	0.06330708
1023.15	0.064209965	0.078742182	0.06419637
1123.15	0.064834572	0.086362247	0.06482392
1223.15	0.06527883	0.094910886	0.06526629
1323.15	0.065602676	0.104470442	0.06558124
1423.15	0.06584396	0.11510461	0.06581047
1523.15	0.06602706	0.126860845	0.06598237
1623.15	0.066168661	0.139772754	0.06611477
1723.15	0.066279757	0.153862503	0.06621774
1823.15	0.066367966	0.169143209	0.06629628
1923.15	0.066439261	0.18562135	0.06635313
2023.15	0.066497186	0.203299155	0.0663915
2123.15	0.066544825	0.222177012	0.06641785
2223.15	0.066584042	0.242255862	0.0664446

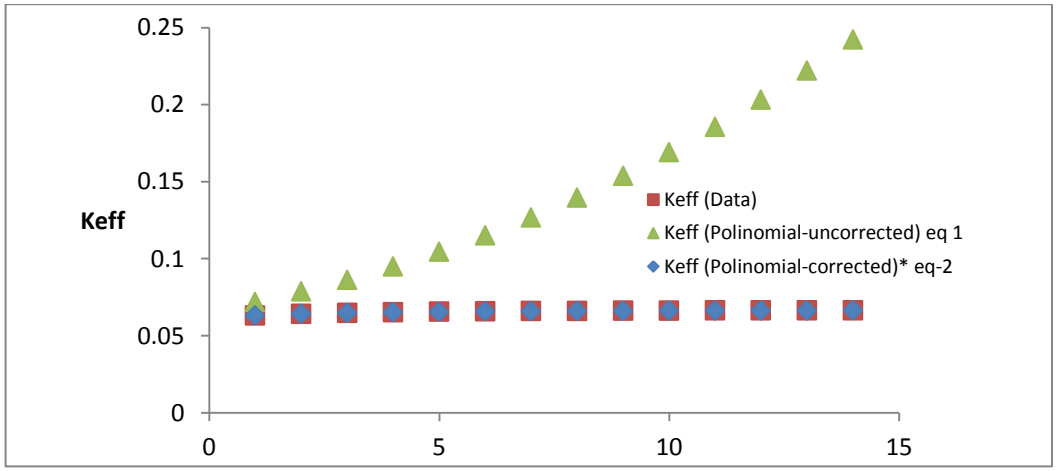

$$k_{eff}(T) := \sum_{i=0}^{5} \left(C_i \cdot T^i\right) \qquad k^*_{eff}(T) := \sum_{i=0}^{5} \left(C^*_i \cdot T^i\right)$$

Regression coefficients-uncorrected			Regression coefficients-corrected	
Equation 1 C =	0.0151		Equation 2 C* =	1.508E-02
	0.0001			1.305E-04
	-1E-07			-1.384E-07
	8E-11			7.528E-11
	-2E-14			-2.074E-14
	2E-18			2.297E-18

$$k_{eff}(T) = 2.297 * 10^{-18} T^5 - 2.074 * 10^{-14} T^4 + 7.528 * 10^{-11} T^3 - 1.384 * 10^{-07} T^2 + 0.0001305 T + 0.01508 \qquad (2)$$

Appendix G. SFAs Represented by the Respective Fuel Zones in the 2-D Flownex Network Model of the SFP

Total Heat Load (red squares)		**5440**	**kW**	**No of FAs (red squares)**		**160**	**Top Area SFA (m^2)**	**0.049506**
Total Heat Load (blue squares)		**1065**	**kW**	**No of FAs (blue squares)**		**1201**		
Heat load / FA (red squares)		**34**	**kW**	**Top Area SFAs (m^2)**		**Heat load / FA (blue squares)**	**0.886761032**	**kW**
Node/ Fuel zone	**Number of FAs**							
1	90			4.45556				
2	7			0.34654				
3	9			0.44556				
4	9			0.44556				
5	9			0.44556				
6	9			0.44556				
7	9			0.44556				
8	9			0.44556				
9	9			0.44556				
10	12			0.59408				
11	9			0.44556				
12	9			0.44556				
13	9			0.44556				
14	4			0.19803				
15	5			0.24753				
16	4			0.19803				
17	5			0.24753				
18	4			0.19803				
19	6			0.29704				

	Total Heat Load (red squares)		**5440**	**kW**	**No of FAs (red squares)**		**160**	**Top Area SFA (m^2)**	**0.049506**
	Total Heat Load (blue squares)		**1065**	**kW**	**No of FAs (blue squares)**		**1201**		
	Heat load / FA (red squares)		**34**	**kW**	**Top Area SFAs (m^2)**		**Heat load / FA (blue squares)**	**0.886761032**	**kW**
	Node/ Fuel zone	**Number of FAs**							
	20	181			8.96063				
	21	589			29.15918				
	22	364			18.02028				
Total		**1361**			**67.37801**				

Appendix H. Actual Flow Areas and Lengths through the Respective Fuel Zones in the 2-D Flownex Network Model of SFP

Length and Area conversions of scaled up 2-D SFP Layout (using Figures 30 &31 as reference)						
Scale :	**5**	**mm =**	**0.2225**	**m**	**FA Height (m)**	**4.2**
Length ID (between Fuel zones)	**Measured Length (Distance between Fuel zones) (mm)**	**Converted length (m)**		**Measured Heat flow length (mm)**	**Converted Heat Flow length (m)**	**Heat Flow area (m^2)**
1 to 2	45	2.0025		20	0.89	3.738
1 to 3	45	2.0025		15	0.6675	2.8035
1 to 4	48	2.136		15	0.6675	2.8035
1 to 5	37	1.6465		15	0.6675	2.8035
1 to 6	20	0.89		15	0.6675	2.8035
1 to 7	20	0.89		15	0.6675	2.8035
1 to 8	20	0.89		15	0.6675	2.8035
1 to 9	37	1.6465		20	0.89	3.738
2 to 10	15	0.6675		15	0.6675	2.8035
3 to 11	15	0.6675		15	0.6675	2.8035
4 to 12	15	0.6675		15	0.6675	2.8035
4 to 14	15	0.6675		15	0.6675	2.8035
5 to 15	15	0.6675		15	0.6675	2.8035
6 to 16	15	0.6675		15	0.6675	2.8035
7 to 17	15	0.6675		15	0.6675	2.8035
8 to 18	15	0.6675		15	0.6675	2.8035
9 to 19	15	0.6675		20	0.89	3.738
10 to 22	73	3.2485		20	0.89	3.738
11 to 22	70	3.115		15	0.6675	2.8035
12 to 22	70	3.115		15	0.6675	2.8035

13 to 22	74	3.293		15	0.6675	2.8035
13 to 21	86	3.827		20	0.89	3.738
14 to 20	67	2.9815		15	0.6675	2.8035
15 t0 20	58	2.581		15	0.6675	2.8035
16 to 20	52	2.314		15	0.6675	2.8035
17 to 20	50	2.225		15	0.6675	2.8035
18 to 20	52	2.314		15	0.6675	2.8035
19 to 20	58	2.581		20	0.89	3.738
20 to 20.1	52	2.314		95	4.2275	17.7555
20.1 to 21	78	3.471		95	4.2275	17.7555
22 to 21	75	3.3375		155	6.8975	28.9695
10 to 11	15	0.6675		15	0.6675	2.8035
11 to 12	15	0.6675		15	0.6675	2.8035
12 to 13	15	0.6675		15	0.6675	2.8035
2 to 3	15	0.6675		15	0.6675	2.8035
3 to 4	15	0.6675		15	0.6675	2.8035
4 to 14	15	0.6675		15	0.6675	2.8035
9 to 8	15	0.6675		15	0.6675	2.8035
8 to 7	15	0.6675		15	0.6675	2.8035
7 to 6	15	0.6675		15	0.6675	2.8035
6 to 5	15	0.6675		15	0.6675	2.8035
5 to 4	15	0.6675		15	0.6675	2.8035
4 to 12	15	0.6675		15	0.6675	2.8035
19 to 18	15	0.6675		15	0.6675	2.8035
18 to 17	15	0.6675		15	0.6675	2.8035
17 to 16	15	0.6675		15	0.6675	2.8035
16 to 15	15	0.6675		15	0.6675	2.8035
15 to 14	15	0.6675		15	0.6675	2.8035
14 to 13	15	0.6675		15	0.6675	2.8035

Appendix I. Heat Flow Derivation through Checker Box Arrangement of SFAs

$$q_{conduction} = -kA\,\frac{\Delta T}{\Delta x}$$

$$Q_{conduction} = kA\,\frac{\Delta T}{l}$$

Similiarly,

$$\Delta TA = \frac{l}{k}\,Q$$

Also,

For checker box arrangement of SFAs

$$\Delta TA = \left(\frac{l_1}{k_1} + \frac{l_2}{k_2}\right) Q \qquad [\,where:\ k_1 = k_{eff}\,, k_2 = 2k_{eff}]$$

Also,

$$\Delta TA = \left(\frac{l_1\,k_2 + l_2\,k_1}{k_1 k_2}\right) Q$$

Hence,

$$Q = \left(\frac{k_1 k_2}{l_1\,k_2 + l_2\,k_1}\right) \Delta TA$$

Appendix J. Actual Flow Areas and Lengths for Heat Transfer to the Respective SFP Walls of the 2-D Flownex Network Model of SFP

Length and Area conversions of scaled up 2-D SFP Layout (using Figures 30 and 32 as reference)						
Scale :	5	mm =	0.2225	m	FA Height (m)	4.2
Length ID (between Fuel zones and SFP walls)	Measured Length (Distance between Fuel zones and SFP walls) (mm)	Converted length (m)		Measured Heat flow length (mm)	Converted Heat Flow length (m)	Heat Flow area (m^2)
1 to A1 (conduction)	17.5	0.77875		75	3.3375	14.0175
2 to C1 (conduction)	7.5	0.33375		15	0.6675	2.8035
10 to D1 (conduction)	12.5	0.55625		15	0.6675	2.8035
22 to D2 (conduction)	32.5	1.44625		140	6.23	26.166
22 to E (conduction)	77.5	3.44875		65	2.8925	12.1485
21 to F (conduction)	77.5	3.44875		95	4.2275	17.7555
21 to G (conduction)	52.5	2.33625		155	6.8975	28.9695
20 to H (conduction)	52.5	2.33625		95	4.2275	17.7555
20 to I (conduction)	42.5	1.89125		95	4.2275	17.7555
19 to J (conduction)	12.5	0.55625		15	0.6675	2.8035
9 to K1 (conduction & radiation)	7.5	0.33375		15	0.6675	2.8035
1 to B1 conduction & radiation)	42.5	1.89125		30	1.335	5.607
A1 to A2 (radiation)				75	3.3375	40.05
C1 to C2 (radiation)				15	0.6675	8.01

Appendix K. Summary of the Respective Thermal Capacities for each Fuel Zone in the 2-D Flownex Network Model of SFP

Fuel Zone	FAs	FRs	$\rho\ cp\ V_{Uranium}$ $(\frac{J}{K})$	$\rho\ cp\ V_{Zirconium}$ $(\frac{J}{K})$	$\rho\ cp\ V_{Stainless\ steel}$ $(\frac{J}{K})$	L (m)	A_{FLOOR} (m^2)	$V_{Fuel\ Zone}$ (m^3)	V_{SFP} (m^3)	$\sum(\rho\ cp\ V)$	cp $(\frac{J}{kg.K})$	ρ $(\frac{kg}{m^3})$
1	90	26010	1.37E+07	3.68E+06	4.32E+06	0.1	4.45556	0.445556	7.628919	2.17E+07	2.84E+06	1
2	7	2023	1.07E+06	2.87E+05	3.36E+05	0.1	0.34654	0.034654	7.628919	1.69E+06	2.22E+05	1
3	9	2601	1.37E+06	3.68E+05	4.32E+05	0.1	0.44556	0.044556	7.628919	2.17E+06	2.84E+05	1
4	9	2601	1.37E+06	3.68E+05	4.32E+05	0.1	0.44556	0.044556	7.628919	2.17E+06	2.84E+05	1
5	9	2601	1.37E+06	3.68E+05	4.32E+05	0.1	0.44556	0.044556	7.628919	2.17E+06	2.84E+05	1
6	9	2601	1.37E+06	3.68E+05	4.32E+05	0.1	0.44556	0.044556	7.628919	2.17E+06	2.84E+05	1
7	9	2601	1.37E+06	3.68E+05	4.32E+05	0.1	0.44556	0.044556	7.628919	2.17E+06	2.84E+05	1
8	9	2601	1.37E+06	3.68E+05	4.32E+05	0.1	0.44556	0.044556	7.628919	2.17E+06	2.84E+05	1
9	9	2601	1.37E+06	3.68E+05	4.32E+05	0.1	0.44556	0.044556	7.628919	2.17E+06	2.84E+05	1
10	12	3468	1.83E+06	4.91E+05	5.76E+05	0.1	0.59408	0.059408	7.628919	2.90E+06	3.80E+05	1
11	9	2601	1.37E+06	3.68E+05	4.32E+05	0.1	0.44556	0.044556	7.628919	2.17E+06	2.84E+05	1
12	9	2601	1.37E+06	3.68E+05	4.32E+05	0.1	0.44556	0.044556	7.628919	2.17E+06	2.84E+05	1
13	9	2601	1.37E+06	3.68E+05	4.32E+05	0.1	0.44556	0.044556	7.628919	2.17E+06	2.84E+05	1
14	4	1156	6.09E+05	1.64E+05	1.92E+05	0.1	0.19803	0.019803	7.628919	9.65E+05	1.26E+05	1
15	5	1445	7.61E+05	2.05E+05	2.40E+05	0.1	0.24753	0.024753	7.628919	1.21E+06	1.58E+05	1
16	4	1156	6.09E+05	1.64E+05	1.92E+05	0.1	0.19803	0.019803	7.628919	9.65E+05	1.26E+05	1
17	5	1445	7.61E+05	2.05E+05	2.40E+05	0.1	0.24753	0.024753	7.628919	1.21E+06	1.58E+05	1
18	4	1156	6.09E+05	1.64E+05	1.92E+05	0.1	0.19803	0.019803	7.628919	9.65E+05	1.26E+05	1
19	6	1734	9.14E+05	2.46E+05	2.88E+05	0.1	0.29704	0.029704	7.628919	1.45E+06	1.90E+05	1
20	181	52309	2.76E+07	7.41E+06	8.69E+06	0.1	8.96063	0.896063	7.628919	4.37E+07	5.73E+06	1

21	589	170221	8.97E+07	2.41E+07	2.83E+07	0.1	29.15918	2.915918	7.628919	1.42E+08	1.86E+07	1
22	364	105196	5.54E+07	1.49E+07	1.75E+07	0.1	18.02028	1.802028	7.628919	8.78E+07	1.15E+07	1
Total			**2.07E+08**	**5.57E+07**	**6.54E+07**		**67.37806**	**6.737806**	**7.628919**	**3.28E+08**	**4.30E+07**	

Note*

$$\boldsymbol{cp_{zone}} = \frac{\sum(\rho\ cp\ V)_{zone}}{\boldsymbol{V_{SFP}}} \qquad (\boldsymbol{for\ \rho = 1})$$

$\rho_{Uranium\ oxide}$	*10970 kg/m³* [8]
$cp_{Uranium\ oxide}$	*240.7 J/kg.K* [8]
$\rho_{Zirconium}$	*6500 kg/m³* [8]
$cp_{Zirconium}$	*330 J/kg.K* [8]
$\rho_{stainless\ steel}$	*7817 kg/m³* [8]
$cp_{stainless\ steel}$	*460 J/kg.K* [8]

Appendix L. Summary of Input Data in Modified 2-D Flownex Network Model of SFP

A summary of the input data used in Figure 35 are given below:

Fuel Zone	**No of SFAs**	**Specific heat capacity** $(\frac{J}{kg.K})$	**Total Top SFA area (for Radiative heat transfer)** m^2
1	90	2.84E+06	4.45556
2	7	2.22E+05	0.34654
3	9	2.84E+05	0.44556
4	9	2.84E+05	0.44556
5	9	2.84E+05	0.44556
6	9	2.84E+05	0.44556
7	9	2.84E+05	0.44556
8	9	2.84E+05	0.44556
9	9	2.84E+05	0.44556
10	12	3.80E+05	0.59408

11	9	2.84E+05	0.44556
12	9	2.84E+05	0.44556
`13	9	2.84E+05	0.44556
14	4	1.26E+05	0.19803
15	5	1.58E+05	0.24753
16	4	1.26E+05	0.19803
17	5	1.58E+05	0.24753
18	4	1.26E+05	0.19803
19	6	1.90E+05	0.29704
20	181	5.73E+06	8.96063
21	589	1.86E+07	29.15918
22	364	1.15E+07	18.02028

Note*: For all radiative components the following values were used

View factor =1

Emissivity for zirconium = 0.7 [16], Emissivity for concrete = 0.95 [32], [39]

Appendix M. Copy of Signed EBE Faculty – Assessment of Ethics in Research Projects Form

EBE Faculty: Assessment of Ethics in Research Projects

Any person planning to undertake research in the Faculty of Engineering and the Built Environment at the University of Cape Town is required to complete this form before collecting or analysing data. When completed it should be submitted to the supervisor (where applicable) and from there to the Head of Department. If any of the questions below have been answered YES, and the applicant is NOT a fourth year student, the Head should forward this form for approval by the Faculty EIR committee: submit to Ms Zulpha Geyer (Zulpha.Geyer@uct.ac.za; Chem Eng Building, Ph 021 650 4791). Students must include a copy of the completed form with the thesis when it is submitted for examination.

Name of Principal Researcher/Student: VERNON FILLIS Department:

If a Student: Degree: MENG (NUCLEAR POWER) Supervisor: PROF ARNAUD MALAN

If a Research Contract indicate source of funding/sponsorship: (ESKOM FUNDED)

Research Project Title: TOWARD AN EFFECTIVE MODEL OF SPENT FUEL HEAT TRANSFER SUBSEQUENT TO LOSS OF INVENTORY

Overview of ethics issues in your research project:

Question 1: Is there a possibility that your research could cause harm to a third party (i.e. a person not involved in your project)?	YES	(NO)
Question 2: Is your research making use of human subjects as sources of data? If your answer is YES, please complete Addendum 2.	YES	(NO)
Question 3: Does your research involve the participation of or provision of services to communities? If your answer is YES, please complete Addendum 3.	YES	(NO)
Question 4: If your research is sponsored, is there any potential for conflicts of interest? If your answer is YES, please complete Addendum 4.	YES	(NO)

If you have answered YES to any of the above questions, please append a copy of your research proposal, as well as any interview schedules or questionnaires (Addendum 1) and please complete further addenda as appropriate.

I hereby undertake to carry out my research in such a way that

- there is no apparent legal objection to the nature or the method of research; and
- the research will not compromise staff or students or the other responsibilities of the University;
- the stated objective will be achieved, and the findings will have a high degree of validity;
- limitations and alternative interpretations will be considered;
- the findings could be subject to peer review and publicly available; and
- I will comply with the conventions of copyright and avoid any practice that would constitute plagiarism.

Signed by:

	Full name and signature	Date
Principal Researcher/Student: VERNON FILLIS	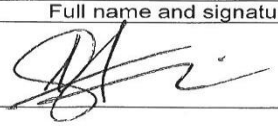	2015-03-17

This application is approved by:

Supervisor (if applicable):		2015/03/17
HOD (or delegated nominee): Final authority for all assessments with NO to all questions and for all undergraduate research.		15/4/15
Chair : Faculty EIR Committee For applicants other than undergraduate students who have answered YES to any of the above questions.		